COMPARTMENTATION OF DE NOVO THYMIDYLATE BIOSYNTHESIS AT THE SITES OF DNA REPLICATION

A Dissertation

Presented to the Faculty of the Graduate School

of Cornell University

In Partial Fulfillment of the Requirements for the Degree of

Doctor of Philosophy

by

Donald Dean Anderson II

January 2012

COMPARTMENTATION OF DE NOVO THYMIDYLATE BIOSYNTHESIS AT THE SITES OF DNA REPLICATION

Donald Dean Anderson II, Ph. D.

Cornell University 2012

Folate mediated one-carbon (1C) metabolism is required for the de novo synthesis of purines, thymidylate, and the remethylation of homocysteine to methionine. Perturbations in folate mediated 1C metabolism are associated with pathologies and developmental defects including cardiovascular disease, cancers, and neural tube defects. Disruption of thymidylate biosynthesis is associated with genome instability resulting from the misincorporation of uracil into DNA. The de novo dTMP pathway consists of serine hydroxymethyltransferase, (SHMT), thymidylate synthase (TYMS), and dihydrofolate reductase (DHFR). Serine hydroxymethyltransferase 1 (SHMT1) expression is limiting for de novo thymidylate synthesis.

Whereas the current literature describes nucleotide biosynthesis occurring in the cytoplasm, the results of these studies demonstrate that de novo dTMP biosynthesis is unique in that it occurs in the nucleus and mitochondria. The entire de novo thymidylate biosynthesis pathway is shown to undergo SUMO dependent nuclear translocation during S-phase. A novel isoform of SHMT, termed SHMT2α, was identified which provides functional redundancy with SHMT1 for nuclear de novo thymidylate biosynthesis and accounts for about 25% of nuclear SHMT activity. SHMT1 protein levels are shown to be regulated by the ubiquitin system where an interplay between SUMOylation and ubiquitination on SHMT1 signals proteasomal

degradation, nuclear export, and mediates stability within the nucleus and cytosol. Nuclear thymidylate biosynthesis is coupled with the formation of multi-enzyme complexes associated with the nuclear lamina. SHMT1 serves as scaffold protein and is essential for metabolic complex formation. The enzymes for de novo dTMP synthesis were found to be associated with PCNA and enriched at origins of replication.

The nuclear compartmentation of de novo dTMP synthesis led to the hypothesis that there is a requirement for dTMP synthesis within the mitochondria. Purified mitochondria were capable of de novo thymidylate biosynthesis. A novel isoform of DHFR previously thought to be a pseudogene called DHFR-like protein 1 (DHFRL1) was identified that is essential for mitochondrial thymidylate biosynthesis. In cells lacking mitochondrial SHMT activity (SHMT2) uracil levels in mtDNA were increased by 40%. These data support a role for de novo dTMP synthesis within the nucleus and mitochondria that supports DNA replication and repair and limits uracil misincorporation.

BIOGRAPHICAL SKETCH

Donald Dean Anderson II was born to Sandra Arline Anderson and Donald Dean Anderson I, Ph.D. on February 14, 1980 in Farmington, MO. He attended Central High School in Ft. Pierce, FL and graduated in 1997. Donald attended Logos Christian College to study Philosophy and Religion. Changing career goals, Donald became interested in the Biological Sciences and moved to Ithaca, NY. Donald eventually transferred to Cornell University where he started doing research as an undergraduate working with Prof. Stewart Gray in the plant virology field. Looking for more human related research, he started working with Prof. Patrick Stover in 2005 and finished his Bachelors in Science in 2006. Donald decided to continue a research career and was accepted to the graduate field of Biochemistry, Molecular and Cell Biology in 2007 where he has continued to work in the lab of Prof. Patrick Stover.

ACKNOWLEDGMENTS

I would like to thank Prof. Patrick Stover for his dedication to research and understanding of the field of folate mediated one-carbon metabolism. I also want to thank Prof. Stover for his patience during difficult times in my life. I am indebted to several people within the lab that have helped me in multiple ways. I want to thank all past and present members of the Stover lab especially Collynn Woeller, PhD; Martha Field, PhD; and Jae Y. Eom. All three of them have been a source of considerable support. I would also like to thank Prof. Andre Bensadoun and Prof. Volker Vogt for interesting discussions and important contributions to my life and work. Finally, I would like to thank the members of my committee, Prof. Gerald Feigenson and Prof. Hening Lin for their help throughout my PhD training.

TABLE OF CONTENTS

CHAPTER 1

Uracil: Friend or Foe?

Introduction

The presence of uracil in DNA is associated with genome instability and DNA mutagenesis (1). Two mechanisms account for the presence of uracil in DNA: cytidine deamination, and misincorporation of dUTP into DNA during DNA replication. Spontaneous or enzymatic cytosine deamination can lead to genetic transitions upon DNA replication; U:G base mispairs result in C to T transitions. Deamination of cytidine occurs in both dsDNA and ssDNA (Figure 1.1). High dUTP/dTTP ratios in cells can also permit the misincorporation of uracil into DNA (Figure 1.1). While A:U base pairs do not lead to transitions or transversions, genome instability can result. Repair enzymes such as uracil DNA glycosylase (UNG) function to remove uracil for replacement with dTTP.

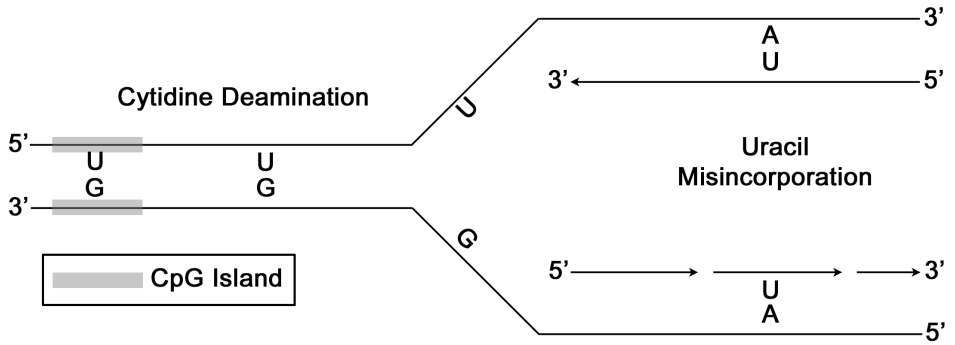

Figure 1.1. The presence of uracil in DNA is due to cytidine deamination and uracil misincorporation. Cytidine deamination can occur in dsDNA or ssDNA. During transcription, replication, or DNA breathing ssDNA can undergo spontaneous or enzymatic cytidine deamination. During replication, dUTP can be misincorporated into DNA in place of dTTP.

Under dTTP deplete conditions, a futile cycle of removal and replacement can result in double strand breaks. Double strand breaks (DSB) can give rise to chromosomal translocations, point mutations and/or cell death. It has been estimated that spontaneous cytidine deamination occurs 70-200 events per day (2) whereas incorporation of dUTP in place of dTTP has been observed to occur up to 10,000 times per genome per day (3) representing a quantitatively larger source of uracil in DNA (4). The presence of uracil in DNA elicits repair mechanisms which are 5-fold redundant. The four human genes encoding uracil repair enzymes include: thymine DNA glycosylase (TDG), methyl-CpG-binding domain protein 4 (MBD4), single strand selective monofunctional uracil DNA glycosylase 1 (SMUG1) and uracil DNA glycosylase (UNG). The UNG gene encodes both mitochondrial (UNG1) and nuclear (UNG2) isoforms. In mice, Nei-like glycosylase 1 (Neil1) has been determined to excise uracil from DNA (5) . Recent evidence also supports a role for NEIL1 in uracil repair in humans (6). Despite the redundancy in uracil repair mechanisms, uracil misincorporation is responsive to folate levels (7). Folate mediated one-carbon metabolism is a metabolic network required for the *de novo* synthesis of purines, thymidylate, and *S*-adenosylmethionine (8). The *de novo* dTMP pathway serves to limit uracil misincorporation by maintaining dTMP levels within compartments where DNA replication occurs: the nucleus and mitochondria (9,10). Although accumulation of uracil in DNA could lead to genome instability, uracil misincorporation may encode information within DNA. The focus of this review will be to outline what is known about uracil misincorporation limiting mechanisms, uracil repair mechanisms and possible outcomes, and the evidence that suggests uracil as an information encoder within DNA.

Uracil misincorporation limiting mechanisms prior to DNA replication.

The inability of DNA polymerase to discriminate between dUTP and dTTP indicates that the ratio of dUTP/dTTP is an important factor in the misincorporation of uracil in DNA (11). Two mechanisms exist that can lower the concentration of dUTP and increase dTTP: deoxyuridine

triphosphatase, (dUTPase) which hydrolyzes dUTP to dUMP and pyrophosphate (12) and the *de novo* thymidylate pathway which uses dUMP to make dTMP. Sources of dUMP include the deamination of dCMP by deoxycytidylate deaminase and the reduction of UDP by the action of ribonucleotide reductase to form dUDP. Following subsequent phosphorylation to dUTP, dUTPase can hydrolyze dUTP to make dUMP for *de novo* dTMP synthesis (Figure 1.2).

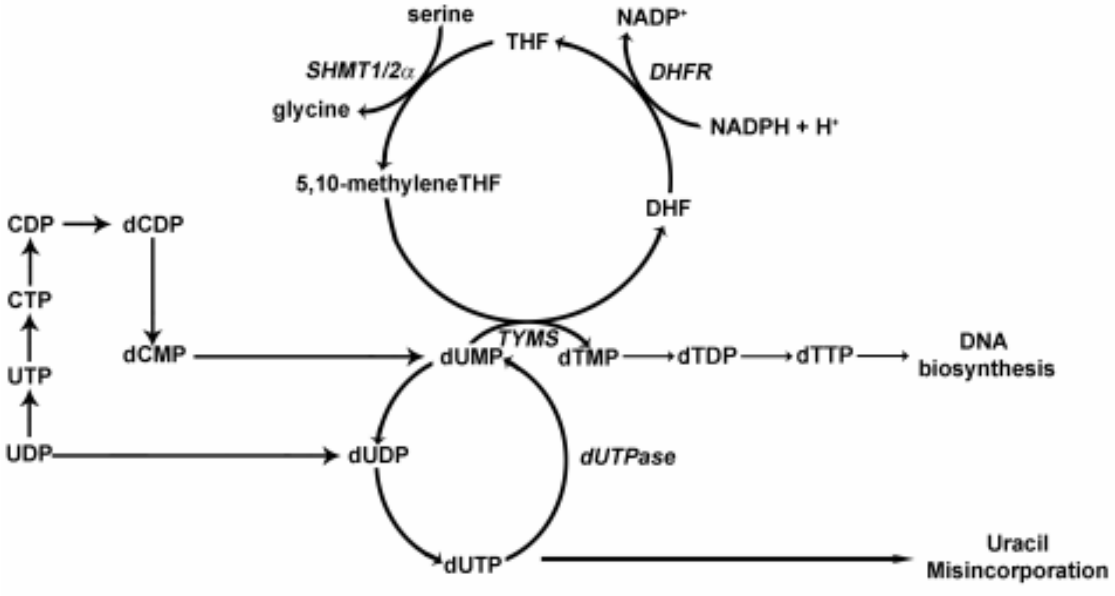

Figure 1.2. Pre-Replication Mechanisms for Limiting the Available dUTP Pool. The *de novo* dTMP biosynthetic cycle is localized to the nucleus in S-phase and G2/M phases. SHMT1 and SHMT2α work to convert serine and THF to glycine and 5,10-methyleneTHF. TYMS uses 5,10-methyleneTHF to methylate dUMP to form dTMP leaving DHF which can be reduced by DHFR to form THF for another round of dTMP synthesis. dTMP can subsequently be phosphorylated for incorporation into DNA. dUTPase can dephosphorylate dUTP to dUMP in order to allow TYMS to convert it to dTMP. Both of these mechanisms work to effectively lower the dUTP/dTTP ratio which governs how much uracil misincorporation can occur.

dUTPase is conserved throughout vertebrate evolution (13) and is essential in *E. coli* (14) and *S. cerevisiae* (15). The dUTPase gene encodes two isozymes: a nuclear form, DUT-N and a mitochondrial form, DUT-M (16). These two isoforms are generated through alternative 5' exon usage which contains either a nuclear localization signal or a mitochondrial localization

signal (17,18). DUT-N and DUT-M are regulated differently with DUT-M being constitutively expressed whereas DUT-N is expressed in replicating cells (19). These isozymes work to limit the available pools of dUTP for misincorporation in their respective compartments and increase the levels of dUMP which can be utilized for *de novo* thymidylate biosynthesis.

De novo thymidylate biosynthesis occurs in both the nucleus (9) and mitochondria (10). The three enzymes that constitute the *de novo* thymidylate biosynthetic pathway, serine hydroxymethyltransferase (SHMT), dihydrofolate reductase (DHFR), and thymidylate synthase (TYMS) also work to control the dUTP/dTTP ratio (Figure 2). SHMT catalyses the reversible conversion of serine and THF to glycine and 5,10-methyleneTHF. 5,10-methyleneTHF is then used by TYMS to methylate dUMP to produce dTMP and dihydrofolate (DHF). DHFR subsequently reduces DHF to THF in a NADPH dependent reaction allowing for the *de novo* thymidylate biosynthetic cycle to continue (8). For nuclear *de novo* dTMP synthesis, the entire *de novo* thymidylate biosynthetic cycle is localized to the nucleus in S and G2/M phases of the cell cycle (20)(Unpublished observation, Anderson et al.). Two cytosolic and nuclear isoforms of SHMT exists: one encoded by the *SHMT1* gene, and another encoded by the *SHMT2* gene we termed SHMT2α (9). SHMT2α was shown to account for ~25% of the thymidylate produced in nuclei. Through cell culture and mouse studies, SHMT1 has been observed to be rate-limiting for *de novo* dTMP biosynthesis. Increasing levels of SHMT1 in MCF-7 and SHSY5Y cells increases the efficiency of de novo dTMP synthesis whereas lowering SHMT1 levels in MCF-7 cells lowers efficiency of dTMP synthesis (21). In mouse models lacking *Shmt1,* levels of uracil misincorporation are increased further showing the importance of SHMT1 and *de novo* dTMP synthesis for limiting uracil within DNA (7). Both SHMT1 and SHMT2α are required as a scaffold protein for the formation of multi-enzyme complexes including SHMT, TYMS, and DHFR that co-localize

with the nuclear lamina. We have also identified SHMT1, TYMS, and DHFR as PCNA interacting proteins. PCNA acts as the sliding clamp for replicative DNA synthesis. Using a model system of replicating episomal DNA and tandem chromatin immunoprecipitation experiments, SHMT1, TYMS, and DHFR were all found to be in association with PCNA on DNA with high enrichment around origins of replication (Unpublished observation, Anderson et al.). These data confirm the presence of the nuclear *de novo* dTMP pathway at replication forks for the processive addition of dTTP into DNA when needed.

Mitochondrial de novo dTMP synthesis has been shown to occur in the human liver cell line, HepG2, and Chinese hamster ovary cells (CHO)(10). Our lab and others have identified TYMS and SHMT2 within mitochondria of mammalian cells (22-25). The entire de novo dTMP pathway also exists in plant mitochondria using a bi-functional TYMS-DHFR enzyme and SHMT2 (26). Within mammalian mitochondria identification of a mitochondrial DHFR was still undetermined until recently (10). We were able to identify a previously uncharacterized mitochondrial DHFR that was thought to be a pseudogene called dihydrofolate reductase-like protein 1 (DHFRL1). Confocal microscopy experiments identified that DHFRL1 localized to mitochondria. Knocking down DHFRL1 with siRNA in HepG2 cells eliminated DHFR activity within mitochondria. All three enzymes in mitochondrial de novo dTMP synthesis including DHFRL1, TYMS, and SHMT2 are available within matrix and inner membrane fractions of mitochondria with the matrix being the compartment in which mtDNA is housed (10). Furthermore, in mitochondria isolated from the glycine auxotrophic CHO cell line, glyA, which lack SHMT2 activity, it was observed that levels of mitochondrial *de novo* dTMP biosynthesis was essentially absent with a concomitant 40% increase in levels of uracil misincorporation in mtDNA. These data support the importance of *de novo* dTMP biosynthesis in limiting uracil misincorporation in mtDNA.

The availability of both dUTPase and de novo dTMP biosynthetic pathways to sites where DNA is synthesized show the importance of maintaining the dUTP/dTTP ratio in limiting uracil misincorporation.

Regardless of the multiple enzymes that exist to remove uracil from DNA, it seems that one of the most important factors in limiting the presence of uracil within DNA is folate. Previous work has observed that in humans deficient in folate, levels of uracil within blood and bone marrow DNA are increased 8 and 9 fold respectively as compared to patients with normal folate levels (27). Upon folate supplementation, levels of uracil within blood DNA decreased 20 fold in patients with the lowest presupplementation folate levels. In normal human lymphocytes grown in medium with decreasing concentrations of folates, the presence of uracil increased as folate levels decreased (28). It has also been observed that in lymphocytes of hooded lister rats fed folate deficient diets that uracil levels increase in response (29). In a DNA repair deficient CHO cell line, CHO-UV5 cells, which are hemizygous at the *aprt* locus, it was observed that cells grown in media lacking folates, thymidine, and hypoxanthine had drastic increases in dUTP/dTTP ratios along with increases in the presence of uracil within DNA as compared to cells grown in replete media (30). Within our lab, we have seen that mice lacking *Shmt1* exhibit increased uracil levels within liver and colon DNA (7,31) and that these increases double when mice are fed a folate and choline deficient diet. These data implicate folate status as a determining factor in regulating uracil content within DNA.

Redundancy in uracil repair mechanisms

Although multiple repair enzymes exist for uracil within DNA, the focus of this review will be in enzymes that work to repair uracil misincorporation and not spontaneous or enzymatic deamination of cytidine within DNA leading to the presence of uracil. The major repair enzymes that work to remove uracil from U:A pairs derived from uracil misincorporation are the mitochondrial and nuclear isoforms of uracil DNA glycosylases, UNG1 and UNG2

respectively. The UNG gene is highly conserved across several species including mammals, bacteria, yeast, and herpes viruses (32). UNG1 and UNG2 have a high catalytic turnover rate, 600-1000 uracils/min (33), consistent with the rapid movement of the replication fork (33-35). Both UNG1 and UNG2 do not have specificities for U:A or U:G pairings and work to repair uracil in DNA in both of those contexts in both single stranded and double stranded DNA (33). In mammalian cells, both UNG1 and UNG2 are derived from the *UNG* gene through mRNA splicing and alternate promoter usage (36). The different N-termini encoded for on these transcripts are required for nuclear and mitochondrial sorting (2).

UNG1

Mitochondrial DNA (mtDNA) is subject to increased mutation rates. The presence of an oxidative environment due to the process of respiration can lead to mtDNA mutagenesis. Respiration has been observed to function abnormally in cells depleted of mtDNA (37). Mutations in mtDNA can result in diseases such as cancer (38), neurodegeneration (39), and diabetes (40). Maintaining mtDNA integrity is essential for maintaining human health. Within mitochondria UNG1 is the only known uracil-DNA glycosylase (41). Like DUT-M and SHMT2 (42), UNG1 exhibits housekeeping-like expression. Highest levels of human UNG1 expression occur in skeletal muscle, heart, and testis (43). UNG1 has been observed to remove uracil from mtDNA in short patch and long patch base excision repair (BER) in human mitochondrial extracts devoid of nuclear proteins (41). It must be noted that species specific differences exist between mice and men. While the Ung gene is organized similarly in both mice and men, murine *Ung1* products sort to both mitochondria and nucleus (36,44) whereas in humans, UNG1 is only mitochondrial (43,44). This is due to a poor conservation of the mitochondrial localization signal in Ung1. A stronger promoter driving Ung1 in mice leads to a higher contribution of Ung1 to total Ung activity within mice compared to humans. In mice, the stronger promoter driving Ung1 and its localization to nuclei suggests that Ung1 acts as a

backup for Ung2 activity and works to ensure nuclear Ung activity. Understanding these species specific difference is important in interpreting data from mouse models. While these differences exist, mouse and rat models can be informative. During rat gestation, transcripts for both Ung1 and Ung2 exhibit high expression in embryos and yolk sacs between gestational days 10 and 12. Both Ung1 and Ung2 transcript levels are increased by 400% in gestational day 12 embryos and yolk sacs versus gestational day 10 embryos and yolk sacs (45). Treatment of embryo and yolk sac cells of rats *in vitro* with 0.5 μM methotrexate showed a 30-40% increase in Ung1 levels in both embryos and yolk sacs while Ung2 levels were only increased in yolk sacs. Within mice, Ung1 is highly expressed in tissues rich in mitochondria similar to humans (43,44). An increase of Ung1 during embryo mid-gestation has been observed. These data may be indicative of important aspects of mitochondrial dUTP misincorporation during embryogenesis which are still unknown although the relative contributions of mouse Ung1 and Ung2 within the nucleus need further research.

Mice deficient in the *Ung* gene show a marked phenotype following ischemic insult and lower numbers of surviving neurons (46). Although the $Ung^{-/-}$ mouse model does not discriminate between the mitochondrial and nuclear isoforms of Ung, disruption of mtDNA repair and mitochondrial damage has been shown to lead to cell death. Both mtDNA and mitochondrial damage are known to occur in response to ischemic brain injury and in *Ung* wild-type mice, the *Ung1* transcript is specifically upregulated in response to stroke (46). The existence of mitochondrial and nuclear isoforms of dUTPase and UNG, as well as the presence of mitochondrial and nuclear *de novo* dTMP synthesis suggests that maintaining uracil levels in both compartments where DNA is synthesized is a critical process.

UNG2

UNG2 is expressed most highly during S-phase in dividing cells and is undetectable in cells that are non-dividing (47) with highest UNG2 mRNA levels in late G1/early S phase (43). In

the nucleus, UNG2 accumulates at replication foci and binds to PCNA and replication factor A (RPA) suggesting a processive removal of uracils during replication which is consistent with its high catalytic rate (35,48). UNG2 has been observed to be in association with complexes containing APE1, POLD, XRCC1, and DNA ligase which are competent for both short-patch and long-patch BER (34). Interestingly, SHMT1 has been shown to interact with BER proteins suggesting a processive repair pathway in which UNG2 removes uracil and thymidylate is synthesized at those repair foci for incorporation in DNA (Unpublished results Anderson). More work must be done in order to understand the role of SHMT1 in repairing and limiting uracil in DNA.

Post-translational modification of UNG2 is an important mediator of degradation and activity. Phosphorylation of serines and threonines in the N-terminus of UNG2 has been observed (49) and UNG2 phosphorylation occurs at the initial start of S-phase (47). Furthermore, phosphorylation was observed to occur on Ser23 at late G1/early S-phase which increases its association with RPA and increases activity (50). Throughout S-phase, a sequential phosphorylation of Thr60 and Ser64 result in decreased affinity for RPA. S64A mutants of UNG2 accumulate in cells suggesting phosphorylation at that site is required for proteosomal degradation (47) via ubiquitination of UNG2 by late G2 phase (50). UNG2 is also phosphorylated at threonines 6 and 126 in response to UV damage. These phospho-forms of UNG2 have increased activity with subsequent dephosphorylation decreasing activity (51). Future work should be done to understand how the various phospho-forms of UNG2 affect protein-protein interactions and if differing partners exist in normal cycling cells versus UV treated cells.

Little phenotypic evidence is available from *Ung-/-* mice. These mice are viable and develop normally (52) whereas later in life these mice develop B cell lymphomas (53,54). As stated previously, species specific differences do exist between mice and men and

accumulating evidence in mammalian cell culture models shows UNG2 as playing a role in proliferation, cell death, and mitotic dysfunction. Previous reports have indicated that treatment of human cells with uracil-DNA glycosylase inhibitor protein (UGi) results in reduced cellular proliferation (55). Knockdown of UNG2 using siRNA has also been observed to decrease cell proliferation and increased apoptosis as compared to controls (56). In rat hippocampal neurons grown in culture, knockdown of Ung induced apoptosis (57). Recent evidence supports a role for UNG2 in mediating kinetochore assembly for mitosis by acting as an assembly factor for the histone H3 variant, CENP-A (58,59). CENP-A is required for kinetochore assembly during mitosis and also binds to sites of DNA damage (60). UNG2 co-localizes at centromeres and sites of double strand breaks (DSB) with CENP-A and phosph-H2AX, a histone H2A variant that rapidly localizes to sites of DSB. Knockdown using siRNA specific to UNG2 results in the inability for CENP-A to assemble and results in cell death, reduced proliferation, and increased frequencies of mitotic dysfunction (59). Mutants of UNG2 lacking catalytic activity still rapidly form foci in cells at sites of laser induced damage suggesting the catalytic activity is not required for this function (59). Future work must be done in order to more fully understand whether all the defects seen in mammalian cell culture models are due to lack of UNG2 mediated CENP-A assembly.

NEIL1

Some recent evidence implicates human NEIL1 as a mediator of increased sensitivity to de novo dTMP synthesis pathway inhibition with addition of dTTP rescuing the phenotype (6). Although this data may be indicative of human NEIL1 playing a role in removal of U:A pairs, mouse Neil1 is selective in removal of U:G mispairs (5). More work should be done in order to fully understand the selectivity and characteristics of human and mouse Neil1.

Uracil in DNA as a controller of gene expression

Evidence supports that uracil misincorporation leads to genomic instability (27,28,61-63). While this may be accurate and responsible for some pathologies, other possibilities exist namely: alterations in the transcriptome and/or nucleotide sensing mechanisms.

Maternal folate supplementation has reduced the numbers of neural tube defects in the population (64,65). Until recently though, no folate-dependent enzymes have been implicated in neural tube defects. Mice deficient in SHMT1 fed folate deficient diets exhibit increased risks of neural tube defects (66). These mice also exhibit increased uracil misincorporation in DNA (7) and decreased capacity for *de novo* dTMP synthesis (9). While uracil in DNA may be a marker of potential genomic instability, Ung-/- mice exhibit 100 fold increased uracil in genomic DNA, yet they develop normally with no evident macroscopic phenotypes (35). Because impaired dTMP synthesis, the presence of uracil in DNA, and folate status are associated with neural tube defects, it would stand to reason that Ung-/- mice on folate deficient diets would also exhibit neural tube defects if it were uracil misincorporation related, which is not the case. Lower folate status would be expected to increase the dUTP/dTTP ratio. It may be that uracil in DNA is simply a marker of increased dUTP/dTTP ratio and that this ratio in the cell signals some downstream event that acts as a master regulator. This has been observed in the bacterium *E. coli,* where the transcription factor RutR was found to be regulated by uracil and thymine levels (67). The RutR regulon contains a large number of genes involved in the degradation of purines and pyrimidines; the synthesis of pyrimidines, glutamine, and arginine; and the transport of glutamate. Future work should identify potential RutR homologues in mammalian cells to determine if similar regulatory processes occur. Master regulatory events may be important in understanding early developmental processes due to aberrant levels of uracil and thymine.

Another intriguing hypothesis of regulation of gene expression by uracil in DNA is supported by several lines of evidence. Pyrimidine C5 methyl groups exist in two forms:

methylation of cytosine by DNA methyltransferases and in thymine. Thymine bases have a methyl group at C5 whereas uracil does not. Interestingly, these methyl groups exist in the major groove of B-form DNA, with the major groove being the more accessible to regulatory proteins such as transcription factors (68). It is known that cytosine methylation plays an important part in epigenetic phenomenon and regulation of gene expression. An intriguing hypothesis emerges in that thymine methyls could be playing a role in regulation with the absence of a methyl group (uracil in place of thymine) also playing a role.

Protein-DNA interactions can be facilitated by the C-5 methyl group of thymine. This was originally identified for restriction enzymes containing thymine in their recognition motifs. The *B. subtilis* phage, PBS2, contains uracil in its DNA in place of thymine. When PBS2 DNA was subjected to restriction enzymes that recognize thymine-containing sequences, such as HpaI and HindIII, DNA was digested inefficiently (69). The efficiency of enzymes containing only G-C base pairs within their recognition motifs was unaffected. Furthermore, site-directed mutagenesis of the EcoRI, EcoRII, and EcoRV recognition sites in which thymines were replaced with uracil lead to a 30%, 50%, and complete reduction of activity respectively (70,71).

The regulatory impact of uracil in place of thymine has been described in the *E. coli* lac operon, a 26 bp region containing 16 A-T base pairs (72). Several thymines within the sequence at positions 6,7,13,25, and 26 were required for normal lac repressor-lac operon (RO) complex formation. Replacing these thymines with uracil resulted in drastic reduction of RO complex stability and solidified a role for thymine methyls in making hydrophobic contacts with the lac repressor.

The promoter regions of *E. coli* also contain thymines. The consensus sequences -35 and -10 upstream of transcription start sites are A-T rich. Replacement of thymines at -35 and -34 with uracil resulted in the abolishment of promoter function showing how critical thymines at

those positions are for transcriptional activity (73). Although several studies have implicated roles for uracil misincorporation regulating protein-DNA interactions in bacteria, evidence exists within higher eukaryotes as well. The yeast transcription factor GCN4 is a transcription factor in the AP-1 family (74). The sequence that GCN4 binds to is ATGACTCAT (75) and contains 6 A-T pairs. Using uracil interference assays this sequence was probed for GCN4 binding when T is replaced with U (76). It was observed that the 4 internal thymines within the sequence were required for the high affinity binding of GCN4 *in vitro*. These data support the importance of thymine methyls in protein-DNA interactions. A model of how uracil in DNA may play a role in protein-DNA interactions is shown in figure 1.3. It can be envisioned that in DNA, transcriptional activators or repressors that recognize thymine methyls could recognize and bind to their DNA binding motif when thymine is present. Upon replacement of thymines with uracil, transcriptional activators or repressors may have a lower or higher affinity for the DNA binding motif which would affect transcriptional processes.

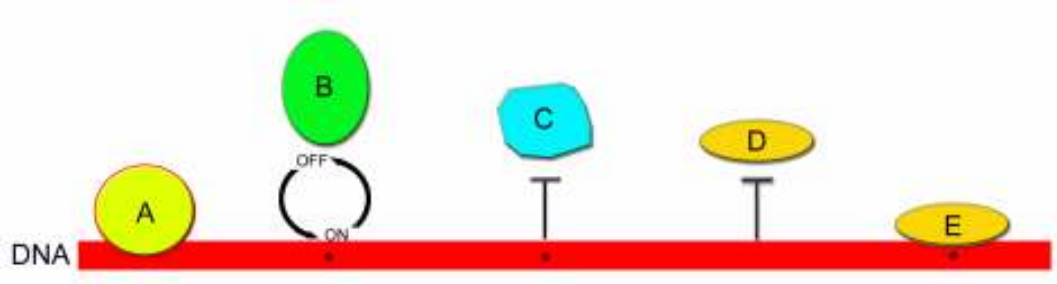

Figure 1.3. Models of Transcriptional Response to Uracil Misincorporation. A) Transcriptional activators or repressors containing critical thymines in their binding sequence can recognize and bind to their motif. B) Upon uracil misincorporation (as denoted by the asterisk) transcriptional activators or repressor DNA binding may be affected by changing binding constants for the cognate site or C) completely inhibiting binding and decreasing or increasing transcription. D) Conversely, a transcriptional activator or repressor inhibited by thymine containing sequence may bind E) when the methyl group of thymine is missing in uracil containing sequence.

In *Drosophila,* no UNG activity has been detected (77). Instead, a nuclease which acts upon uracil containing DNA has been isolated. Using uracil-containing DNA, pull-down

experiments were performed to isolate interactors that contained uracilated DNA nuclease activity. The enzyme that was purified was termed uracil-DNA-degrading factor protein (UDE) (78). It has been determined that a drastic reduction of dUTPase in larval stages prior to pupation and lack of UNG activity could significantly increase uracil in DNA during those developmental stages (79). UDE expression is also under strict control during *Drosophila* development with upregulation just prior to pupation with little expression during the embryonic and larval stages (78). The significant increases in uracil-DNA during larval stages suggests some sort of uracil-mediated control of metamorphosis.

DNA replication, repair, recombination, and transcriptional processes all use DNA as substrate and these processes are inherently connected (80). Increased transcriptional activation occurs in association with genomic instability. In *S. cerevisiae* it has been determined that a link exists between transcription associated mutagenesis and the levels of transcription. The accumulation of abasic sites has been observed to be greatly increased in highly transcribed DNA. Using *ung* deficient mutants in yeast, it was identified that UNG was responsible for generating abasic sites that accumulate under high-transcriptional conditions (81). The authors went on to overexpress dUTPase in yeast and observed lower mutation rates showing that most uracil present in highly-transcribed DNA is derived from dUTP misincorporation versus cytosine deamination. These data provide a direct link between the presence of uracil in DNA and transcriptional response.

Although evidence of these types of regulatory events is lacking in mammalian cells, models of hypotheses that uracil misincorporation in DNA leads to transcriptional changes can be made. GATA-1 is a transcription factor that is required for erythroid and megakaryocyte differentiation. The DNA binding motif that GATA-1 recognizes is (A/T)GATA(A/G) (82). A model of GATA-1 (83) in complex with DNA is shown in figure 1.4.

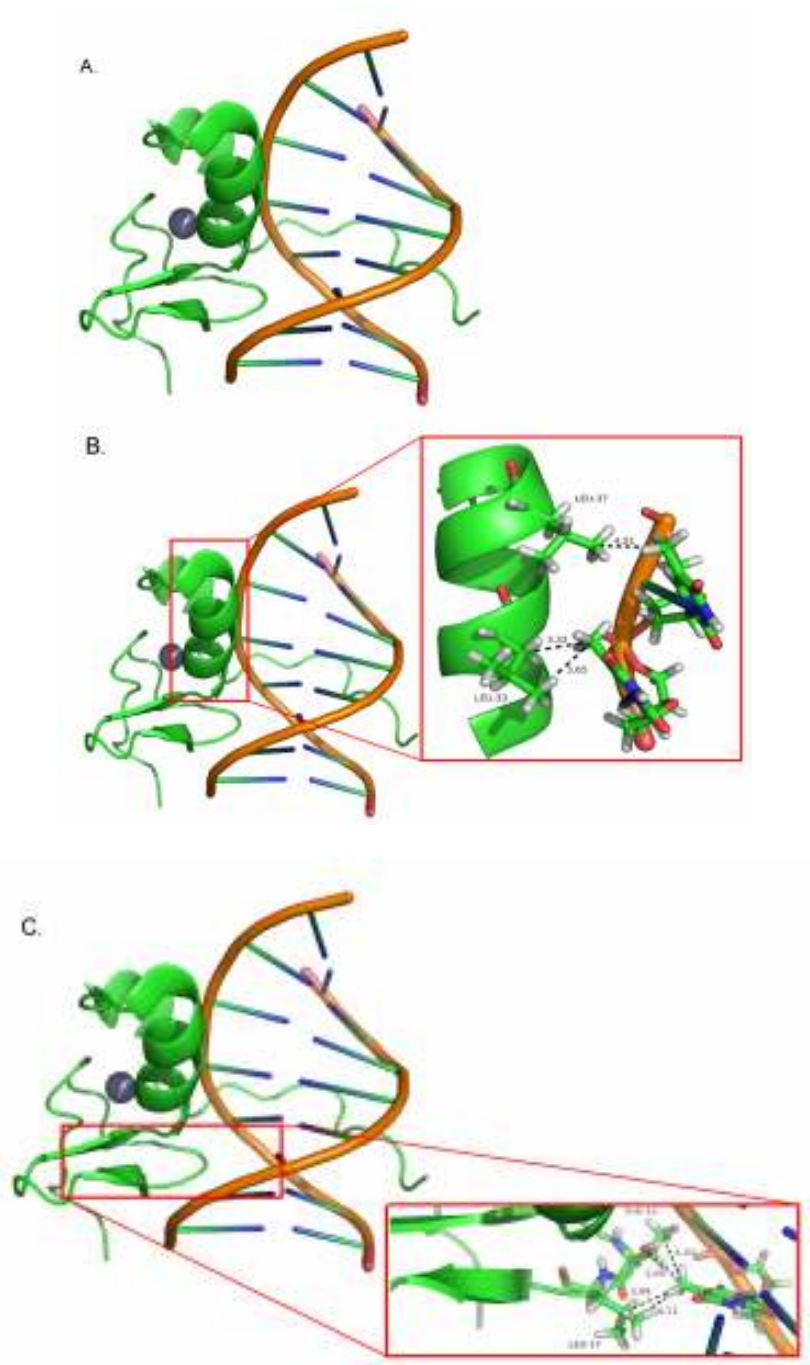

Figure 1.4. GATA-1 as an example of thymine recognition transcription factors. PyMOL generated figures of the zinc-finger protein GATA-1 (PDB Entry: 1GAT). A) A cartoon of the co-crystal structure of the GATA-1 DNA binding region interacting with DNA. The GATA-1 DNA element is (A/T)GATA(A/G). A GATA-1 α-helix and loop structure fit into the major groove of DNA where thymine methyl groups are always located. B) and C) The α-helix and loop structures shown contain hydrophobic residues which are close enough for van der Waals contacts allowing for the recognition of thymine methyls.

The α-helix and loop structure shown are present within the major groove of DNA with potential van der Waals contacts between DNA thymine methyls and Leu33 and Leu37 in the α-helix (Figure 1.4B) and Thr16 and Leu17 on the loop structure (Figure 1.4C). Due to these interactions, it could be postulated that uracil in place of thymine in these sequences would decrease GATA-1 binding.

Another intriguing aspect of GATA-1 as a model is that multiple GATA-1 binding sites exist within the same promoters that drive both the mouse α-globin gene cluster and the mouse high affinity receptor for IgE (FcεRI) β-chain. The mouse FcεRI β-chain promoter is activated through binding to four different GATA motifs (Figure 1.5A) (84).

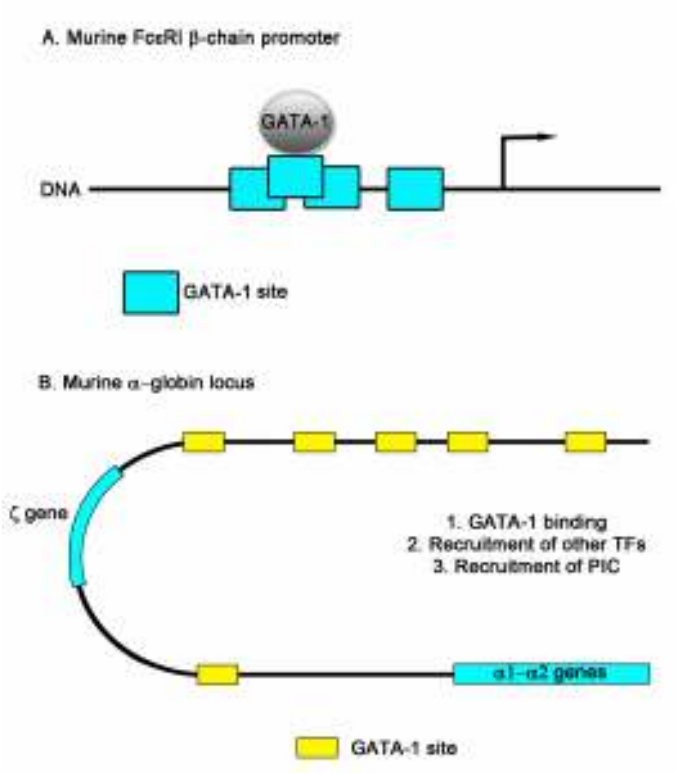

Figure 1.5.Multiple GATA-1 motifs are required for transcription. Two examples of GATA-1 driven genes are shown. A) In the mouse FcεRI β-chain promoter, recruitment of GATA-1 to four separate GATA-1 binding motifs is required for wild-type levels of FcεRI β-chain to be produced. B) The mouse α-globin locus requires the nucleation of multi-protein complexes by GATA-1. GATA-1 recruits multiple transcription factors which allow for the recruitment of the PIC for α-globin production.

At the mouse α-globin gene cluster, it has been reported that the binding of GATA-1 to multiple motifs recruits several different proteins including the pre-initiation complex and RNA polymerase II for transcription (85,86). Promoter sequence containing multiple GATA sites in several different genes have higher affinities for GATA-1 than promoter sequence containing only 1 GATA site (87). Uracil-misincorporation is driven by the dUTP/dTTP ratio and so incorporation of uracil is both dUTP concentration and DNA sequence dependent. Therefore, DNA regions that have higher numbers of thymines in the sequence are more likely to contain uracil in place of thymine than in regions where thymine is not prevalent within the sequence. If uracil is expected to cause changes in transcription through changes in transcription factor binding, then it would be a more likely event in regions where multiple thymine containing binding sites exist.

Another important hypothesis to consider is that a more general process controlling transcription is occurring. Approximately 24% of human genes contain TATA box elements (88). TATA-containing genes are generally non-housekeeping genes which are under tight control. Multiple transcription factors bind to the TATA box prior to recruitment of RNA polymerase II for transcription. More research is required to fully understand how uracil containing DNA may regulate transcription globally.

Genomic instability

As previously stated, much evidence supports uracil misincorporation associated with genomic instability. Following the criteria for uracil misincorporation into regions enriched in thymine, several regions of the genome become of interest, such as telomeric sequence that is enriched in long TTAGGG repeats (89).

Telomeres are essential for maintaining genome stability. Because of the linear nature of human chromosomes, the progressive loss of DNA sequence at chromosome ends occurs with

every replication. Once chromosomes lose a critical amount of sequence, cells enter senescence and programmed cell death (90,91). Shortening of telomeres occurs with age (92), with loss of telomeres resulting in susceptibility to chromosome fusion and/or DSBs which can result in chromosomal rearrangements (93). Embryonic stem cells, germ cells, and some cancer cells exhibit telomerase activity, whereas somatic cells exhibit low levels of telomerase (94) . Telomerase is essential for the maintenance of chromosome ends during development and has been proposed to be a mechanism of transformation in cancer cells. Telomerase has reverse transcriptase activity and uses its own RNA molecule (TERC) as a template for addition of repeats (94). Following the addition of long repeats of the aforementioned sequence, DNA polymerase α uses the ssDNA sequence made by telomerase as a template to synthesize the complementary strand and form dsDNA. Although DNA polymerase does not differentiate between dUTP and dTTP, it is still unknown whether telomerase makes a choice between the two nucleotides. If dUTP is not as good a substrate for telomerase, telomerase stalling may occur. Because telomerase is highly active during embryogenesis, this may have extreme deleterious effects on cell differentiation and growth. Furthermore, if dUTP is misincorporated into telomeric DNA, DSBs may be induced because the repeated TTAGGG sequence would result in strings of thymine on both strands of DNA. Repair occurring on both strands simultaneously would likely produce DSB. Both of these mechanisms could lead to increased telomere loss and potentially induce programmed cell death.

DSB either within telomeric regions or in other DNA regions have to be repaired either by homologous recombination, or non-homologous end joining (NHEJ). Homologous recombination requires a significant amount of homology while NHEJ is a process that requires no homologous sequence and can occur at any time during the cell cycle (95). When the formation of DSB at telomeric or other DNA regions occurs, the potential for aneuploidy increases due to bridge fusion break cycles (96). Aneuploidy is associated with folate

deficiency although the molecular mechanisms are still poorly understood (97-99). Aneuploidy is a hallmark of cancer cells and is also one of the major contributors to spontaneous abortion (100). An interesting caveat is that although aneuploidy occurs in populations of cells undergoing uncontrolled proliferation, most aneuploidies reduce fitness of organisms. Only after enough aneuploidy tolerating mutations have been acquired do these cells proliferate unchecked (101).

Conclusions

Uracil misincorporation may reflect a new form of transcriptional regulation (Figure 1.6). Uracil in DNA may lead to altered gene expression through some unknown mechanism (Figure 1.6A). Uracil in DNA may also lead to chromosomal aberrations through increasing genome instability.

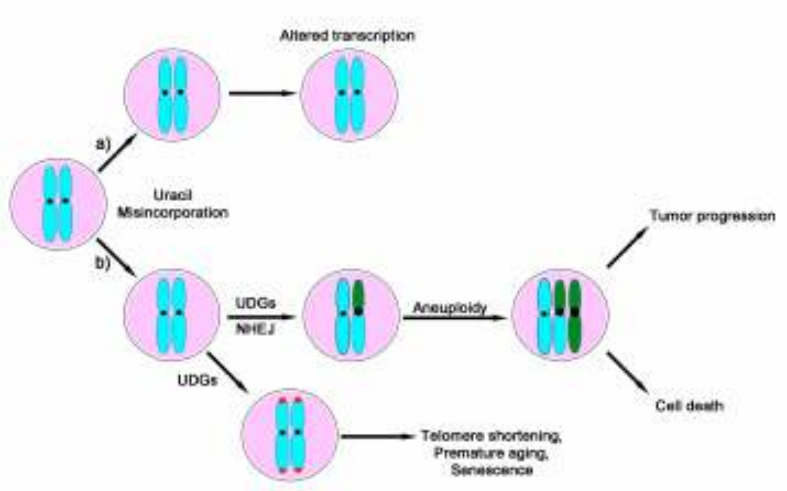

Figure 1.6. Uracil: Friend or Foe? Models showing potential consequences of uracil misincorporation. A) Upon uracil misincorporation in folate depleted individuals, as uracil is removed from DNA and repaired, high dUTP/dTTP ratios could favor the continued incorporation of uracil into DNA. If this occurs in regulatory sequence, changes in transcription may be observed. B) If uracil misincorporation occurs on adjacent strands of DNA upon uracil removal, double strand breaks (DSBs) can occur. Upon homologous recombination or NHEJ it can be hypothesized that translocations could occur potentially leading to other chromosomal aberrations such as aneuploidy. Aneuplody can lead to cell death or upon aneuploidy tolerating mutations, tumor progression can take place. Human telomeres contain long TTAGGG repeats. The high number of thymines in telomeric DNA in adjacent strands could lead to DSBs in telomeric DNA leading to telomere shortening, premature aging, and cell senescence.

This may occur in several ways (Figure 1.6B): decreased dTTP availability for telomerase causing stalling; increased dUTP incorporation into telomeres resulting in DSB; increases in telomere fusion, homologous recombination, or NHEJ in response to DSB leading to aneuploidy. Following aneuploidy tolerating mutations, tumor progression can occur. Telomeric shortening may lead to cell death. During embryogenesis telomere shortening could be catastrophic resulting in decreased cell proliferation. Telomeric fusion resulting from shortening could lead to aneuploidy. Aneuploidy is seen in many spontaneous abortions and could be partially due to maternal nutritional status. Future work will need to be done to understand if telomerase is affected by altered dTTP levels and if dU in telomeres is problematic.

We have seen that increased uracil in DNA and deficiencies in dTMP synthesis result in increased risk for neural tube defects and intestinal cancers. We have also seen that mice deficient in nuclear SHMT1 on folate deficient diets exhibit drastic increases in uracil levels within DNA and it is protective against cancer (Unpublished results, MacFarlane et al). Neural tube defects could be caused by aberrant uracil in DNA which leads to telomere shortening and/or an increase in aneuploidy leading to decreased cell proliferation. Aneuploidy does occur in NTDs (102,103). Neural tube closure could also be affected by global changes in gene expression during critically timed events due to uracil in DNA. Future work will need to determine if any of these hypotheses are valid.

Cancer could also be due to altered gene expression from uracil within DNA. Altered expression of oncogenes or tumor suppressors could lead to aberrant cell growth. For genomic instability to be causal in cancer progression, cells would have to overcome the programmed cell death induced by both telomere shortening and aneuploidy. If mutations arose that tolerated these genomic problems then those cells could progress. There may be a critical threshold of uracil in DNA which may be protective such that increasing uracil above that

point causes severe DNA damage and increased cell death. Because uracil misincorporation is not mutagenic, as is the case in cytosine deamination, the likelihood of tolerating mutations would be less.

Future work should identify which regions, if any, in DNA are enriched with uracil. Understanding how DNA acts as a sink for dUTP and what outcomes can arise will give insight into multiple biological processes. Another interesting question would be to determine if any RutR homologues exist within humans and to characterize it. The coordination of nucleotide pools and master regulatory processes could also lend insight to our understanding of these pathways. Finally, more work should be done to understand uracil misincorporation into mtDNA. It is intriguing that UNG1 is the only uracil dna glycosylase in mitochondria. Limiting levels of dUTP in mitochondria may therfore be more important. Little work has been done on UNG1, but what is known is that loss of SHMT2 results in increased uracil misincorporation into mtDNA. Future work should determine how folate deficiency affects uracil misincorporation in mtDNA and if critical levels of uracil in mtDNA cause metabolic changes or lead to apoptosis.

REFERENCES

1. Berger, S. H., Pittman, D. L., and Wyatt, M. D. (2008) *Biochem Pharmacol* **76**(6), 697-706
2. Kavli, B., Otterlei, M., Slupphaug, G., and Krokan, H. E. (2007) *DNA Repair (Amst)* **6**(4), 505-516
3. Mosbaugh, D. W., and Bennett, S. E. (1994) *Prog Nucleic Acid Res Mol Biol* **48**, 315-370
4. Andersen, S., Heine, T., Sneve, R., Konig, I., Krokan, H. E., Epe, B., and Nilsen, H. (2005) *Carcinogenesis* **26**(3), 547-555
5. Takao, M., Kanno, S., Kobayashi, K., Zhang, Q. M., Yonei, S., van der Horst, G. T., and Yasui, A. (2002) *J Biol Chem* **277**(44), 42205-42213
6. Taricani, L., Shanahan, F., Pierce, R. H., Guzi, T. J., and Parry, D. (2010) *Cell Cycle* **9**(24), 4876-4883
7. MacFarlane, A. J., Liu, X., Perry, C. A., Flodby, P., Allen, R. H., Stabler, S. P., and Stover, P. J. (2008) *J Biol Chem* **283**(38), 25846-25853
8. Fox, J. T., and Stover, P. J. (2008) *Vitam Horm* **79**, 1-44
9. Anderson, D. D., and Stover, P. J. (2009) *PLoS One* **4**(6), e5839
10. Anderson, D. D., Quintero, C. M., and Stover, P. J. (2011) *Proc Natl Acad Sci U S A*, published ahead of print
11. Olinski, R., Jurgowiak, M., and Zaremba, T. (2010) *Mutat Res* **705**(3), 239-245
12. Ladner, R. D. (2001) *Curr Protein Pept Sci* **2**(4), 361-370
13. McIntosh, E. M., Ager, D. D., Gadsden, M. H., and Haynes, R. H. (1992) *Proc Natl Acad Sci U S A* **89**(17), 8020-8024
14. el-Hajj, H. H., Zhang, H., and Weiss, B. (1988) *J Bacteriol* **170**(3), 1069-1075
15. Gadsden, M. H., McIntosh, E. M., Game, J. C., Wilson, P. J., and Haynes, R. H. (1993) *Embo J* **12**(11), 4425-4431

16. Tinkelenberg, B. A., Fazzone, W., Lynch, F. J., and Ladner, R. D. (2003) *Exp Cell Res* **287**(1), 39-46

17. Ladner, R. D., and Caradonna, S. J. (1997) *J Biol Chem* **272**(30), 19072-19080

18. Ladner, R. D., McNulty, D. E., Carr, S. A., Roberts, G. D., and Caradonna, S. J. (1996) *J Biol Chem* **271**(13), 7745-7751

19. Ladner, R. D., Lynch, F. J., Groshen, S., Xiong, Y. P., Sherrod, A., Caradonna, S. J., Stoehlmacher, J., and Lenz, H. J. (2000) *Cancer Res* **60**(13), 3493-3503

20. Woeller, C. F., Anderson, D. D., Szebenyi, D. M., and Stover, P. J. (2007) *J Biol Chem* **282**(24), 17623-17631

21. Oppenheim, E. W., Adelman, C., Liu, X., and Stover, P. J. (2001) *J Biol Chem* **276**(23), 19855-19861

22. Bogenhagen, D. F., Rousseau, D., and Burke, S. (2008) *J Biol Chem* **283**(6), 3665-3675

23. Samsonoff, W. A., Reston, J., McKee, M., O'Connor, B., Galivan, J., Maley, G., and Maley, F. (1997) *J Biol Chem* **272**(20), 13281-13285

24. Da Cruz, S., Xenarios, I., Langridge, J., Vilbois, F., Parone, P. A., and Martinou, J. C. (2003) *J Biol Chem* **278**(42), 41566-41571

25. Cybulski, R. L., and Fisher, R. R. (1976) *Biochemistry* **15**(15), 3183-3187

26. Neuburger, M., Rebeille, F., Jourdain, A., Nakamura, S., and Douce, R. (1996) *J Biol Chem* **271**(16), 9466-9472

27. Blount, B. C., Mack, M. M., Wehr, C. M., MacGregor, J. T., Hiatt, R. A., Wang, G., Wickramasinghe, S. N., Everson, R. B., and Ames, B. N. (1997) *Proc Natl Acad Sci U S A* **94**(7), 3290-3295

28. Duthie, S. J., and Hawdon, A. (1998) *Faseb J* **12**(14), 1491-1497

29. Duthie, S. J., Grant, G., and Narayanan, S. (2000) *Br J Cancer* **83**(11), 1532-1537

30. Melnyk, S., Pogribna, M., Miller, B. J., Basnakian, A. G., Pogribny, I. P., and James, S. J. (1999) *Cancer Lett* **146**(1), 35-44

31. Macfarlane, A. J., Perry, C. A., McEntee, M. F., Lin, D. M., and Stover, P. J. (2011) *Cancer Res* **71**(6), 2098-2107

32. Olsen, L. C., Aasland, R., Wittwer, C. U., Krokan, H. E., and Helland, D. E. (1989) *Embo J* **8**(10), 3121-3125

33. Kavli, B., Sundheim, O., Akbari, M., Otterlei, M., Nilsen, H., Skorpen, F., Aas, P. A., Hagen, L., Krokan, H. E., and Slupphaug, G. (2002) *J Biol Chem* **277**(42), 39926-39936

34. Akbari, M., Otterlei, M., Pena-Diaz, J., Aas, P. A., Kavli, B., Liabakk, N. B., Hagen, L., Imai, K., Durandy, A., Slupphaug, G., and Krokan, H. E. (2004) *Nucleic Acids Res* **32**(18), 5486-5498

35. Nilsen, H., Rosewell, I., Robins, P., Skjelbred, C. F., Andersen, S., Slupphaug, G., Daly, G., Krokan, H. E., Lindahl, T., and Barnes, D. E. (2000) *Molecular cell* **5**(6), 1059-1065

36. Nilsen, H., Otterlei, M., Haug, T., Solum, K., Nagelhus, T. A., Skorpen, F., and Krokan, H. E. (1997) *Nucleic Acids Res* **25**(4), 750-755

37. Shen, J., Khan, N., Lewis, L. D., Armand, R., Grinberg, O., Demidenko, E., and Swartz, H. (2003) *Biophys J* **84**(2 Pt 1), 1291-1298

38. Kamp, D. W., Shacter, E., and Weitzman, S. A. (2011) *Oncology (Williston Park)* **25**(5), 400-410, 413

39. Schon, E. A., and Przedborski, S. (2011) *Neuron* **70**(6), 1033-1053

40. van den Ouweland, J. M., Lemkes, H. H., Ruitenbeek, W., Sandkuijl, L. A., de Vijlder, M. F., Struyvenberg, P. A., van de Kamp, J. J., and Maassen, J. A. (1992) *Nat Genet* **1**(5), 368-371

41. Akbari, M., Visnes, T., Krokan, H. E., and Otterlei, M. (2008) *DNA Repair (Amst)* **7**(4), 605-616

42. Stover, P. J., Chen, L. H., Suh, J. R., Stover, D. M., Keyomarsi, K., and Shane, B. (1997) *J Biol Chem* **272**(3), 1842-1848

43. Haug, T., Skorpen, F., Aas, P. A., Malm, V., Skjelbred, C., and Krokan, H. E. (1998) *Nucleic Acids Res* **26**(6), 1449-1457

44. Nilsen, H., Steinsbekk, K. S., Otterlei, M., Slupphaug, G., Aas, P. A., and Krokan, H. E. (2000) *Nucleic Acids Res* **28**(12), 2277-2285

45. Vinson, R. K., and Hales, B. F. (2002) *Biochemical pharmacology* **64**(4), 711-721

46. Endres, M., Biniszkiewicz, D., Sobol, R. W., Harms, C., Ahmadi, M., Lipski, A., Katchanov, J., Mergenthaler, P., Dirnagl, U., Wilson, S. H., Meisel, A., and Jaenisch, R. (2004) *J Clin Invest* **113**(12), 1711-1721

47. Fischer, J. A., Muller-Weeks, S., and Caradonna, S. (2004) *DNA Repair (Amst)* **3**(5), 505-513

48. Otterlei, M., Warbrick, E., Nagelhus, T. A., Haug, T., Slupphaug, G., Akbari, M., Aas, P. A., Steinsbekk, K., Bakke, O., and Krokan, H. E. (1999) *Embo J* **18**(13), 3834-3844

49. Muller-Weeks, S., Mastran, B., and Caradonna, S. (1998) *J Biol Chem* **273**(34), 21909-21917

50. Hagen, L., Kavli, B., Sousa, M. M., Torseth, K., Liabakk, N. B., Sundheim, O., Pena-Diaz, J., Otterlei, M., Horning, O., Jensen, O. N., Krokan, H. E., and Slupphaug, G. (2008) *Embo J* **27**(1), 51-61

51. Lu, X., Bocangel, D., Nannenga, B., Yamaguchi, H., Appella, E., and Donehower, L. A. (2004) *Molecular cell* **15**(4), 621-634

52. Hagen, L., Pena-Diaz, J., Kavli, B., Otterlei, M., Slupphaug, G., and Krokan, H. E. (2006) *Exp Cell Res* **312**(14), 2666-2672

53. Nilsen, H., Stamp, G., Andersen, S., Hrivnak, G., Krokan, H. E., Lindahl, T., and Barnes, D. E. (2003) *Oncogene* **22**(35), 5381-5386

54. Andersen, S., Ericsson, M., Dai, H. Y., Pena-Diaz, J., Slupphaug, G., Nilsen, H., Aarset, H., and Krokan, H. E. (2005) *DNA Repair (Amst)* **4**(12), 1432-1441

55. Studebaker, A. W., Ariza, M. E., and Williams, M. V. (2005) *Biochem Biophys Res Commun* **334**(2), 509-515

56. Pulukuri, S. M., Knost, J. A., Estes, N., and Rao, J. S. (2009) *Molecular cancer research : MCR* **7**(8), 1285-1293

57. Kruman, II, Schwartz, E., Kruman, Y., Cutler, R. G., Zhu, X., Greig, N. H., and Mattson, M. P. (2004) *J Biol Chem* **279**(42), 43952-43960

58. Zeitlin, S. G., Patel, S., Kavli, B., and Slupphaug, G. (2005) *DNA Repair (Amst)* **4**(7), 760-772

59. Zeitlin, S. G., Chapados, B. R., Baker, N. M., Tai, C., Slupphaug, G., and Wang, J. Y. (2011) *PLoS One* **6**(3), e17151

60. Zeitlin, S. G. (2010) *Epigenetics : official journal of the DNA Methylation Society* **5**(1), 34-40

61. Dianov, G. L., Timchenko, T. V., Sinitsina, O. I., Kuzminov, A. V., Medvedev, O. A., and Salganik, R. I. (1991) *Molecular & general genetics : MGG* **225**(3), 448-452

62. Mashiyama, S. T., Courtemanche, C., Elson-Schwab, I., Crott, J., Lee, B. L., Ong, C. N., Fenech, M., and Ames, B. N. (2004) *Anal Biochem* **330**(1), 58-69

63. Duthie, S. J., Narayanan, S., Blum, S., Pirie, L., and Brand, G. M. (2000) *Nutrition and cancer* **37**(2), 245-251

64. Czeizel, A. E., and Dudas, I. (1992) *The New England journal of medicine* **327**(26), 1832-1835

65. (1991) *Lancet* **338**(8760), 131-137

66. Beaudin, A. E., Abarinov, E. V., Noden, D. M., Perry, C. A., Chu, S., Stabler, S. P., Allen, R. H., and Stover, P. J. (2011) *Am J Clin Nutr* **93**(4), 789-798

67. Shimada, T., Hirao, K., Kori, A., Yamamoto, K., and Ishihama, A. (2007) *Molecular microbiology* **66**(3), 744-757

68. Rohs, R., Jin, X., West, S. M., Joshi, R., Honig, B., and Mann, R. S. (2010) *Annu Rev Biochem* **79**, 233-269

69. Berkner, K. L., and Folk, W. R. (1979) *J Biol Chem* **254**(7), 2551-2560

70. Fliess, A., Wolfes, H., Rosenthal, A., Schwellnus, K., Blocker, H., Frank, R., and Pingoud, A. (1986) *Nucleic Acids Res* **14**(8), 3463-3474

71. Yolov, A. A., Vinogradova, M. N., Gromova, E. S., Rosenthal, A., Cech, D., Veiko, V. P., Metelev, V. G., Kosykh, V. G., Buryanov, Y. I., Bayev, A. A., and et al. (1985) *Nucleic Acids Res* **13**(24), 8983-8998

72. Goeddel, D. V., Yansura, D. G., and Caruthers, M. H. (1978) *Proc Natl Acad Sci U S A* **75**(8), 3578-3582

73. Dubendorff, J. W., deHaseth, P. L., Rosendahl, M. S., and Caruthers, M. H. (1987) *J Biol Chem* **262**(2), 892-898

74. Curran, T., and Franza, B. R., Jr. (1988) *Cell* **55**(3), 395-397

75. Sellers, J. W., Vincent, A. C., and Struhl, K. (1990) *Mol Cell Biol* **10**(10), 5077-5086

76. Pu, W. T., and Struhl, K. (1992) *Nucleic Acids Res* **20**(4), 771-775

77. Deutsch, W. A., and Spiering, A. L. (1982) *J Biol Chem* **257**(7), 3366-3368

78. Bekesi, A., Pukancsik, M., Muha, V., Zagyva, I., Leveles, I., Hunyadi-Gulyas, E., Klement, E., Medzihradszky, K. F., Kele, Z., Erdei, A., Felfoldi, F., Konya, E., and Vertessy, B. G. (2007) *Biochem Biophys Res Commun* **355**(3), 643-648

79. Bekesi, A., Zagyva, I., Hunyadi-Gulyas, E., Pongracz, V., Kovari, J., Nagy, A. O., Erdei, A., Medzihradszky, K. F., and Vertessy, B. G. (2004) *J Biol Chem* **279**(21), 22362-22370

80. Aguilera, A. (2002) *Embo J* **21**(3), 195-201

81. Kim, N., and Jinks-Robertson, S. (2009) *Nature* **459**(7250), 1150-1153

82. Viger, R. S., Guittot, S. M., Anttonen, M., Wilson, D. B., and Heikinheimo, M. (2008) *Mol Endocrinol* **22**(4), 781-798

83. Omichinski, J. G., Clore, G. M., Robien, M., Sakaguchi, K., Appella, E., and Gronenborn, A. M. (1992) *Biochemistry* **31**(16), 3907-3917

84. Maeda, K., Nishiyama, C., Tokura, T., Akizawa, Y., Nishiyama, M., Ogawa, H., Okumura, K., and Ra, C. (2003) *J Immunol* **170**(1), 334-340

85. Anguita, E., Hughes, J., Heyworth, C., Blobel, G. A., Wood, W. G., and Higgs, D. R. (2004) *Embo J* **23**(14), 2841-2852

86. Vernimmen, D., De Gobbi, M., Sloane-Stanley, J. A., Wood, W. G., and Higgs, D. R. (2007) *Embo J* **26**(8), 2041-2051

87. Trainor, C. D., Omichinski, J. G., Vandergon, T. L., Gronenborn, A. M., Clore, G. M., and Felsenfeld, G. (1996) *Mol Cell Biol* **16**(5), 2238-2247

88. Yang, C., Bolotin, E., Jiang, T., Sladek, F. M., and Martinez, E. (2007) *Gene* **389**(1), 52-65

89. Zhang, P., Dilley, C., and Mattson, M. P. (2007) *Neuroscience* **145**(4), 1439-1448

90. Harley, C. B., Futcher, A. B., and Greider, C. W. (1990) *Nature* **345**(6274), 458-460

91. Lundblad, V., and Szostak, J. W. (1989) *Cell* **57**(4), 633-643

92. Lindsey, J., McGill, N. I., Lindsey, L. A., Green, D. K., and Cooke, H. J. (1991) *Mutat Res* **256**(1), 45-48

93. Latre, L., Tusell, L., Martin, M., Miro, R., Egozcue, J., Blasco, M. A., and Genesca, A. (2003) *Exp Cell Res* **287**(2), 282-288

94. Martinez, P., and Blasco, M. A. (2011) *Nature reviews. Cancer* **11**(3), 161-176

95. Lieber, M. R., Gu, J., Lu, H., Shimazaki, N., and Tsai, A. G. (2010) *Sub-cellular biochemistry* **50**, 279-296

96. Martinez, A. C., and van Wely, K. H. (2010) *Cell Cycle* **9**(12), 2275-2280

97. Ni, J., Lu, L., Fenech, M., and Wang, X. (2010) *Environmental and molecular mutagenesis* **51**(1), 15-22

98. Coppede, F. (2009) *Mutat Res* **682**(1), 54-70

99. Beetstra, S., Thomas, P., Salisbury, C., Turner, J., and Fenech, M. (2005) *Mutat Res* **578**(1-2), 317-326

100. Treff, N. R., Su, J., Taylor, D., and Scott, R. T., Jr. (2011) *PLoS Genet* **7**(6), e1002161

101. Williams, B. R., Prabhu, V. R., Hunter, K. E., Glazier, C. M., Whittaker, C. A., Housman, D. E., and Amon, A. (2008) *Science* **322**(5902), 703-709

102. Babcook, C. J., Ball, R. H., and Feldkamp, M. L. (2000) *Journal of ultrasound in medicine : official journal of the American Institute of Ultrasound in Medicine* **19**(9), 619-623; quiz 625-616

103. Drugan, A., Johnson, M. P., Dvorin, E., Moody, J., Krivchenia, E. L., Schwartz, D., and Evans, M. I. (1989) *Fetal therapy* **4**(2-3), 88-92

CHAPTER 2

SHMT1 and SHMT2 Are Functionally Redundant in Nuclear *De novo* Thymidylate Biosynthesis

Introduction

Tetrahydrofolate (THF) is a metabolic cofactor that carries and activates single carbons for the synthesis of nucleotides and methionine (1). Folate-mediated one-carbon metabolism is compartmentalized in the mitochondria and cytoplasm of eukaryotic cells (Figure 1).

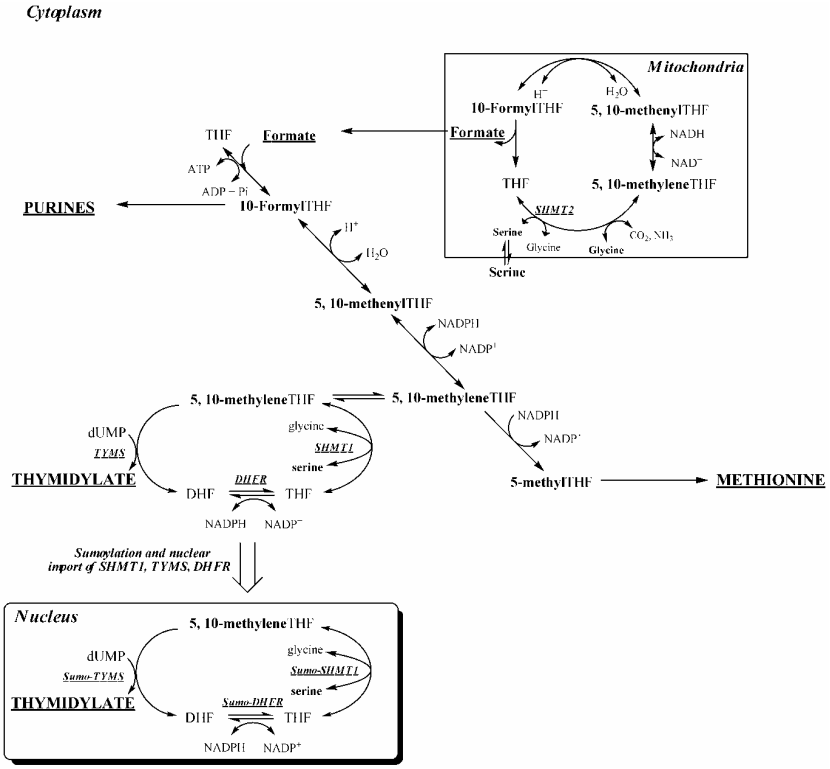

Figure 2.1. Compartmentation of folate-mediated one-carbon metabolism in the cytoplasm, mitochondria and nucleus. One-carbon metabolism in the cytoplasm is required for the *de novo* synthesis of purines and thymidylate, and for the remethylation of homocysteine to methionine. One-carbon metabolism in mitochondria generates one-carbon units for cytoplasmic one-carbon metabolism by generating formate from serine and glycine. One-carbon metabolism in the nucleus synthesizes dTMP from dUMP and serine. SHMT2, mitochondrial serine hydroxymethyltransferase; SHMT1, cytoplasmic serine hydroxymethyltransferase; TYMS, thymidylate synthase; DHFR, dihydrofolate reductase; THF, tetrahydrofolate.

In the cytoplasm, this metabolic network is required for the biosynthesis of purines, thymidylate, and the remethylation of homocysteine to form methionine. Serine is a major source of one-carbon units for this network through its reversible and tetrahydrofolate-dependent conversion to glycine and methyleneTHF catalyzed by serine hydroxymethyltransferase (SHMT). There are cytoplasmic and mitochondrial SHMT isozymes. *SHMT1* encodes the cytoplasmic isozyme (SHMT1) and *SHMT2* encodes the mitochondrial isozyme (SHMT2) (2-4). Mitochondrial one-carbon metabolism generates one-carbons from serine through the activity of SHMT2, and the one-carbon is oxidized and exported to the cytoplasm as formate, supporting cytoplasmic one-carbon metabolism (5). The SHMT1 enzyme generates methyleneTHF for thymidylate and methionine biosynthesis, but isotope tracer studies indicate that SHMT1 preferentially partitions methyleneTHF to thymidylate biosynthesis (6). The *de novo* thymidylate biosynthesis pathway requires three enzymes: thymidylate synthase (TYMS), dihydrofolate reductase (DHFR), and SHMT1. MethyleneTHF generated by SHMT is the one-carbon donor for the TYMS catalyzed conversion of dUMP to dTMP generating dihydrofolate (DHF). DHFR catalyzes the NADPH-dependent reduction of DHF to regenerate THF for subsequent cycles of *de novo* thymidylate synthesis. Recently, the enzymes that constitute the thymidylate synthesis cycle were shown to undergo post-translational modification by the small ubiquitin-like modifier (SUMO) and nuclear translocation during S and G2/M phases (7,8). Although the synthesis of thymidylate in the nucleus has never been demonstrated, others have found folate cofactors present in liver nuclei (9), and multi-enzyme complexes containing ribonucleotide reductase and thymidylate synthase have been isolated from nuclear extracts (10). In this study, intact nuclei are shown to catalyze the formation of dTMP from dUMP, which accounts for the results of stable isotope studies that indicate SHMT preferentially partitions methyleneTHF to thymidylate

biosynthesis. Furthermore, both *Shmt1* and *Shmt2* are shown to contribute to nuclear *de novo* thymidylate biosynthesis.

Results

Shmt1 and *Shmt2* contribute to nuclear dTMP biosynthesis. The ability of purified nuclei to catalyze the formation of tritiated dTMP from unlabeled dUMP, NADPH and [2,3-^{3}H]-L-serine *in vitro* was investigated (Figure 2.2).

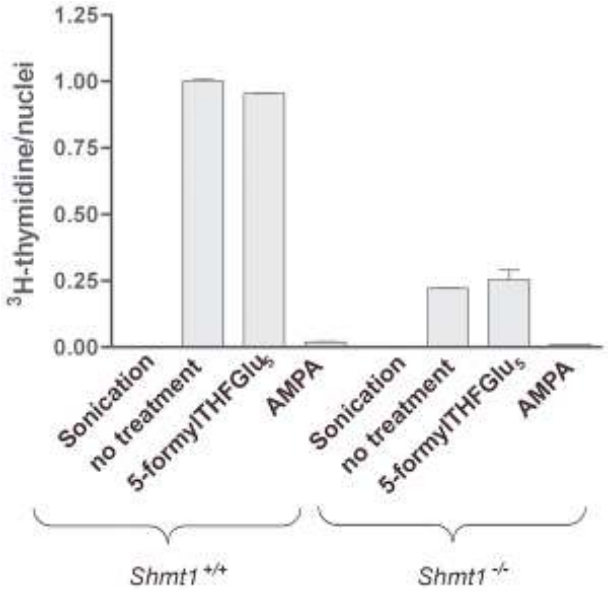

Figure 2.2. Thymidylate biosynthesis occurs in purified nuclei. Liver nuclei were isolated from *SHMT1*$^{+/+}$ and *SHMT1*$^{-/-}$ mice and capacity to convert dUMP and [2,3-^{3}H]-L-serine to [^{3}H]dTMP was determined in reactions that contained: 1) sonicated nuclei; 2) intact nuclei; 3) intact nuclei with 200 μM 5-CHOTHFGlu$_5$; and 4) intact nuclei with 100 mM aminomethyl phosphonate (AMPA). *De novo* thymidylate biosynthesis activities were normalized to activity generated from *SHMT1*$^{+/+}$ intact nuclei which was given an arbitrary value of 1.0. Reactions containing sonicated nuclei contained no activity. All reactions were performed in duplicate and the experiment repeated twice. Variation is expressed as the standard deviation.

Intact nuclei isolated from the livers of wild type mice were capable of generating tritiated dTMP, demonstrating that folate-dependent nuclear dTMP synthesis occurs in liver. The addition of the SHMT inhibitor and amino acid analog, aminomethylphosphonate, to the reaction mixture inhibited dTMP synthesis by greater than 95%, demonstrating the essentiality of the SHMT reaction in generating folate-activated one-carbons from serine for dTMP

synthesis in nuclei. 5-formyltetrahydrofolate pentaglutamate, a natural inhibitor of SHMT (11), did not inhibit nuclear dTMP biosynthesis but may not have been able to traverse the nuclear membrane. Disruption of nuclei by sonication eliminated all dTMP synthesis activity, indicating that cytoplasmic contamination was not responsible for the observed dTMP synthesis activity in nuclei, and suggesting that maintenance of nuclear architecture is essential for nuclear dTMP synthesis. Surprisingly, *intact* nuclei isolated from the liver of *Shmt1*$^{-/-}$ mice were capable of generating tritiated dTMP at approximately 25% of the level observed from nuclei isolated from *Shmt1*$^{+/+}$ mice (Figure 2.2). Aminomethylphosphonate inhibited dTMP synthesis in nuclei generated from *Shmt1*$^{-/-}$ mice, indicating that a second SHMT activity is present in nuclei which is not derived from *Shmt1*. PCR was used to confirm the genotype of the purified nuclei and immunoblotting was performed to verify that the nuclei lacked Shmt1 (Figure 2.3A).

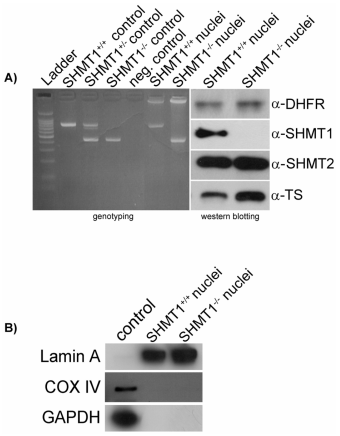

Figure 2.3. Identification of SHMT2 in purified nuclei. Panel A) PCR was used to confirm the genotype of nuclei isolated from *SHMT1*$^{+/+}$ and *SHMT1*$^{-/-}$ mice. *SHMT1*$^{-/-}$ mice were generated through deletion of exon 7 which encodes the PLP binding site. *SHMT1*$^{+/+}$ mice exhibit a 740-bp PCR product whereas the *SHMT1*$^{-/-}$ mice exhibit a 460-bp PCR product. Western blotting confirmed the presence of TYMS and DHFR in nuclei of both genotypes. SHMT1 was present in purified liver nuclei from *SHMT1*$^{+/+}$ mice, but absent in liver nuclei from *SHMT1*$^{-/-}$ mice. SHMT2 was present in nuclei from both genotypes. Panel B) Western blots confirm the purity of the isolated liver nuclei. The control lane represents purified cytosol from NIH/3T3 cells for both the Lamin A (nuclear marker) and GAPDH (cytoplasmic marker). The control for the COX IV immunoblot represents a purified mitochondrial fraction from NIH/3T3 cells. The absence of GAPDH and COX IV in nuclear extracts indicated that no cytosolic or mitochondrial contamination was present in the nuclear dTMP assays.

Furthermore, the nuclei were shown to be free of cytosolic and mitochondrial contamination (Figure 2.3B). DHFR and TYMS protein were observed in purified nuclei isolated from the livers of wild type and *Shmt1*$^{-/-}$ mice, and surprisingly, SHMT2 protein was also observed in nuclei isolated from the livers of wild type and *Shmt1*$^{-/-}$ mice (Figure 2.3A).

Previous evidence suggests that *Shmt2* contains two translation initiation sites. Expression of a *SHMT2* gene fragment lacking exon 1 in *glyA* CHO cells, which lack SHMT2 activity, rescued the glycine auxotrophy (4). Exon 1 encodes the first translation initiation start site and most of the peptide sequence required for efficient import into mitochondria. *Shmt2* contains a potential second translation initiation codon within exon 2, and translation initiation from this site generated a protein capable of import into mitochondria, albeit at lower efficiency (Figure 2.4) (4).

Figure 2.4. The mouse *Shmt2* encodes two transcripts and contains two translation initiation sites.The SHMT2 transcript is denoted by the color red. The first nucleotide of the translation initiation site contained in exon 1 is numbered as +1. The first translation initiation site in exon 1, which encodes for the mitochondrial leader sequence, is boxed in blue. The mitochondrial leader sequence is cleaved co-translationally in the mitochondria denoted by the scissors (2). The second translation initiation site, present in exon 2, is boxed in blue. A transcription start site in intron 1 deduced from a mouse liver EST (AA793217) is denoted by the arrow and starts at −166 from the second ORF.

To determine if two transcripts were generated from *Shmt2*, one containing exon 1 and one lacking exon 1, the mouse EST database was probed for *Shmt2* cDNA sequences that contained nucleotide sequence from the *Shmt2* intron 1/exon 2 boundary. An EST (AA793217) that lacked exon 1 but contained 166 nucleotides from the 3′ end of intron 1 at its 5′ end was identified. Similarly, the human EST database was probed and two *SHMT2* transcripts containing 131 nucleotides from the 3′ end of intron 1 were identified (DB184899 and DA597551). These data indicate that *SHMT2* encodes two transcripts and an alternative promoter within intron 1.

Subcellular localization of SHMT2 gene products

The cellular localization of the two SHMT2 isoforms was determined by expression of SHMT-yellow fluorescent protein (YFP) and red fluorescent protein (RFP) fusion proteins. Cyan fluorescent protein fused to a mitochondrial leader sequence (CFP-mito) at its amino terminus and Draq5 DNA binding dye were used as mitochondrial and nuclear markers respectively. Confocal microscopy revealed that the SHMT protein expressed from the *SHMT2* transcript containing exon 1 (referred to as SHMT2-YFP) and CFP-mito protein co-localized to mitochondria. However, SHMT protein expressed from the *SHMT2* transcript lacking exon 1 (referred to as SHMT2α-RFP) localized predominantly to the cytoplasm and nucleus (Figure 2.5A). The nuclear localization of the SHMT2α-RFP fusion protein exhibited similar cell cycle dependence as observed for SHMT1 (8). The SHMT2α-RFP fusion protein localized exclusively to the cytoplasm in G1 phase whereas in S and G2/M phases it localized to both the cytoplasm and nucleus (Figure 2.5B).

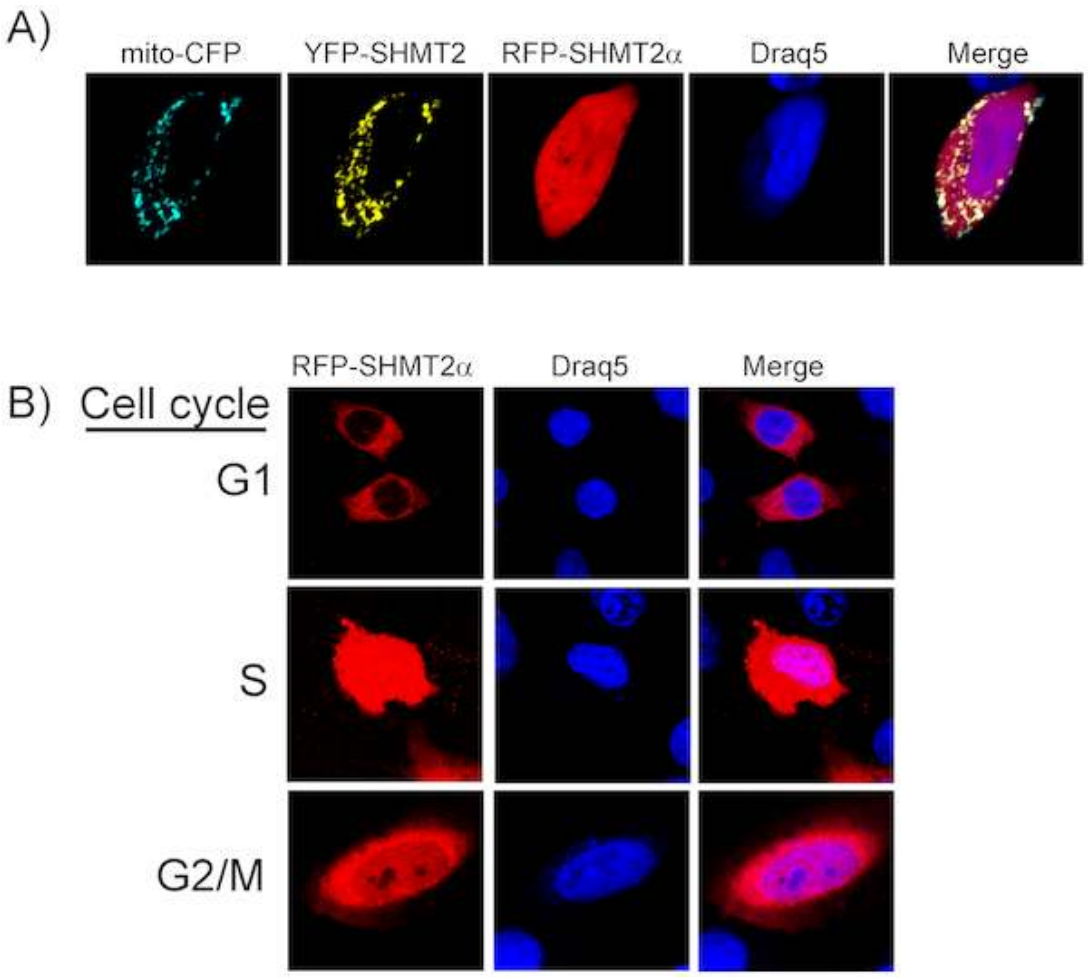

Figure 2.5. SHMT2α localizes to the cytoplasm and nucleus. HeLa cells were transfected with cDNAs encoding SHMT2-YFP, mito-CFP, and SHMT2α-RFP. A) The SHMT2-YFP fusion protein expressed in HeLa cells localizes to mitochondria. The mitochondrial marker, mito-CFP has a similar localization pattern as that of SHMT2. The SHMT2α-RFP fusion protein expressed in HeLa cells localizes to both the cytoplasm and the nucleus. B) SHMT2α-RFP localizes to the nucleus in a cell cycle dependent manner during S-phase and G2/M, whereas it is absent from the nucleus in G1 phase.

Both SHMT2 and SHMT2α rescue the glycine auxotrophy in GlyA Chinese Hamster Ovary cells

Previously, transfection of a human *SHMT2* gene fragment that lacked exon 1 into CHO *GlyA* cells, which lack SHMT2 activity in mitochondria and exhibit a glycine auxotrophy, resulted in very low levels of SHMT2 activity in mitochondria which was sufficient to rescue the glycine auxotrophy (4). In this study, the ability of SHMT2α to rescue the glycine auxotrophy

in *GlyA* cells was determined. Twelve to fifteen stable transfectants were selected for G418 resistance from *GlyA* cells electroporated with either an empty TagRFP-N plasmid, a plasmid expressing the cDNA encoding SHMT2, or a plasmid expressing the cDNA encoding SHMT2α. All plasmids were driven by the immediate early promoter of cytomegalovirus. Stable transfectants containing the RFP empty vector did not rescue glycine auxotrophy and no revertants were observed in the 12 colonies screened. However, the glycine auxotrophy was rescued in all selected cell lines expressing either the SHMT2-RFP or the SHMT2α-RFP fusion protein (Figure 2.6). This data confirms that SHMT2α localizes to mitochondria and can rescue mitochondrial one-carbon metabolism.

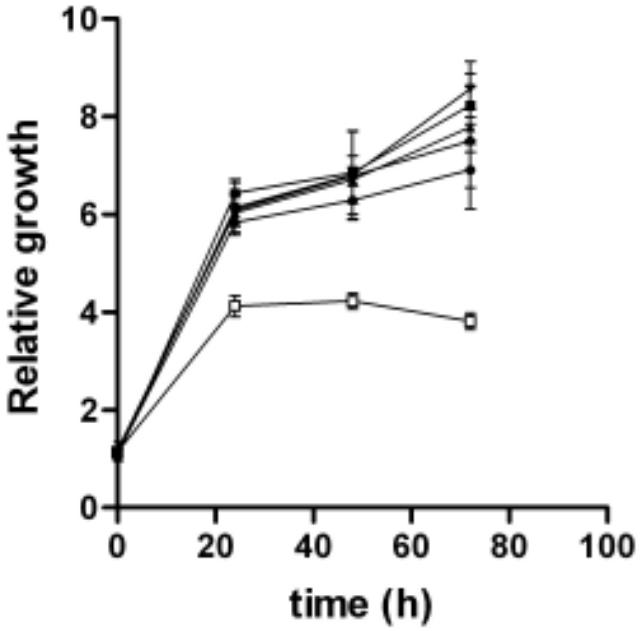

Figure 2.6. SHMT2 and SHMT2α rescue the glycine auxotrophy in CHO *glyA* cells.CHO *glyA* cells were transfected with cDNAs encoding human SHMT2-RFP, SHMT2α−RFP, and a RFP-empty vector control. Stable cells lines were selected for G418 resistance in the presence of 200 mM glycine. For growth assays, cells were cultured with and without glycine and MTT assays were used to quantify growth. Twelve independent lines were assayed per transfection and experiments were done in triplicate. All values are normalized to RFP-empty vector transfectants. There was no significant difference in growth among the cells transfected with SHMT2 and SHMT2α with or without glycine. RFP-empty vector transfectants with and without glycine are shown as a circle and open box respectively. SHMT2-RFP transfectants with and without glycine are shown as a closed box and triangle respectively. SHMT2α−RFP transfectants with and without glycine are shown as an inverted triangle and diamond respectively.

Expression of SHMT2 and SHMT2α in mouse tissues

The relative levels of each SHMT2 isoform was determined in mouse liver and kidney by western blot analyses (Figure 2.7).

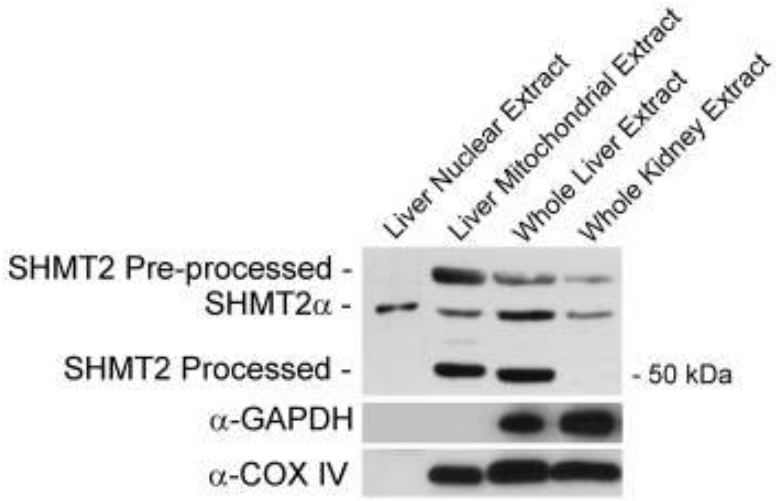

Figure 2.7. SHMT2 and SHMT2α are present in mouse tissues. Immunoblots using a sheep-anti-human SHMT2 antibody revealed the presence of three immunoreactive bands. Protein masses were determined by the migration distance and relative mobility of standards. Purified liver nuclei, whole liver and whole kidney extracts contained an immunoreactive band at ~53 kDa, the predicted mass of SHMT2α. Purified liver mitochondria, whole liver and whole kidney extracts contained a band at ~56 kDa, the predicted mass of the SHMT2 pre-processed protein. Purified liver mitochondria and whole liver, but not whole kidney extracts contained a band at ~50 kDa, the predicted mass of the SHMT2 processed protein. The nuclear fraction was free of cytosolic and mitochondrial contamination as shown by the GAPDH and COX IV immunoblots.

A single immunoreactive band that migrated at 53 kD was present in nuclear extracts isolated from mouse liver when probed with an antibody against SHMT2. This molecular mass corresponds to the predicted size of the SHMT2α protein expressed from the *Shmt2* transcript lacking exon 1. Purified liver mitochondrial extracts exhibited three immunoreactive bands. The upper band, which migrated with a molecular mass of approximately 56 kDa, is consistent with the predicted mass of the full length SHMT2 pre-processed protein. A lower band, which migrated with a molecular mass of approximately 50 kDa, corresponds to the processed SHMT2 protein lacking its leader sequence as present in mitochondria. These 3 bands were

also observed in whole liver extract, and the blot indicates that the predominant SHMT2 isoform is the processed mitochondrial form. However, a substantial amount of the SHMT2α protein was also present in liver. In kidney, only the pre-processed SHMT2 and SHMT2α form of the enzyme were observed.

A single nucleotide polymorphism in SHMT1 impairs nuclear localization

Previously, we demonstrated that a common polymorphism in *SHMT1*, L474F impairs SUMO modification of the SHMT1 protein (8). To determine if this polymorphism impairs nuclear localization and to explore the potential for the redundancy between SHMT1 and SHMT2α, MEFS derived from *Shmt1*$^{-/-}$ mice were electroporated with plasmids that express the wild-type human SHMT1-YFP fusion protein, the human L474F SHMT1-YFP fusion protein or a mutated K38R/K39R SHMT1-YFP fusion protein, which lacks a SUMO-modification site (8). MEFs isolated from *Shmt1*$^{-/-}$ mice were used to eliminate the possibility that endogenous mouse SHMT1 protein could oligomerize with the human SHMT1 fusion proteins thereby allowing nuclear import. The SHMT1-YFP fusion protein localized to both the cytoplasm and nucleus in S-phase, whereas the K38R/K39R SHMT1-YFP fusion protein localized exclusively to the cytoplasm in S-phase (Figure 2.8).

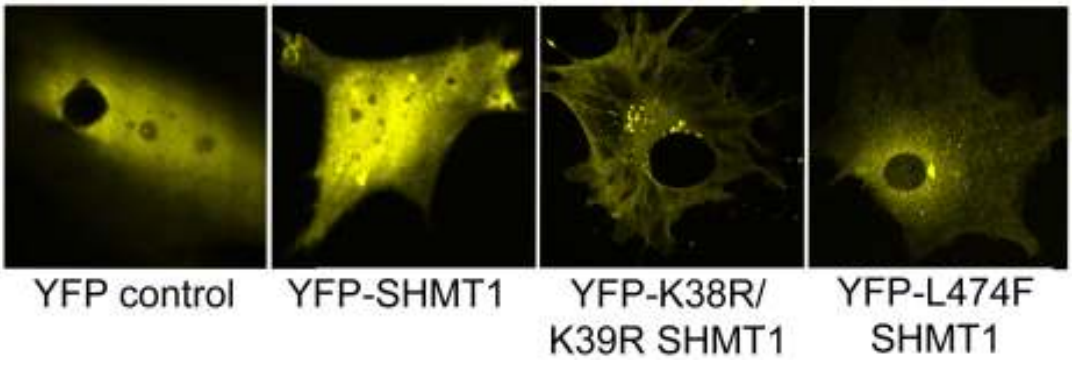

Figure 2.8. The L474F polymorphism in *SHMT1* impairs nuclear localization. *SHMT1*$^{-/-}$ MEF cells were transfected with cDNAs encoding the YFP-empty vector, YFP-SHMT1 wild-type, YFP-SHMT1-K38R/K39R, and YFP-SHMT1-L474F. S-phase blocked transfectants showed that YFP-SHMT1 is greatly increased in the nucleus in S-phase. Empty vector control and K38R/K39R mutation eliminated nuclear localization, and the L474F polymorphism inhibited nuclear localization.

The L474F SHMT1-YFP fusion protein was found in both the cytoplasm and nucleus at S-phase, but in contrast to the SHMT1-YFP protein, its localization was primarily cytoplasmic. These data demonstrate that the *SHMT1* L474 polymorphism impairs nuclear localization. The potential for functional redundancy between SHMT1 and SHMT2α in nuclear folate metabolism may have been the permissive factor that allowed this mutation to expand in human populations.

Discussion

The results from this study demonstrate directly the existence of nuclear thymidylate biosynthesis. Pardee and co-workers (10,12,13) first proposed the concept of nuclear nucleotide biosynthesis and put forward the concept of a nuclear multi-enzyme complex termed the replitase, which synthesized nucleotides at the replication fork during DNA synthesis. Both DHFR and TYMS activities were found in these purified complexes isolated from nuclei, but no direct evidence for nuclear nucleotide biosynthesis was reported. The concept of nuclear folate metabolism is also supported by early studies that demonstrated 10% of the total cellular hepatic folate was present within the nucleus (9). Previous studies have shown that TYMS localizes to the nucleus at S-phase (8), (14), and recently SHMT1, DHFR, and TYMS proteins have all been shown to be SUMOylated, providing a mechanism by which all the enzymes required for *de novo* thymidylate biosynthesis can be localized to the nucleus (7,8). Recent evidence indicates that nuclear folate-dependent nucleotide biosynthesis is limited to thymidylate biosynthesis, as the multi-enzyme complex responsible for *de novo* purine biosynthesis, the purineosome, localizes to the cytoplasm (15).

In this study, we demonstrated that one-carbon units generated from serine are used for nuclear *de novo* thymidylate biosynthesis, and that the three enzymes that participate in *de novo* thymidylate pathway are present in nuclei. Compartmentalization of these enzymes to

the nucleus accounts for previous isotope tracer studies that demonstrate SHMT1 preferentially shuttles one-carbon units towards thymidylate biosynthesis (6).

The data also demonstrate functional redundancy between *Shmt1* and *Shmt2* in nuclear folate metabolism. The observation that *Shmt2* (and human *SHMT2*) encodes a nuclear/cytoplasmic isozyme, SHMT2α, may account for the unexpected viability of *Shmt1*$^{-/-}$ mice, and potentially the emergence in human populations of the L474F *SHMT1* polymorphism, which impairs nuclear SHMT1 import. However, SHMT2α cannot fully replace SHMT1 function as *Shmt1*$^{-/-}$ mice exhibit elevated uracil content in DNA (16). The S-phase and G2/M phase dependence of SHMT2α nuclear localization suggests that it is available for *de novo* thymidylate biosynthesis during DNA synthesis and repair as observed for SHMT1 (8). The mechanism by which SHMT2α localizes to the nucleus is currently under investigation.

To our knowledge, *SHMT2* is the only gene identified that encodes proteins that can localize to the cytoplasm, nucleus and mitochondria. Previously, zebrafish SHMT2 protein was shown to localize exclusively to mitochondria (17). The zebrafish *Shmt2* gene lacks the second translation initiation site in exon 2 and thus can only encode a mitochondrial isozyme. Mammalian *SHMT2* genes, with the exception of the lagomorph gene, encode a translation initiation codon in exon 2 and therefore likely encode the cytoplasmic/nuclear SHMT2α isozyme. These data also provide evidence for tissue-specific expression of the SHMT2 isoforms. The SHMT2/SHMT2α ratio differs between liver and kidney, with SHMT2 being the predominant form in liver, whereas only the SHMT2α and the SHMT2 unprocessed protein precursor were observed in kidney. Mitochondria are a primary source of one-carbon units for cytoplasmic one-carbon metabolism through the activity of SHMT2, and the SHMT2α protein lacks most of the mitochondrial targeting sequence and may not be imported into mitochondria efficiently (4). Therefore, the lack of processed SHMT2 protein in kidney

mitochondria may account for previous findings that glycine catabolism through the mitochondrial glycine cleavage system is a major source of one-carbon units in kidney (18). The molecular mechanisms underlying the differential promoter usage in *SHMT2* that results in the synthesis of the SHMT2 isoforms is currently under investigation.

Compartmentation of SHMT2α and the other *de novo* thymidylate biosynthetic pathway enzymes in the nucleus may allow for folate dependent dTTP biosynthesis directly at the replication fork. It is likely that nuclear thymidylate synthesis requires the formation of an enzyme complex, as sonicated nuclei were not capable of dTMP biosynthesis. It has been shown that the processivity factor PCNA interacts with SHMT1 in both *C. elegans* and HeLa cDNA yeast two hybrids (8), (19). Additional studies are required to determine why thymidylate biosynthesis, unlike purine nucleotide biosynthesis (15), occurs in the nucleus and if a thymidylate-specific replitase-like complex exists that enables the *de novo* dTMP synthesis pathway to function at the replication fork and prevent uracil misincorporation into DNA.

Materials and Methods

Nuclear Biosynthesis Assay

The generation and characterization of $SHMT1^{-/-}$ mice has been described previously (16). All study protocols were approved by the Institutional Animal Care and Use Committee of Cornell University and conform to the NIH Guide for the Care and Use of Laboratory Animals. Twelve livers were isolated from $Shmt1^{+/+}$ or $Shmt1^{-/-}$ mice on a 129SvEv background and placed immediately in cold phosphate buffered saline at 5°C. Liver extracts from six age-matched males and females were combined and used for each genotype group. Nuclei were prepared using an iodixanol gradient as previously described (20). Purified nuclei

were suspended in 500 μL of nuclear assay buffer containing 5 mM NADPH (Sigma), 100 mM β-mercaptoethanol, 25 mM HEPES, pH 7.5, 50 mM Sucrose, 5 mM $MgCl_2$, 25 mM KCl, and 1 mM dUMP (Sigma) and quantified using a hemocytometer. 125 μL of assay buffer containing suspended nuclei were aliquoted into four 1.5 ml plastic tubes and 8 μCi of [2,3-^{3}H]-L-Serine (Moravek Biochemicals) was added to each tube. The assay was conducted under 4 different experimental conditions: Experiment 1, nuclei that were lysed with sonication (Branson Sonifier 150) at 5°C using two 10 sec pulses at 10 watts separated by a 10 sec resting interval; experiment 2, intact nuclei; experiment 3, intact nuclei with 5-formyltetrahydrofolate pentaglutamate (Schirks Laboratory) added to at a final concentration of 200 μM; experiment 4, intact nuclei with aminomethylphosphonate added to a final concentration of 100 mM (Sigma). Reactions were incubated for 12 h at 37°C with shaking at 300 rpm. Nuclei were pelleted by centrifugation at 2000 rpm for 5 min and the supernatant was collected and analyzed for radiolabeled thymidylate by high performance liquid chromatography (HPLC). Sample preparation and HPLC was performed as previously described (21,22). Fractions were collected and tritium quantified with a scintillation counter. The retention times of [2,3-^{3}H]-L-serine (9 min) and ^{3}H-thymidine (17 min) (Moravek Biochemicals) were verified prior to separation of the reaction mixtures. All experiments were performed in duplicate.

Genotyping and immunoblotting

After completion of the nuclear thymidylate biosynthesis reactions, pelleted nuclei were genotyped and analyzed by western blots. DNA was isolated using the DNeasy Blood and Tissue Kit (Qiagen) per manufacturer's protocol and genotyping as previously described to confirm the *Shmt1* genotype (16). For western blots, nuclei were disrupted by boiling in SDS-PAGE loading buffer for 10 min and protein concentrations quantified by the Lowry-

Bensadoun assay (23). 20 μg of protein were loaded into each lane of a 10% SDS-PAGE gel (23). Protein transfers, western blotting and DHFR and TYMS detection were performed as previously described (7). SHMT1 and SHMT2 detection were completed as previously described (24,25). Equal loading and/or purity of nuclear fractions was confirmed through the detection of GAPDH using α-GAPDH (Novus Biologicals, 1:20000 dilution), Lamin A using α-Lamin A (Santa Cruz Biotechnology, 1:500 dilution), and COX IV using α-COX IV (Abcam, 1:5000 dilution). For Lamin A detection, goat anti-rabbit IgG-horseradish peroxidase-conjugated secondary (Pierce) was used at a1:20000 dilution. For COX IV and GAPDH detection, a 1:10000 dilution of goat anti-mouse IgG-horseradish peroxidase-conjugated secondary (Pierce) was used.

The sizes of the SHMT2α isoforms were determined using the Precision Plus Protein All Blue (BIORAD) and Kaleidoscope Prestained Standard (BIORAD). Processed mitochondrial SHMT2 migrated with the Precision Plus Protein All Blue 50 kDa marker. To determine the size of the bands corresponding to preprocessed SHMT2 and SHMT2α proteins, a standard curve was generated by measuring the migration distances of the protein standards. These distances were plotted as a function of $\log_{10}$ of the molecular mass standards, and the molecular mass of preprocessed SHMT2 and SHMT2α were determined using the equation $MM = -1.4D+137.9$; $R^2 = 0.98$, where MM is molecular mass in kDa and D is migration distance in mm. The migration distance of the largest molecular mass band corresponding to preprocessed SHMT2 migrated 58 mm and SHMT2α migrated 61 mm, corresponding to approximately 56 kDa and 53 kDa respectively.

Identification of Shmt2α expression

The nucleotide sequences of the human *SHMT2* and mouse *shmt2* intron 1/exon 2 boundaries were BLASTED against both the human and mouse EST databases to identify alternative *SHMT2* and *Shmt2* transcripts lacking sequence encoded by exon 1 but containing intron 1 sequence within the 5′-untranslated region. To identify *shmt2* protein products expressed from alternative *shmt2* transcripts, liver and kidney were isolated from *SHMT1*$^{+/+}$ mice on a C57Bl/6 background. The tissues were washed with phosphate-buffered saline and proteins solubilized using the Mammalian Protein Extraction Reagent (Pierce) containing 10 mM β-mercaptoethanol and a 1:100 dilution of mammalian protease inhibitor (Sigma). Immunoblotting was performed as described above.

Cell lines and culture

HeLa cells (CCL2) and NIH/3T3 cells (CRL-1658) were obtained from ATCC. Mouse embryonic fibroblasts were isolated and maintained as previously described (8). *GlyA*, a CHO cell mutant lacking SHMT2 activity, was obtained from Dr. Larry Thompson, Lawrence Livermore Labs. All cells were cultured at 37°C in a 5% CO_2 atmosphere. HeLa cells were maintained in minimal essential medium (α-MEM) (Hyclone) with 10% fetal bovine serum (Hyclone) and penicillin/streptomycin (Gibco). NIH/3T3 cells were cultured in DMEM (Gibco) supplemented with 10% fetal bovine serum and penicillin/streptomycin. *GlyA* cells were cultured in DMEM supplemented with 10% dialyzed and charcoal treated fetal bovine serum (*d*DMEM), 20 nM leucovorin (Sigma), 200 μM glycine (Sigma), and penicillin/streptomycin.

Subcellular localization of SHMT2 and SHMT2α

The human *SHMT2* full length open reading frame was purchased from Open Biosystems. The cDNAs for the full length transcript (encoding SHMT2), and the transcript lacking exon 1 but

containing 131 nucleotides of intron 1 in the 5′UTR (encoding SHMT2α) were amplified by PCR amplified and cloned into PhiYFP-N (Evrogen) and TagRFP-N (Evrogen) vectors respectively. The forward primer used to amplify the *SHMT2* transcript was 5′-ATATCTCGAGATGCTGTACTTCTCTTTGTT-3′. The forward primer to amplify the *SHMT2α* transcript was 5′-ATATCTCGAGGTATGGCCATTCGGGCTCAGCAC-3′. The underlined sequence signifies a *XhoI* (Promega) restriction site. The same reverse primer was used for both amplifications: 5′-ATATAAGCTTCTAATGCTCATCAAAACCAG-3′. The underlined sequence denotes a *HindIII* (Promega) restriction site. The PCR conditions for amplification of both the *SHMT2* and *SHMT2α* transcripts were as follows: 95°C for 45 s, 52°C for 45 s, and 72°C for 2 min. A vector containing a mitochondrial marker, pTagCFP-mito (Evrogen) was used for control transfections to identify mitochondria. Plasmids were transfected into HeLa cells using Lipofectamine 2000 (Invitrogen) per manufacturer's protocol. The DNA binding dye, Draq5 (Biostatus Limited) was used to visualize nuclei. For cell cycle analysis, HeLa cells were treated with 1 mM hydroxyurea, 30 μM Lovastatin or 60 ng/ml nocodazole to block at S, G_1 and G2/M phase respectively as previously described (8). Confocal fluorescence microscopy (Leica TCS SP2 system) was used to image all cells at the Cornell Microscope and Imaging Facility.

Rescue of the glycine auxotrophy in GlyA cells

GlyA cells were cultured in *d*DMEM supplemented with 200 μM glycine and 20 nM leucovorin. TagRFP-N-*SHMT2* and TagRFP-N-*SHMT2α* and TagRFP-N vectors were linearized using *NheI* (Promega) and electroporated into *GlyA* cells as previously described (26). Following electroporation, cells were plated on BD Primaria 100×20 mm culture dishes (BD Bioscience) containing 10 ml of *d*DMEM medium, supplemented with 20 nM leucovorin, 200 μM glycine and 200 μg/ml Geneticin (Gibco). 12–15 colonies from each transfection

were isolated and plated in 6-well plates (Corning) containing 3 ml *d*DMEM medium supplemented with glycine, leucovorin, and Geneticin. Cell growth assays were completed in media with and without glycine as previously reported (27).

Site-directed mutagenesis and subcellular localization of SHMT1

The *SHMT1* cDNA (28) was used as a template to generate SHMT1-YFP fusion proteins. The *SHMT1* cDNA was amplified for cloning into PhiYFP-N by PCR. The forward and reverse primers used were 5′- ATATCTCGAGATGACGATGCCAGTCAAC-3′ and 5′-ATATAAGCTTTTAGAAGTCAGGCAGGCC-3′ respectively. The PCR conditions were as follows: 95°C for 45 s, 55°C for 45 s, and 72°C for 2 min. The underlined regions depict *XhoI* and *HindIII* restriction sites respectively. Coding mutations K38R/K39R and L474F mutations were made as previously described (8). PhiYFP-N vectors containing the *SHMT1* cDNA, the *SHMT1* cDNA containing a K38R/K39R mutation, and a *SHMT1* cDNA containing the L474F mutation were transfected into *Shmt1*$^{-/-}$ MEFs using electroporation protocols described above. Cells were blocked at S-phase by exposure to 1 mM hydroxyurea (Sigma) for 24 h. Confocal fluorescence microscopy (Leica TCS SP2 system) was used to image the SHMT1-YFP fusion proteins at the Cornell Microscope and Imaging Facility.

REFERENCES

1. Fox JT, Stover PJ (2008) Folate-mediated one-carbon metabolism. Vitam Horm 79: 1–44.
2. Garrow TA, Brenner AA, Whitehead VM, Chen XN, Duncan RG, et al. (1993) Cloning of human cDNAs encoding mitochondrial and cytosolic serine hydroxymethyltransferases and chromosomal localization. J Biol Chem 268: 11910–11916.
3. Girgis S, Nasrallah IM, Suh JR, Oppenheim E, Zanetti KA, et al. (1998) Molecular cloning, characterization and alternative splicing of the human cytoplasmic serine hydroxymethyltransferase gene. Gene 210: 315–324.
4. Stover PJ, Chen LH, Suh JR, Stover DM, Keyomarsi K, et al. (1997) Molecular cloning, characterization, and regulation of the human mitochondrial serine hydroxymethyltransferase gene. J Biol Chem 272: 1842–1848.
5. Appling DR (1991) Compartmentation of folate-mediated one-carbon metabolism in eukaryotes. Faseb J 5: 2645–2651.
6. Herbig K, Chiang EP, Lee LR, Hills J, Shane B, et al. (2002) Cytoplasmic serine hydroxymethyltransferase mediates competition between folate-dependent deoxyribonucleotide and S-adenosylmethionine biosyntheses. J Biol Chem 277: 38381–38389.
7. Anderson DD, Woeller CF, Stover PJ (2007) Small ubiquitin-like modifier-1 (SUMO-1) modification of thymidylate synthase and dihydrofolate reductase. Clin Chem Lab Med 45: 1760–1763.
8. Woeller CF, Anderson DD, Szebenyi DM, Stover PJ (2007) Evidence for small ubiquitin-like modifier-dependent nuclear import of the thymidylate biosynthesis pathway. J Biol Chem 282: 17623–17631.
9. Shin YS, Chan C, Vidal AJ, Brody T, Stokstad EL (1976) Subcellular localization of gamma-glutamyl carboxypeptidase and of folates. Biochim Biophys Acta 444: 794–801.

10. Prem veer Reddy G, Pardee AB (1980) Multienzyme complex for metabolic channeling in mammalian DNA replication. Proc Natl Acad Sci U S A 77: 3312–3316.
11. Stover P, Schirch V (1991) 5-Formyltetrahydrofolate polyglutamates are slow tight binding inhibitors of serine hydroxymethyltransferase. J Biol Chem 266: 1543–1550.
12. Noguchi H, Prem veer Reddy G, Pardee AB (1983) Rapid incorporation of label from ribonucleoside disphosphates into DNA by a cell-free high molecular weight fraction from animal cell nuclei. Cell 32: 443–451.
13. Boorstein RJ, Pardee AB (1983) Coordinate inhibition of DNA synthesis and thymidylate synthase activity following DNA damage and repair. Biochem Biophys Res Commun 117: 30–36.
14. Bissoon-Haqqani S, Moyana T, Jonker D, Maroun JA, Birnboim HC (2006) Nuclear expression of thymidylate synthase in colorectal cancer cell lines and clinical samples. J Histochem Cytochem 54: 19–29.
15. An S, Kumar R, Sheets ED, Benkovic SJ (2008) Reversible compartmentalization of de novo purine biosynthetic complexes in living cells. Science 320: 103–106.
16. MacFarlane AJ, Liu X, Perry CA, Flodby P, Allen RH, et al. (2008) Cytoplasmic serine hydroxymethyltransferase regulates the metabolic partitioning of methylenetetrahydrofolate but is not essential in mice. J Biol Chem 283: 25846–25853.
17. Chang WN, Tsai JN, Chen BH, Huang HS, Fu TF (2007) Serine hydroxymethyltransferase isoforms are differentially inhibited by leucovorin: characterization and comparison of recombinant zebrafish serine hydroxymethyltransferases. Drug Metab Dispos 35: 2127–2137.
18. Cowin GJ, Willgoss DA, Bartley J, Endre ZH (1996) Serine isotopmer analysis by 13C-NMR defines glycine-serine interconversion in situ in the renal proximal tubule. Biochim Biophys Acta 1310: 32–40.

19. Li S, Armstrong CM, Bertin N, Ge H, Milstein S, et al. (2004) A map of the interactome network of the metazoan C. elegans. Science 303: 540–543.
20. Graham JM (2001) Isolation of Nuclei and Nuclear Membranes From Animal Tissues. In: Bonifacino MD JS, Harford JB, Lippincott-Schwartz J, Yamada KM, editors. Current Protocols in Cell Biology. Malden, MA: John Wiley & Sons, Inc. pp. 3.10.11–13.10.19.
21. Field MS, Szebenyi DM, Stover PJ (2006) Regulation of de novo purine biosynthesis by methenyltetrahydrofolate synthetase in neuroblastoma. J Biol Chem 281: 4215–4221.
22. Friso S, Choi SW, Dolnikowski GG, Selhub J (2002) A method to assess genomic DNA methylation using high-performance liquid chromatography/electrospray ionization mass spectrometry. Anal Chem 74: 4526–4531.
23. Bensadoun A, Weinstein D (1976) Assay of proteins in the presence of interfering materials. Anal Biochem 70: 241–250.
24. Liu X, Szebenyi DM, Anguera MC, Thiel DJ, Stover PJ (2001) Lack of catalytic activity of a murine mRNA cytoplasmic serine hydroxymethyltransferase splice variant: evidence against alternative splicing as a regulatory mechanism. Biochemistry 40: 4932–4939.
25. Perry C, Yu S, Chen J, Matharu KS, Stover PJ (2007) Effect of vitamin B6 availability on serine hydroxymethyltransferase in MCF-7 cells. Arch Biochem Biophys 462: 21–27.
26. Potter H (2003) Tranfection by Electroporation. In: Bonifacino MD JS, Harford JB, Lippincott-Schwartz J, Yamada KM, editors. Current Protocols in Cell Biology. Malden, MA: John Wiley & Sons, Inc. pp. 20.25.21–20.25.26.
27. Anguera MC, Field MS, Perry C, Ghandour H, Chiang EP, et al. (2006) Regulation of folate-mediated one-carbon metabolism by 10-formyltetrahydrofolate dehydrogenase. J Biol Chem 281: 18335–18342.
28. Zanetti KA, Stover PJ (2003) Pyridoxal phosphate inhibits dynamic subunit interchange among serine hydroxymethyltransferase tetramers. J Biol Chem 278: 10142–10149.

CHAPTER 3

Identification of a *de novo* dTMP biosynthesis pathway in mammalian mitochondria

Introduction

Regulation of cellular dTTP pools is essential for faithful replication of nuclear and mitochondrial DNA (mtDNA), with both depletion and expansion of the pool affecting DNA integrity and human health (1). Depletion of de novo dTMP synthesis results in deoxyuridine misincorporation into nuclear DNA leading to genome instability (2), whereas depletion of mitochondrial dTTP pools, due to mitochondrial deoxyribonucleoside kinases, deoxyguanosine kinase, or thymidine kinase 2 (TK2) mutations are associated with mtDNA-depletion syndromes and severe mitochondrial dysfunction in humans (3). Elevations in dTTP pools, as observed in mitochondrial neurogastrointestinal encephalomyopathy (4), an autosomal recessive disease resulting from decreased levels of cytoplasmic thymidine phosphorylase, results in mtDNA depletion (5), deletions (6), and site-specific point mutations (6).

There are two distinct pathways for thymidine nucleotide synthesis (Figure 3.1).

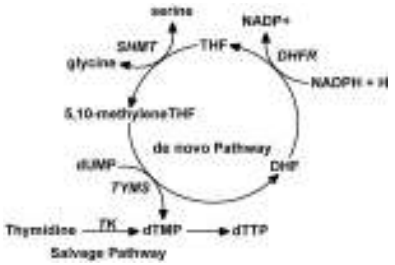

Figure 3.1. De novo and salvage pathway synthesis of dTTP. There are two distinct pathways for dTTP synthesis. In the de novo pathway, SHMT catalyzes the conversion of serine and tetrahydrofolate (THF) to methyleneTHF and glycine. TYMS converts methyleneTHF and dUMP to dihydrofolate (DHF) and dTMP. DHF is converted to THF for subsequent rounds of dTMP synthesis in an NADPH-dependent reaction catalyzed by DHFR. In the salvage pathway, thymidine is phosphorylated by TK to form dTMP.

The salvage pathway involves the conversion of thymidine to thymidylate, and occurs in the mitochondria and cytoplasm catalyzed by TK2 and thymidine kinase 1 (TK1), respectively (7). Salvage pathway synthesis of dTTP is not sufficient to sustain mtDNA replication (3) and therefore requires de novo dTMP synthesis, which involves the conversion of dUMP to dTMP, catalyzed by the tetrahydrofolate (THF)-dependent enzymes serine hydroxymethyltransferase (SHMT), thymidylate synthase (TYMS), and dihydrofolate reductase (DHFR) (8). In this pathway, 5,10-methyleneTHF, a one-carbon donor, is generated from serine by SHMT and used for the conversion of dUMP to dTMP in a reaction catalyzed by TYMS. The TYMS catalyzed reaction generates dihydrofolate, which is converted to THF in an NADPH-dependent manner by DHFR. The regenerated THF can then be used for subsequent rounds of thymidylate biosynthesis.

Both de novo and salvage dTMP synthesis have been assumed to occur in the cytoplasm to support both nuclear and mtDNA replication, but recent studies have demonstrated nuclear localization of TK1 (9) and the de novo dTMP biosynthesis pathway during S-phase and as a result of DNA damage (10, 11). The inability of the mitochondrial dTMP salvage pathway to support mtDNA synthesis, and recent studies indicating that de novo dTMP synthesis occurs in the nucleus, raised the possibility for a requirement for de novo thymidylate biosynthesis in mitochondria.

De novo thymidylate synthesis has been shown to occur in plant mitochondria through the activities of an SHMT isozyme [mitochondrial serine hydroxymethyltransferase (SHMT2)] and a bifunctional enzyme containing both TYMS and DHFR (12). Interestingly, previous studies have localized TYMS to the mitochondria in mammalian cells (1, 13) and in neurospora crassa (14). In mammalian cells, mitochondria contain SHMT2, which is required for formate and glycine synthesis (15), but the third enzyme in the pathway, DHFR, does not localize to the mitochondria (16).

In this study, a de novo dTMP biosynthesis pathway was identified in mammalian mitochondria that includes a unique mitochondrial isozyme of DHFR called DHFRL1, which was previously thought to be a pseudogene (17). De novo dTMP synthesis is shown to be necessary to prevent uracil accumulation in mtDNA.

Results

Mammalian Mitochondria Contain a De Novo dTMP Synthesis Pathway

Purified intact mitochondria from Chinese hamster ovary (CHO) cells and HepG2 cells (Table 3.1 and Figure 3.2) were capable of catalyzing the formation of 3H-dTMP from unlabeled dUMP, NADPH, and [2,3-3H]-L-serine in vitro.

Cell line	Treatment	Normalized ^{3}H-dT
WT CHO	Sonicated	0.54 ± 0.14
	Intact	1 ± 0.092
	MTX	0.0002 ± 0.02
glyA CHO	Sonicated	0.01 ± 0.02
	Intact	0.06 ± 0.02
	MTX	0.05 ± 0.02
HepG2	Sonicated	0.3 ± 0.005
	Intact	1 ± 0.05

Table 3.1 Mitochondrial de novo thymidylate biosynthesis. Mitochondria were isolated from HepG2, wild-type CHO, and glyACHOcells which lack SHMT2 activity. The capacity to convert dUMP and [2,3-^{3}H]-L-serine to ^{3}H-dTMP was determined in reactions that contained: (i) sonicated mitochondria, (ii) intact mitochondria for both the HepG2 and CHO cell reactions; and (iii) intact mitochondria with 100 μM methotrexate (MTX), a dihydrofolate reductase inhibitor for CHO cell reactions. The reactions were all normalized to the activity obtained from intact mitochondria isolated from wild-type CHO or HepG2 cells and given an arbitrary value of 1.0. Thymidylate synthesis was inhibited in MTX treated reactions ($p < 0.001$, n=3) and in CHO glyA cells ($p< 0.001$, n=3) compared to the activity obtained in intact mitochondria isolated from wild-type CHO cells. Data were analyzed by two-way ANOVA with Tukey's post hoc test for treatment. For HepG2, thymidylate synthesis was inhibited in the sonicated mitochondria ($p <0.002$, n=3, t-test). Variation is expressed as SEM.

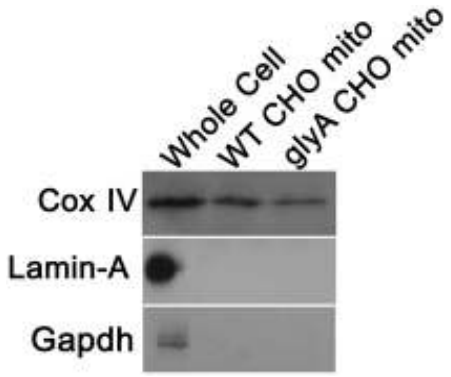

Figure 3.2. Purity of Chinese hamster ovary (CHO) mitochondria. Mitochondria that were purified from CHO cells for the experiment described in Table 1 exhibited no nuclear or cytosolic contamination using immunoblots against GAPDH and Lamin A.

This activity is a unique demonstration of folate-dependent de novo dTMP biosynthesis in mammalian mitochondria. Methotrexate inhibited dTMP production in mitochondria isolated from wild-type CHO cells. Mitochondria isolated from glyA CHO cell mutants, which lack SHMT2, exhibited a 94% reduction in dTMP synthesis capacity, indicating the essentiality of SHMT2 within mitochondria for mitochondrial de novo dTMP synthesis. Disruption of mitochondria by sonication-reduced de novo dTMP synthesis activity, indicating that compartmentalization within mitochondria, or the formation of complexes within mitochondria, may be important for de novo dTMP synthesis. Alternatively, the reduced activity may reflect dilution or loss of the endogenous folate cofactor pool following sonication.

Identification of DHFRL1 as an Expressed Gene.

To determine if alternative human DHFR transcripts are expressed that encode a mitochondrial leader sequence, 5' rapid amplification of cDNA ends (RACE) was conducted using total mRNA isolated from HepG2 cells. Two prominent bands were observed from the 5' RACE experiment. Upon sequencing the two bands, both DHFR and DHFRL1 were identified (Fig. 3.3A). DHFRL1 is annotated as a mammalian pseudo gene in Entrez Gene, and expressed sequence tags are present (GenBank accession no. DN994912).

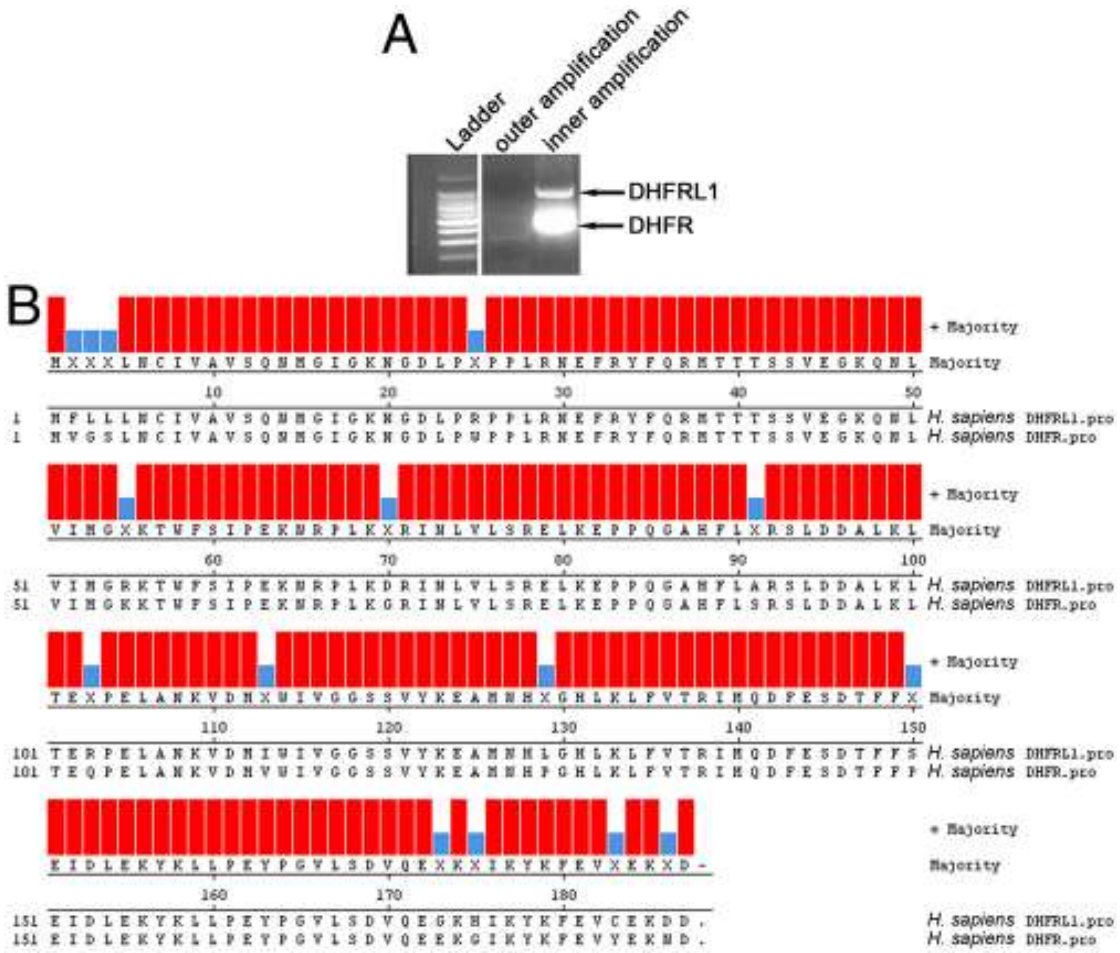

Figure 3.3. Identification of DHFRL1 and alignment to DHFR. (A) 5'RACE was performed to identify DHFR transcripts that encoded a mitochondrial DHFR isozyme. Using a primer complementary to DHFR sequence, two bands were obtained following electrophoresis. The bands were isolated, cloned, and sequenced revealing DHFRL1 as an expressed transcript. (B) The sequence of DHFR and DHFRL1 were aligned using ClustalW in Lasergene Megalign software. The sequences are 92% identical.

The DHFR and DHFRL1 primary sequences are 92% identical (Fig. 3.3B). An energy minimized three-dimensional model of DHFRL1 was constructed using the crystal structure of human DHFR [Protein Data Bank (PDB) ID code 3GHW] as a template. The model of DHFRL1 structure and DHFR structure are highly similar with an rms value of 0.0034 (Figure 3.4).

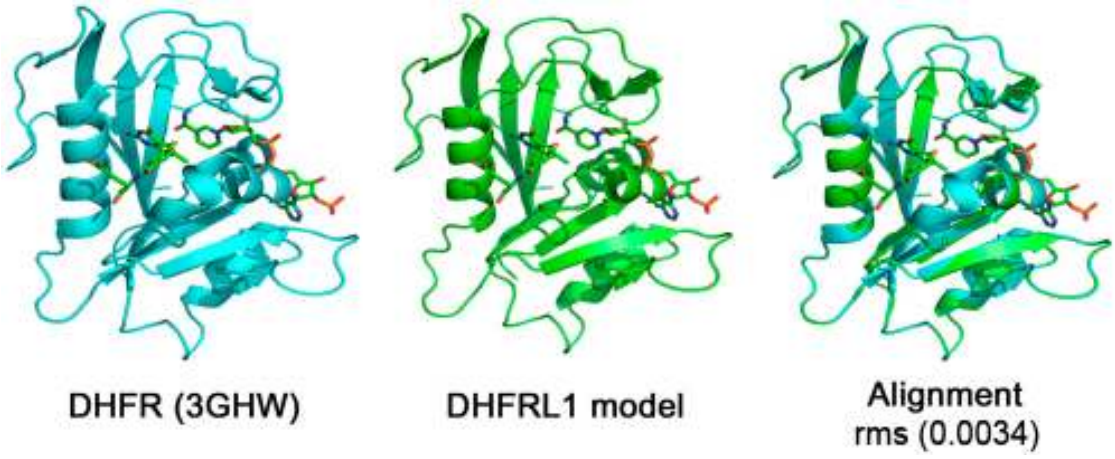

Figure 3.4. Model of dihydrofolate reductase-like protein 1 (DHFRL1) protein. The protein sequence of DHFRL1 was modeled using the structure of human dihydrofolate reductase (DHFR) [Protein Data Bank (PDB) ID code 3GHW] as a template. The energy minimized model of DHFRL1 was produced in SWISS-PDB viewer and the model alignment and images were made in PyMOL. The rms between DHFR and the DHFRL1 model was determined to be 0.0034 indicating high similarity in structure.

Localization of DHFRL1 and TYMS to Mitochondria

The subcellular localization of DHFRL1 and TYMS were determined by confocal microscopy following the transfection of pCMV6-ACDHFRL1-GFP and pCMV6-AC-TYMS-GFP constructs into HeLa cells. The mitochondrial control vector pTagCFP-mito was also transfected to visualize mitochondria, and DRAQ5 nuclear stain was used to visualize nuclei. Colocalization of the mitochondrial control protein, and both TYMS-GFP and DHFRL1-GFP fusion proteins, was observed. TYMS-GFP localized to the cytoplasm, mitochondria, and nuclei (Figure 3.5A), whereas DHFRL1-GFP was present exclusively within mitochondria (Figure 3.5B). DHFRL1, SHMT2, and TYMS endogenous to HepG2 mitochondria were localized to the mitochondrial matrix and inner membrane in fractionated mitochondria (Figure 3.5C), consistent with previous localization studies of SHMT2 (18, 19). Using MITOPRED (20, 21), a bioinformatics program for prediction of mitochondrial proteins, no canonical mitochondrial leader sequence was identified for DHFRL1. The primary sequence of DHFRL1 shown in Figure 3.3 was sufficient for mitochondrial import.

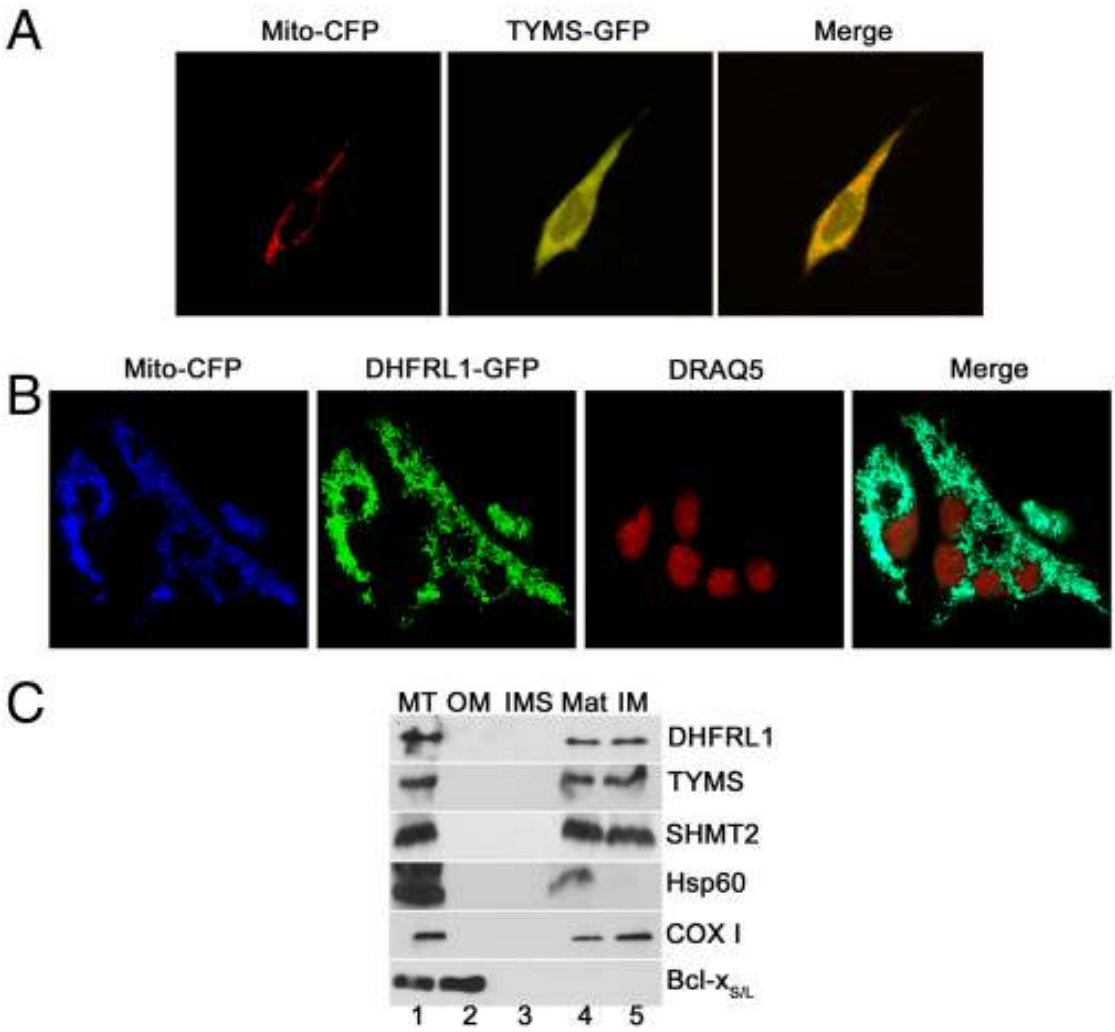

Figure 3.5. TYMS and DHFRL1 localize to mitochondria. TYMS-GFP fusion proteins (A) and DHFRL1-GFP fusion proteins (B) were expressed in HeLa cells, as well as a mitochondrial marker mito-CFP. (A) TYMS-GFP localizes to the nucleus, cytoplasm, and colocalizes with the mito-CFP mitochondrial marker. (B) DHFRL1-GFP localizes exclusively to mitochondria. (C) TYMS, DHFRL1, and SHMT2 proteins localize to the matrix and inner membrane of fractionated HepG2 cells. Lane 1, mitochondrial extract; lane 2, outer membrane fraction; lane 3, innermembrane space; lane 4, matrix; lane 5, inner membrane. Hsp60 is the inner membrane/matrix marker, Cox I is an inner membrane marker, and Bcl-xS/L is an outer membrane marker.

These data demonstrate that both TYMS and DHFRL1 are present in human mitochondria, and indicate that mitochondria contain a complete pathway to conduct de novo thymidylate biosynthesis.

DHFRL1 is a Functional Enzyme in Mitochondria

The presence of DHFR activity in mitochondria was investigated in human HepG2 cells treated with scrambled control siRNA, and siRNA specific to the DHFRL1 5' untranslated region and not present in the DHFR transcript. The DHFR activity in extracts from mitochondria isolated from the control siRNA (32.4 ±4.0 nmol/min/mg protein) and DHFRL1-specific siRNA treatments (0.17 ±0.008 nmol/ min/mg protein) were significantly different with a p value of 0.0002 (n=3) where error is expressed as SEM. The mitochondria isolated for these assays exhibited no nuclear or cytosolic contamination as determined by immuno-blotting against Lamin A and GAPDH, respectively (Figure 3.6A).

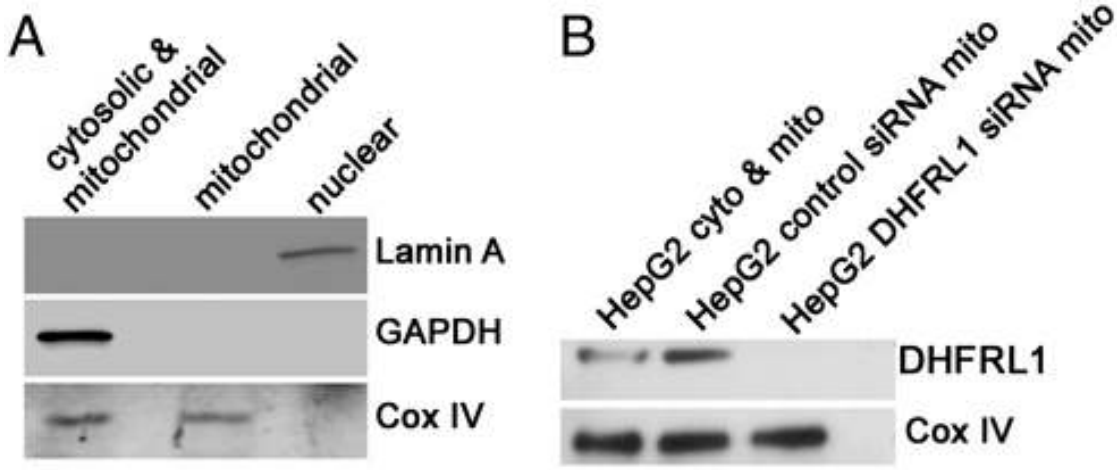

Figure 3.6. Knockdown of DHFRL1 inhibits DHFR activity in mitochondrial extracts. Scrambled siRNA and siRNA against DHFRL1 were transfected into HepG2 cells and DHFRL1 protein and activity was measured. (A)Mitochondria from HepG2 cells that were purified for de novo dTMP synthesis assays (Table 3.2), and DHFRL1 activity experiments exhibited no nuclear or cytosolic contamination using immunoblots against GAPDH and Lamin A. (B) No DHFRL1 was present in mitochondria of HepG2 cells transfected with siRNA against DHFRL1.

Cell line	Uracil (pg)/ DNA (μg)
WT CHO	1.0 ± 0.072
glyA CHO	1.6 ± 0.25
p value	0.015 ($n = 3$)

Table 3.2. Uracil content in mtDNA from wild-type CHO and glyA CHO cells. MtDNA was isolated from wild-type CHO and glyA CHO cells and levels of uracil were determined using GC/MS. Uracil levels were higher in mtDNA isolated from glyA CHO cells compared to wild-type CHO cells using a t-test (p= 0.01, n=3). Variation is expressed as SD.

In the samples in which DHFRL1 was knocked down, no DHFRL1 protein was present in the mitochondrial extracts. COX-IV immunoblotting was used as a positive mitochondrial control. DHFR activity in the cytosolic extracts was unaffected by both scrambled and DHFRL1-specific siRNA treatment with specific activities of 4.5 ±2.6 and 4.5 ±2.8 nmol/ min /mg protein, respectively, indicating that DHFRL1 knockdown did not affect DHFR expression. For comparison, DHFR activity in purified nuclei from HepG2 cells exhibited a specific activity of 14.3±1.0 nmol/ min /mg protein.

De Novo Thymidylate Biosynthesis is Required to Prevent Uracil Accumulation in mtDNA

mtDNA was isolated from both wild-type and glyA CHO cells and uracil content in mtDNA was quantified. GlyA CHO cells lack SHMT2 activity and are auxotrophic for glycine (22, 23). mtDNA isolated from wild-type cells contained 40% less uracil than mtDNA from glyA CHO cells (Table 3.2). These data confirm the importance of SHMT2 activity within mitochondria for the production of dTMP, and demonstrate the importance of mitochondrial dTMP de novo biosynthesis in protecting mtDNA from uracil misincorporation.

DHFRL1 Expression Rescues the Glycine Auxotrophy in glyC CHO Cells

To verify the function of DHFRL1 in mitochondrial folate metabolism, the ability of DHFRL1 to rescue the glycine auxotrophy caused by disrupted mitochondrial folate-metabolism in a previously uncharacterized CHO cell line, glyC, was determined (Figure 3.7).

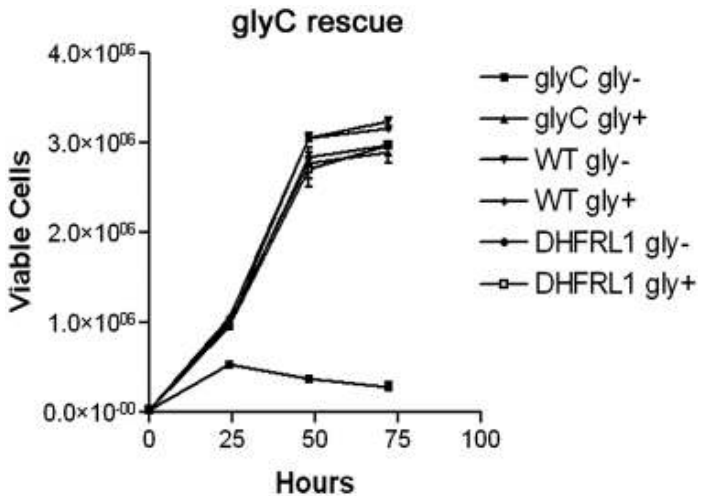

Figure 3.7. DHFRL1 cDNA rescues glycine auxotrophy in glyC CHO cells. CHO glyC cells were transfected with cDNAs encoding human DHFRL1-GFP, or a GFP-empty vector control. Stable cells lines were selected for G418 resistance in the presence of 200 μM glycine and 10 mg⁄L thymidine. For growth assays, cells were cultured with and without glycine and trypan blue exclusion was used to quantify viable cells. Four independent lines were assayed per transfection and experiments were done in triplicate. There was no significant difference in growth among the cells transfected with DHFRL1-GFP with or without glycine. CHO glyC cells transfected with GFP-empty vector and cultured without glycine failed to proliferate over the 72 h time period.

Four stable transfectants were selected for G418 resistance from glyC cells electroporated with either an empty pCMV6-AC-GFP plasmid, or a plasmid containing the DHFRL1 cDNA with a 5' CMV promoter. Stable transfectants containing the pCMV6-AC-GFP empty vector did not rescue the glycine auxotrophy. However, the glycine auxotrophy was rescued in all selected cell lines transfected with the vector that contained the DHFRL1 cDNA. These results confirm that DHFRL1 localizes to mitochondria and can rescue mitochondrial one-carbon metabolism.

Discussion

This study demonstrates that human mitochondria contain an active de novo thymidylate biosynthesis pathway, composed of SHMT2, TYMS and DHFRL1. This study supports two previous studies that have observed TYMS protein localized within mammalian mitochondria,

although the functional significance of these observations was never established (1, 13). Folate-activated one-carbon units for mammalian mitochondrial thymidylate biosynthesis are derived from serine through the catalytic activity of SHMT2; mitochondria lacking functional SHMT2, isolated from glyA CHO cells, exhibited impaired de novo thymidylate synthesis. The discovery of DHFRL1 as the functional mitochondrial enzyme completes the de novo thymidylate synthesis cycle. Inhibition of DHFRL1 expression by siRNA significantly reduced DHFR activity in mitochondria isolated from HepG2 cells. DHFRL1 was previously thought to be a pseudogene and was mapped to chromosome 3q11.2 (17). The mechanism whereby TYMS and DHFRL1 are localized to mitochondria remains to be established as neither protein contains a canonical mitochondrial leader sequence at its amino terminus. Disruption of mitochondrial folate metabolism results in a glycine auxotrophy due to loss of SHMT2 function (22). In this study, we show that DHFRL1 complements the previously uncharacterized CHO glycine auxotrophic mutant, glyC. Previous reports have observed that glyC mutants have normal SHMT levels in both the cytosol and mitochondria (15, 24). Because the mitochondrial and cytoplasmic folate pools are not in equilibrium, loss of DHFR activity in mitochondria is expected to result in an accumulation of mitochondrial folate as dihydrofolate, thereby depleting THF pools for the SHMT2-catalyzed conversion of serine to glycine.

De novo thymidylate synthesis appears to be required to maintain mtDNA integrity, as glyA cells were observed to have elevated levels of uracil in DNA. During nuclear DNA replication, dTTP is the only deoxyribonucleotide that is not essential for DNA synthesis as dUTP can be incorporated into DNA when dTTP levels fall (2). Results from these studies indicate that impaired de novo thymidylate synthesis in mitochondria also results in deoxyuridylate incorporation in mtDNA. A recent report observed increases in mtDNA deletions in mice lacking the Ung gene undergoing folate deprivation compared to wild-type

controls (25). Other studies support a role for de novo thymidylate biosynthesis in maintaining DNA integrity. Patients with the mitochondrial disorder, Friedrich's ataxia, which leads to large increases in mtDNA damage, exhibited elevated DHFRL1 mRNA (26). Elevated DHFRL1 expression may help limit some deleterious changes in mtDNA. Other studies have demonstrated that TYMS inhibition leads to caspase-dependent apoptosis and changes in mitochondrial membrane potential (27, 28). mtDNA damage has been shown to initiate apoptosis rapidly, independent of deleterious mutations (29). Mitochondrial DNA damage due to inhibition of mitochondrial dTMP synthesis could explain the increases in apoptosis observed (27). Further investigation should be undertaken to determine if TYMS inhibition-dependent apoptosis is due to uracil misincorporation within mtDNA and/or reduced mitochondrial thymidylate biosynthesis.

Unlike the synthesis of purine and cytosine deoxyribonucleotides, dTMP synthesis is compartmentalized to the nucleus and mitochondria, both sites of DNA replication. Elevated uracil content in DNA results from both nutritional deficiency of folate (2) and impaired expression of the thymidylate biosynthesis pathway genes (30); genetic disruption of SHMT1 in mice increases uracil levels in nuclear DNA (31). To our knowledge, impairment of de novo thymidylate biosynthesis has not been shown previously to elevate uracil in mtDNA. These data also indicate that a high level of organization within the mitochondria may be required for efficient dTMP biosynthesis, such as the proposed complex in nuclei for dTMP biosynthesis (11, 32, 33). As observed previously in nuclei, disruption of mitochondria by sonication inhibited thymidylate biosynthesis (11). Others have observed that SHMT2 cross-links to mtDNA in HeLa cells upon formaldehyde treatment (34, 35). Collectively, these data suggest that a multienzyme complex may exist within mitochondria at mtDNA replication forks. Ongoing studies will address the biological necessity for thymidylate biosynthesis

within both the nuclei and mitochondria, whereas purine biosynthesis occurs in the cytosol (11, 36).

Methods

Cell Lines and Culture

HeLa and HepG2 cells were acquired from American Type Culture Collection (ATCC). GlyA, a CHO cell mutant lacking SHMT2 activity, was obtained from Larry Thompson, Lawrence Livermore Labs, Livermore, CA. GlyC, an uncharacterized CHO cell mutant which is auxotrophic for glycine was obtained from Barry Shane, University of California, Berkeley, CA. All cells were cultured at 37 °C in a 5% CO2 atmosphere. HeLa and HepG2 cells were maintained in minimal essential medium (α-MEM) (Hyclone) with 10% fetal bovine serum (Hyclone) and penicillin/streptomycin (Gibco). GlyA and GlyC cells were cultured in defined minimal essential medium which lacks glycine and supplemented with 10% dialyzed and charcoal treated fetal bovine serum (dDMEM), pencillin/streptomycin, and 20 nM leucovorin (Sigma). For the complementation assays, positive growth controls included 200 μM glycine.

5′ Rapid Amplification of cDNA Ends (5′ RACE) Identifies DHFRL1 Transcript.

Polyadenylated mRNA was isolated from HepG2 cells using the Dynabeads mRNA purification kit (Invitrogen) as per manufacturer's instructions. The isolated mRNA was then used for 5′ RACE using the FirstChoice RNA Ligase Mediated-RACE kit (Ambion, Inc.) as per manufacturer's instructions. For the outer and inner amplifications the primers used were 5′-TGG AGG TTC CTT GAG TTC TCTGCT-3′ and 5′- AGG TCG ATT CTT CTC AGG AAT GGA GA-3′, respectively. The primers were made to detect DHFR but also identified DHFRL1. The outer and inner primers are made to nucleotides 229–252 and 176–201 of both DHFR and DHFRL1 coding sequence. The outer primer has a sequence identity of 96% to DHFRL1. The inner primer has 100% sequence identity to DHFRL1.

The nested PCR products were run on a 2% agarose gel. Bands were cut from the gel and purified using the QIAquick gel extraction kit (Qiagen). The isolated cDNA was then Topo cloned using the pCR-Blunt II-Topo vector (Invitrogen) as per manufacturer's instructions. Topo clones were picked and grown overnight at 37 ℃ for DNA isolation. Plasmid DNA was isolated using a Miniprep kit from Qiagen as per manufacturer's instructions. The isolated plasmid DNA was sent to sequencing at the Biotech Resource Center at Cornell University. Primers against the T7 promoter priming site present in the pCR-Blunt II-Topo vector was used for sequencing.

Homology Modeling and Alignment of DHFRL1.

The primary protein sequence of DHFRL1 (GenBank accession no. AAH63379.1) was modeled against the structure of human DHFR (PDB ID code 3GHW) using DeepView/Swiss-PDB viewer 3.7. The Iterative Magic Fit of all atoms tool was used to generate a structural alignment. The structure model was then energy minimized using GROMOS96 energy minimization tool. PyMOL was used to generate three-dimensional structures and the RMS was determined using the align action within PyMOL. Primary protein sequences alignments between DHFR (GenBank accession no. AAH71996.1) and DHFRL1 were generated using the ClustalW tool in Lasergene Megalign software.

Localization of TYMS and DHFRL1 by Confocal Microscopy in HeLa Cells.

TYMS and DHFRL1 cDNAs were fused to the N terminus of GFP within the pCMV6-AC-GFP vector (Origene). A vector expressing a mitochondrial marker, pTagCFP-mito (Evrogen) was used for control transfections to identify mitochondria. Plasmids were transfected into HeLa cells using the Nucleofector II and the nucleofection kit R (Lonza) as per manufacturer's protocol. The DNA binding dye, Draq5 (Biostatus Limited) was used to visualize nuclei. Confocal fluorescence microscopy (Zeiss 710 Confocal system) was used to image all cells at the Cornell Microscope and Imaging Facility.

Rescue of the Glycine Auxotrophy in CHO GlyC Cells.

GlyC CHO cells were cultured in dDMEM supplemented with 200 μM glycine and 20 nM leucovorin. pCMV6-DHFRL1-GFP and pCMV6-GFP vectors were linearized using ScaI (New England Biolabs), electroporated into CHO GlyC cells, and selected as previously described (11). Trypan blue exclusion assays were completed in media with and without glycine as previously reported (37).

Knockdown of DHFRL1 and Dihydrofolate Reductase Activity in Mitochondria.

DHFRL1-specific siRNA and control scrambled siRNA (Qiagen) were transfected into HepG2 cells using Nucleofection (Lonza) as per manufacturer's instructions. After a 24 h incubation, mitochondria were isolated using the same protocol described below for the mitochondrial dTMP biosynthesis assays. Mitochondria were lysed using mammalian protein extraction reagent (Pierce) supplemented with 1 mMEDTA, 10 mM PMSF (Alexis Biochemicals), and 1□1;000 dilution of protease inhibitor (Sigma). DHFR enzyme activity was determined in isolated mitochondria from both control siRNA treated and DHFRL1 siRNA-treated HepG2 cells using the DHFR activity kit (Sigma) as per manufacturer's instructions. To control for cytoplasmic and nuclear contamination, immunoblotting was performed as previously reported (11). To determine if DHFRL1 was present in mitochondria and knocked down in the siRNA-treated samples, immunoblots were performed using a mouse polyclonal antibody toward DHFRL1 (Abnova) at a concentration of 1:5;000. Goat anti-mouse HRP (Pierce) conjugated secondary was used at a concentration of 1:10;000. Cox IV antibody was used as a mitochondrial control as previously described (11).

Mitochondrial Thymidylate Biosynthesis Assay.

Mitochondria were isolated from 109 cells of each HepG2, wild-type CHO and glyA CHO cells. Cells were grown in Hyperflasks (Corning) in DMEM (Gibco) supplemented with 10% fetal bovine serum (Hyclone) and penicillin/streptomycin (Gibco). Cells were

trypsinized and collected in 50 mL conical tubes and centrifuged at 2,000 rpm for 5 min. The cell pellets were washed twice with phosphate buffered saline with centrifugation at 2,000 rpm between washes. Isolation of mitochondrial fractions were completed as previously reported (38). The mitochondrial pellets were resuspended in buffer containing 0.3 M sucrose, 1.0 mM EGTA, 5.0 mM MOPS, 5.0 mM K2PO4, and 0.1% BSA, and adjusted to pH 7.4 with KOH. The mitochondria were then distributed equally into 1.5 mL tubes, nine fractions for each of wild-type CHO cells and glyA CHO cells and six fractions for HepG2 cells. These tubes were centrifuged at 5;000 × g for 10 min at 4 °C. The pelleted mitochondria were then resuspended in 600 μL of thymidylate reaction buffer containing 5 mM NADPH (Sigma), 100 mM β-mercaptoethanol (Sigma), 50 mM Hepes, pH 7.4, 2 mM MgCl2, 50 mMKCl, 25 mM K2HPO4, 1 mM dUMP, and 0.3 M sucrose. The mitochondria used for the sonicated reactions were then subjected to five 10 s pulses with 10 s rests between pulses on ice. The small probe on a Branson sonifier was used at 20% power. O2 gas was bubbled into each reaction vessel for 3 min. prior to addition of 8 μL [2,3-3H]-L-serine (Moravek). The reactions were put in a shaking incubator at 300 rpm and 37 °C for 12 h. The samples were then centrifuged at 5;000 × g for 10 min to pellet mitochondria and the supernatant was collected. The mitochondria were then lysed using 500 μL 1% SDS and sonication as previously stated. The lysate was then analyzed using HPLC as previously reported (11).

mtDNA Purification and Determination of Uracil Misincorporation in glyA and Wild-Type CHO Cells.

Mitochondria were isolated from both CHO wild-type and CHO glyA cells. The mitochondrial pellet was resuspended in 50 mM glucose (Sigma), 20 mM Tris·HCl pH 8.0 (Fisher), and 10 mM EDTA (Fisher) at 1 mL buffer per 500 μg mitochondria. Lysozyme (Sigma) was added at a concentration of 2 mg⁄mL and incubated on ice for 20 min. Two milliliters of 0.2 M NaOH (Fisher) containing 1% SDS (Fisher) were added and incubated on

ice for 5 min. One and a half milliliters of 3 M potassium acetate dissolved in 2 M acetic acid was used to neutralize the sample to pH 7.0. The samples were incubated on ice for 1 h. The samples were then centrifuged at 11;000 × g for 30 min. The supernatant was decanted and then treated with 1⁄10 the volume of 3 M sodium acetate and two volumes of ethanol. The mtDNA was precipitated for 2 h at −20 °C. The samples were centrifuged at 10;000 × g for 20 min at 4 °C. The pellet was resuspended in 0.6 mL of 10 mM Tris/1 mM EDTA, pH 8.0 containing 0.1 mg⁄mL RNaseA. The mtDNA was purified using 1 mL of the Wizard Plus Resin from the Wizard Plus Miniprep kit (Promega) as per manufacturer's instructions. Analysis of uracil levels was performed as previously reported with modifications; a Shimadzu QP2010 Plus GC/MS was used for analysis (31).

Mitochondrial Subfractionation.

Purified mitochondria from HepG2 cells were subfractionated into matrix, outer membrane, and inner membrane fractions as previously reported (39) and immunoblots were performed on each fraction to determine submitochondrial localization of DHFRL1, TYMS, and SHMT2. DHFRL1 immunoblots were performed as mentioned above. TYMS and SHMT2 immunoblots were performed as previously reported (11). Mouse anti-hsp60 (inner membrane/matrix marker), mouse anti-Cox I (inner membrane marker), and mouse anti-Bcl-xS⁄L (outer membrane marker) were purchased from Santa Cruz Biotechnology and were used at a dilution of 1:200. HRP conjugated goat anti-mouse (Pierce) secondary antibodies were used at a dilution of 1:10;000.

REFERENCES

1. Samsonoff WA, et al. (1997) Intracellular location of thymidylate synthase and its state of phosphorylation. J Biol Chem 272:13281–13285.

2. Blount BC, et al. (1997) Folate deficiency causes uracil misincorporation into human DNA and chromosome breakage: Implications for cancer and neuronal damage. Proc Natl Acad Sci USA 94:3290–3295.

3. Zhou X, et al. (2008) Progressive loss of mitochondrial DNA in thymidine kinase 2-deficient mice. Hum Mol Genet 17:2329–2335.

4. Nishino I, Spinazzola A, Hirano M (1999) Thymidine phosphorylase gene mutations in MNGIE, a human mitochondrial disorder. Science 283:689–692.

5. Pontarin G, et al. (2006) Mitochondrial DNA depletion and thymidine phosphate pool dynamics in a cellular model of mitochondrial neurogastrointestinal encephalomyopathy. J Biol Chem 281:22720–22728.

6. Nishigaki Y, Marti R, HiranoM(2004) ND5 is a hot-spot for multiple atypical mitochondrial DNA deletions in mitochondrial neurogastrointestinal encephalomyopathy.Hum Mol Genet 13:91–101.

7. Pontarin G, Gallinaro L, Ferraro P, Reichard P, Bianchi V (2003) Origins of mitochondrial thymidine triphosphate: Dynamic relations to cytosolic pools. Proc Natl Acad Sci USA 100:12159–12164.

8. Fox JT, Stover PJ (2008) Folate-mediated one-carbon metabolism. Vitam Horm 79:1–44.

9. Chen YL, Eriksson S, Chang ZF Regulation and functional contribution of thymidine kinase 1 in repair of DNA damage. J Biol Chem 285:27327–27335.

10. Fox JT, Shin WK, Caudill MA, Stover PJ (2009) A UV-responsive internal ribosome entry site enhances serine hydroxymethyltransferase 1 expression for DNA damage repair. J Biol Chem 284:31097–31108.

11. Anderson DD, Stover PJ (2009) SHMT1 and SHMT2 are functionally redundant in nuclear de novo thymidylate biosynthesis. PLoS One 4:e5839.

12. Neuburger M, Rebeille F, Jourdain A, Nakamura S, Douce R (1996) Mitochondria are a major site for folate and thymidylate synthesis in plants. J Biol Chem 271:9466–9472.

13. Brown SS, Neal GE, Williams DC (1965) Subcellular distribution of some folic acidlinked enzymes in rat liver. Biochem J 97:34C–36C.

14. Rossi M, Woodward DO (1975) Enzymes of deoxythymidine triphosphate biosynthesis in Neurospora crassa mitochondria.. J Bacteriol 121:640–647.

15. Appling DR (1991) Compartmentation of folate-mediated one-carbon metabolism in eukaryotes. FASEB J 5:2645–2651.

16. Wang FK, Koch J, Stokstad EL (1967) Folate coenzyme pattern, folate linked enzymes and methionine biosynthesis in rat liver mitochondria. Biochem Z 346:458–466.

17. Anagnou NP, Antonarakis SE, O'Brien SJ, Modi WS, Nienhuis AW (1988) Chromosomal localization and racial distribution of the polymorphic human dihydrofolate reductase pseudogene (DHFRP1). Am J Hum Genet 42:345–352.

18. Da Cruz S, et al. (2003) Proteomic analysis of the mouse liver mitochondrial inner membrane.. J Biol Chem 278:41566–41571.

19. Cybulski RL, Fisher RR (1976) Intramitochondrial localization and proposed metabolic significance of serine transhydroxymethylase.. Biochemistry 15:3183–3187.

20. Guda C, Fahy E, Subramaniam S (2004) MITOPRED: A genome-scale method for prediction of nucleus-encoded mitochondrial proteins. Bioinformatics 20:1785–1794.

21. Guda C, Guda P, Fahy E, Subramaniam S (2004) MITOPRED: A web server for the prediction of mitochondrial proteins. Nucleic Acids Res 32:W372–374.

22. Pfendner W, Pizer LI (1980) The metabolism of serine and glycine in mutant lines of Chinese hamster ovary cells. Arch Biochem Biophys 200:503–512.

23. Stover PJ, et al. (1997) Molecular cloning, characterization, and regulation of the human mitochondrial serine hydroxymethyltransferase gene. J Biol Chem 272:1842–1848.
24. Taylor RT, Hanna ML (1982) Folate-dependent enzymes in cultured Chinese hamster ovary cells: Impaired mitochondrial serine hydroxymethyltransferase activity in two additional glycine-auxotroph complementation classes. Arch Biochem Biophys 217:609–623.
25. Kronenberg G, et al. (2011) Folate deficiency increases mtDNA and D-1 mtDNA deletion in aged brain of mice lacking uracil-DNA glycosylase. Exp Neurol 228(2):253–258.
26. Haugen AC, et al. Altered gene expression and DNA damage in peripheral blood cells from Friedreich's ataxia patients: Cellular model of pathology. PLoS Genet 6: e1000812.
27. Sakoff JA, Ackland SP (2000) Thymidylate synthase inhibition induces S-phase arrest, biphasic mitochondrial alterations and caspase-dependent apoptosis in leukaemia cells. Cancer Chemother Pharmacol 46:477–487.
28. Pritchard DM, Hickman JA (1999) Genetic determinants of cell death and toxicity. Antifolate Drugs in Cancer Therapy, ed ALJackman(HumanaPress, Totowa, NJ), pp437–451.
29. Ricci C, et al. (2008) Mitochondrial DNA damage triggers mitochondrial-superoxide generation and apoptosis. Am J Physiol Cell Ph 294:C413–422.
30. Goulian M, Bleile B, Tseng BY (1980) Methotrexate-induced misincorporation of uracil into DNA. Proc Natl Acad Sci USA 77:1956–1960.
31. MacFarlane AJ, et al. (2008) Cytoplasmic serine hydroxymethyltransferase regulates the metabolic partitioning of methylenetetrahydrofolate but is not essential in mice. J Biol Chem 283:25846–25853.
32. Anderson DD, Woeller CF, Stover PJ (2007) Small ubiquitin-like modifier-1 (SUMO-1) modification of thymidylate synthase and dihydrofolate reductase. Clin Chem Lab Med 45:1760–1763.

33. Woeller CF, Anderson DD, Szebenyi DM, Stover PJ (2007) Evidence for small ubiquitinlike modifier-dependent nuclear import of the thymidylate biosynthesis pathway. J Biol Chem 282:17623–17631.

34. Wang Y, Bogenhagen DF (2006) Human mitochondrial DNA nucleoids are linked to protein folding machinery and metabolic enzymes at the mitochondrial inner membrane. J Biol Chem 281:25791–25802.

35. Bogenhagen DF, Rousseau D, Burke S (2008) The layered structure of human mitochondrial DNA nucleoids. J Biol Chem 283:3665–3675.

36. An S, Kumar R, Sheets ED, Benkovic SJ (2008) Reversible compartmentalization of de novo purine biosynthetic complexes in living cells. Science 320:103–106.

37. Field MS, Anguera MC, Page R, Stover PJ (2009) 5,10-Methenyltetrahydrofolate synthetase activity is increased in tumors and modifies the efficacy of antipurine LY309887. Arch Biochem Biophys 481:145–150.

38. Graham JM (2001) Isolation of mitochondria from tissues and cells by differential centrifugation. Curr Protoc Cell Biol 3.3.1–3.3.15.

39. Bolusani S, et al. Mammalian MTHFD2L encodes a mitochondrial methylenetetrahydrofolate dehydrogenase isozyme expressed in adult tissues. J Biol Chem 286:5166–5174.

CHAPTER 4

Sumoylation-ubiquitination antagonism in SHMT1 Nuclear Localization and Accumulation

Introduction

Folate-mediated one-carbon metabolism is compartmentalized in the mitochondria, nucleus and cytoplasm of eukaryotic cells (1) (Figure 4.1).

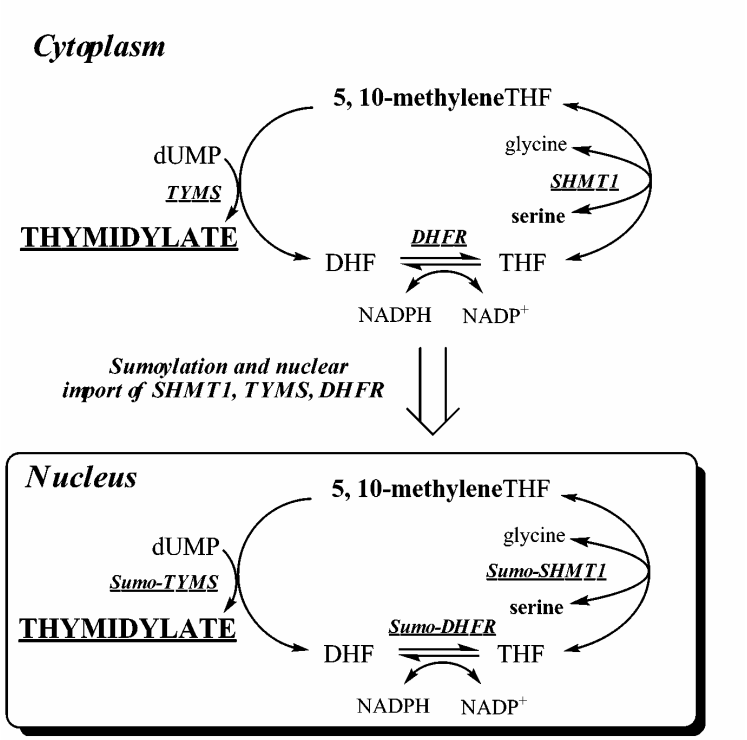

Figure 4.1. Folate-mediated one carbon metabolism**.** Schematic of folate-mediated one-carbon metabolism in the cytoplasm and nucleus. One-carbon metabolism in the cytoplasm is required for the *de novo* synthesis of purines and thymidylate, and for the remethylation of homocysteine to methionine. One-carbon metabolism in the nucleus synthesizes dTMP from dUMP and serine. MTHFD1, Methylenetetrahydrofolate Dehydrogenase; MTR, Methionine Syntase; MTHFR, Methylenetetrahydrofolate Reductase; SHMT1, Cytoplasmic Serine Hydroxymethyltransferase; TYMS, Thymidylate Synthase; DHFR, Dihydrofolate Reductase.

This metabolic network is required for the *de novo* biosynthesis of purines and thymidylate, and for the remethylation of homocysteine to methionine. Nuclear *de novo* thymidylate biosynthesis requires three enzymes: thymidylate synthase (TYMS), dihydrofolate reductase (DHFR), and serine hydroxymethyltransferase (SHMT1 and SHMT2α). SHMT generates an activated single carbon from serine and tetrahydrofolate (THF) in the form of methylenetetrahydrofolate (methyleneTHF), which serves as the one-carbon and two-electron donor for the TYMS catalyzed conversion of dUMP to dTMP generating dihydrofolate (DHF). DHFR catalyzes the NADPH-dependent reduction of DHF to regenerate THF for subsequent rounds of *de novo* thymidylate synthesis. The enzymes that constitute the *de novo* dTMP synthesis pathway are post-translationally modified by Ubc9 with the small ubiquitin-like modifier 1 (SUMO-1) and undergo nuclear translocation during S and G2/M phases (2-4), and in response to UV (5) for nuclear dTMP synthesis (4). Studies in cell cultures and mice have shown that SHMT1 expression determined capacity for de novo dTMP synthesis (Anderson et al Unpublished) (6). Regulation of cellular dTTP pools is essential for maintaining both nuclear and mitochondrial DNA integrity and previous studies have indicated the importance of maintaining dNTP pool size throughout the cell cycle to avoid genome instability (7,8).

We have previously observed that SHMT1 interacts with Ubc13, an E2 conjugase for ubiquitination (2), although the functional significance of this interaction has yet to be determined. Previous studies have indicated that SUMO and ubiquitin (Ub) can modify the same consensus motif, ΨKXE/D, on target proteins, and in some cases have antagonistic effects and allow pathway choice (9). Whereas SUMO-1 modification is essential for nuclear translocation of the *de novo* dTMP pathway, the role of ubiquitination in the regulation of SHMT1 and *de novo* thymidylate biosynthesis is unknown. In this study we demonstrate that Ubc13-mediated modification of SHMT1 leads to nuclear export and acts as a mediator of SHMT1 stability within the nucleus. Furthermore, we demonstrate that SHMT1 is degraded in

the cytoplasm via the proteasome through K48 linkage specific poly-ubiquitination. The study indicates competition between SHMT1 SUMOylation and Ubiquitination to regulate SHMT1 nuclear localization and levels by competing for the same consensus motif on SHMT1.

EXPERIMENTAL PROCEDURES

Cell Lines, Media, and Transfection conditions— HeLa cells were obtained and maintained as previously reported (4). Cells were grown in α-MEM (Hyclone) supplemented with 10% fetal bovine serum (Hyclone) and penicillin/streptomycin (Mediatech) at 37° C and 5% CO_2. All transfections were performed using the Nucleofector II and kitR for HeLa cells per manufacturer's instructions (Lonza).

Vectors and vector construction- A construct encoding a V5-SHMT1 fusion protein, pcDNA3.1-SHMT1-V5-HisA, was generated to differentiate between endogenous SHMT1 and SUMO site mutants. pcDNA3.1/V5-HisA was purchased from Invitrogen. The human SHMT1 cDNA from phiYFP-SHMT1 (4) was amplified by PCR using the forward primer 5'-ATAT**AAGCTT**ATGACGATGCCAGTCAAC-3' where the bold text indicates a HindIII restriction site (New England Biolabs Inc.). The reverse primer was 5'-ATAT**CTCGAG**GAAGTCAGGCAGGCCAGG-3' where the bold text indicates a Xho*I* restriction site. PCR reactions were conducted as follows: 95°C for 45 s, 55°C for 45 s, and 72°C for 2 min. PCR products were gel purified using the QIAquick Gel extraction kit (Qiagen). Vectors and PCR products were restriction digested with their respective restriction enzymes as per manufacturer's protocol. Ligation was completed using T4 DNA ligase (Invitrogen) as per manufacturer's protocol. Ligations were transformed into Top10 cells (Invitrogen) and selected for ampicillin (Fisher) resistance. Following plasmid purification and isolation using plasmid mini-preps (Qiagen), vectors were sequenced at the Cornell University Life Sciences Core Laboratories Center. Mutations within the conserved SUMO motif were performed as previously reported (2). The pCMV-HA-Ub vector was generously provided by

Dr. Shu-Bing Qian, Cornell University, Ithaca, NY. The K48R and K63R Ub mutants were made using the primers 5'-ATCTTTGCAGGCA**G**GCAGCTGGAAGA -3' and 5'-CTACAATATTCAAA**G**GGAGTCTACTC-3' respectively and reverse complements (mutation is bold) using the QuikChange II Site-directed mutagenesis kit (Stratagene) per manufacturer's instruction. All siRNA was purchased from Qiagen.

Preparation of cDNA and real-time PCR – HeLa cells were cell cycle arrested as described below and total RNA was isolated using a RNeasy kit (Qiagen) per manufacturer's protocol after 1 h. treatment of samples with DNase I (Qiagen) at 37° C to remove residual DNA. Total RNA was converted to cDNA using Superscript III first-strand cDNA synthesis kit (Invitrogen) using oligo-dT primers per manufacturer's protocol. Real-time PCR was completed using Quantifast SYBR green PCR kit (Qiagen) and SHMT1 primers (Qiagen). PCR products were quantified using Applied Biosystems 7500 real-time PCR system.

Immunoblotting—Cellular proteins were quantified, separated, transferred, and detected as previously described (2). GAPDH, Lamin-A, and Ubc13 immunoblotting were performed as previously described (2,4). All antibodies were diluted in 5% non-fat dry milk (Carnation) containing 1% NP40 (US Biologicals). For Ub detection, mouse anti-Ub antibody (BIOMOL) was diluted 1:1000. For V5-tag detection, mouse anti-V5 antibody (Invitrogen) was diluted 1:5000. Mouse anti-β-Actin antibody (Abcam) was used at a 1:5000 dilution. For detection of HA tagged Ub, Mouse anti-HA antibody (Santa Cruz Biotechnology, Inc.) was used. For detection of Ub, V5, HA, and β-Actin, goat anti-mouse IgG-horse radish peroxidase (HRP) (Thermo Scientific) was diluted 1:10,000. For detection of SUMO-2/3 conjugates, Rabbit anti-SUMO-2/3 (Cell Signaling) was used at a dilution of 1:1000. Goat anti-rabbit-HRP secondary was used at a dilution of 1:20,000 (Thermo Scientific).

Immunoprecipitation—Immunoprecipitation was conducted using the Dynabeads Protein G Immunoprecipitation Kit (Invitrogen). For whole cell immunoprecipitation, HeLa cells were

lysed using mammalian protein extraction reagent (Pierce) supplemented with 1 mM *N*-ethylmaleimide (Sigma), 100 μM ALLN (Sigma), 2 mM β-mercaptoethanol (Calbiochem), 0.1 mM EDTA (Fisher Scientific), 1 mM PMSF (Alexis Biochemicals), and 1:1000 Protease Inhibitor Cocktail (Sigma). For immunoprecipitations of nuclear and cytosolic extracts, nuclei were purified using the Active Motif Nuclear extract kit per manufacturer's protocol. 1 mg of total protein per sample was incubated with 5 μg of either anti-K63-linkage Ub (Millipore), anti-Ub (BIOMOL) or anti-V5 tag (Invitrogen) antibody overnight at 4^{o}C. For the nuclear immunoprecipitations, anti-SHMT1 antibody was used with the same parameters. The beads were collected and washed four times with 1 mL PBS. 40 μLs SDS-PAGE sample buffer were added to the beads to elute with heating at 100°C.

Cell Cycle Synchronization and Analysis—HeLa cells at 60% confluence were arrested at various cell cycle stages using 30 μM lovastatin for G1 (Sigma), 2 mM hydroxyurea for S-phase (Sigma), or 100 ng/mL nocodazole for G2/M phase (Sigma). Preparation for fluorescence activated cell sorting (FACS) was performed as previously described (2). FACS analysis was performed by Biomedical Sciences Flow Cytometry Core Laboratory at Cornell University.

Proteasomal Inhibition and Half-life Analysis—HeLa cells were treated with 50 μg/mL cycloheximide (Sigma) to stabilize cellular protein levels and 100 μM ALLN (Sigma) to stabilize Ub linkages. Proteasome inhibition was achieved using 20 μM MG132 (Sigma). Cells were isolated at either 0, 1, 2, 4, and 8 hrs or 0, 2, 4, 8 hrs as described in the figure legends. For determination of SHMT1 nuclear versus cytoplasmic half-life, nuclei and cytosol were isolated from cells using a nuclear extraction kit (Active Motif) at the appropriate time points as per manufacturer's protocol.

Immunofluorescence – SHMT1 antibody was labeled with Cy3 dye using the Amersham Cy3 bis-reactive labeling kit (GE Lifesciences) per manufacturer's protocol. HeLa cells were

grown on cover slips in 6-well plates. Cells were treated with DMSO (Fisher) or 50 μM Mg132 (Sigma) for 3 h. Cells were washed and medium added back and cells were incubated for 12 h for recovery. Cells were then fixed using 4% formaldehyde solution at room temperature for 10 min. Fixation was quenched in 100 mM glycine in PBS for 5 min. Cells were permeabilized in 0.1% Triton X-100 (Fisher) in PBS for 5 min at room temperature. Immunohistochemistry was performed using antibodies against SHMT1, 20S α + β subunits (Abcam), and the 19S S7 subunit (Abcam) diluted in 1% BSA (Sigma) in PBS at 1 μg/mL, 1:500 and 1:1000 respectively. Primary antibodies were incubated on the fixed and permeabilized cells for 1 h at room temperature. Following 4 washes of each coverslip with 3 mL of PBS, secondary antibodies were incubated on coverslips for 1 h at room temperature. Alexa Fluor 555 Donkey anti-rabbit secondary was used for detection of 20S α + β subunits and the 19S S7 subunit diluted in 1% BSA in PBS at 1:1000. Coverslips were washed as previously stated. DRAQ5 (Alexis Biochemicals) was used for nuclear staining as per manufacturer's protocol. Cells were mounted to slides using Mowiol mounting solution (Calbiochem) and allowed to harden overnight at 4° then visualized using confocal microscopy.

Leptomycin B treatment – HeLa cells were treated with or without 20 μM Mg132 and either 0, 2.5, or 5 ng/mL of the nuclear export inhibitor leptomycin B (LMB) (Sigma) for 24 h. Nuclei were isolated as stated above from cells and lysed using SDS-PAGE loading buffer for immunoblotting.

Nuclear localization of SHMT1 as a function of Ubc13 expression - cDNAs encoding SHMT1- YFP (4), Ubc13 (Open Biosystems), or siRNA against Ubc13 (Qiagen) were transfected into HeLa cells. Cells were visualized using confocal microscopy with DRAQ5 as the nuclear control. Cells with nuclear SHMT1 versus cytosolic were counted (n = 200) for each of the following treatments: YFP-SHMT1 with endogenous Ubc13 levels; YFP-SHMT1

and Ubc13 siRNA; YFP-SHMT1 and Ubc13 overexpression; and YFP-SHMT1 with Ubc13 overexpression and 2.5 ng/mL LMB treatment.

RESULTS

SHMT1 protein levels and ubiquitination change with the cell cycle – The levels of cellular SHMT1 protein and Ub-modified SHMT1 (Ub-SHMT1) were quantified as a function of cell cycle in HeLa cells (Figure 4.2).

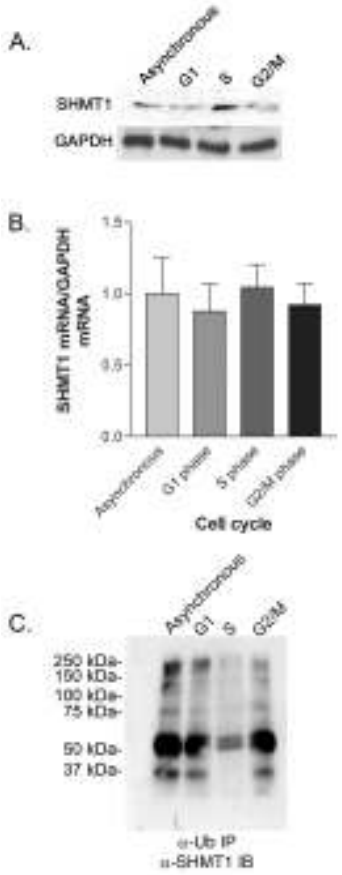

Figure 4.2. SHMT1 protein levels change with the cell cycle. HeLa cells were cell cycle blocked by 24 h treatment with Lovastatin (30 μM) for G1 phase, Hydroxyurea (1 mM) for S phase, and Nocodazole (100 ng/mL) for G2/M phase. Panel A: SHMT1 protein levels were determined by immumoblotting of 20 μg protein extract. Panel B: SHMT1 mRNA levels were quantified from whole cell extract. Panel C: Ub-SHMT1 levels were quantified by immunoprecipitation of ubiquitinated substrates from whole cell extracts (20 μg) followed by SHMT1 immunoblotting. IP; immunoprecipitation; IB: Immunoblots

SHMT1 protein levels were elevated during S-phase (Figure 4.2A) whereas SHMT1 mRNA levels did not change as a function of cell cycle (Figure 4.2B). Ub-SHMT1 was detected in whole-cell extracts at all phases of the cell cycle, but was diminished at S-phase. These data demonstrate that SHMT1 is a cell-cycle regulated protein, and that Ub-SHMT1 levels are lowest at S-phase when SHMT1 undergoes SUMO modification and nuclear transport.

Proteasome inhibition stabilizes SHMT1 and increases ubiquitinated SHMT1 levels. – HeLa cells were treated with the translation inhibitor cycloheximide (CHX) and proteasome inhibitors Mg132 and ALLN to determine if Ub-modification mediates SHMT1 half-life. SHMT1 exhibited a half-life of approximately 2 hours in HeLa cells treated with CHX, whereas SHMT1 levels increased over an 8 h in HeLa cells treated with CHX and proteosome inhibitors (Figure 4.3A), indicating that SHMT1 is subject to Ub-dependent proteasomal processing.

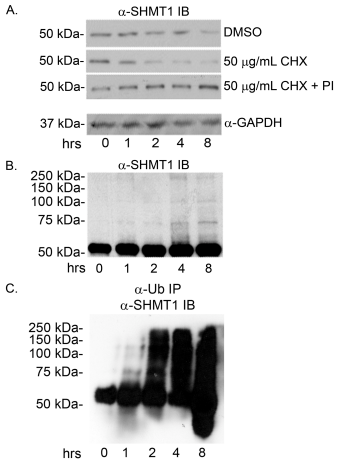

Figure 4.3. Proteasome inhibition stabilizes SHMT1 and increases ubiquitinated SHMT1 levels. HeLa cells were treated with DMSO (control), cycloheximide (CHX), or CHX and 20 μM Mg132 + 100 μM ALLN proteasome inhibitors (PI) for 8 h. SHMT1 immunoblots were performed as described in materials and Methods. Panel A: Total cellular protein extracts (20 μg) were separated by electrophoresis and SHMT1 protein levels determined by immunoblotting. The half-life of endogenous SHMT1 when CHX treated is approximately 2 hours. DMSO control and CHX + PI treatments were stable over 8 hours. Panel B: SHMT1 was visualized in cell extracts by immunoblotting as described above. Accumulation of higher molecular weight bands was observed in CHX + PI treatment over 8 h. Panel C: Ub-SHMT1 was visualized in total cell protein extracts (20 μg) by immunoprecipitation of Ub-conjugated proteins followed by SHMT1 immunoblotting.

Cells treated with CHX and proteosome inhibitors accumulated higher molecular weight SHMT1 immunoreactive bands over time (Figure 4.3B), indicating that Ub-SHMT1 is an intermediated in SHMT1 degradation by the proteosome. These higher molecular weight bands were identified as SHMT1 polyUb conjugates through Ub immunoprecipitation and SHMT1 immunoblotting (Figure 4.3C).

SHMT1 K39 is the ubiquitin modification site – We previously observed that SHMT1 SUMO-1 modification occurs at either K38 or K39 (Figure 4.4C) and that mutation of either lysine to arginine resulted in the ablation of SUMOylation (2,4).

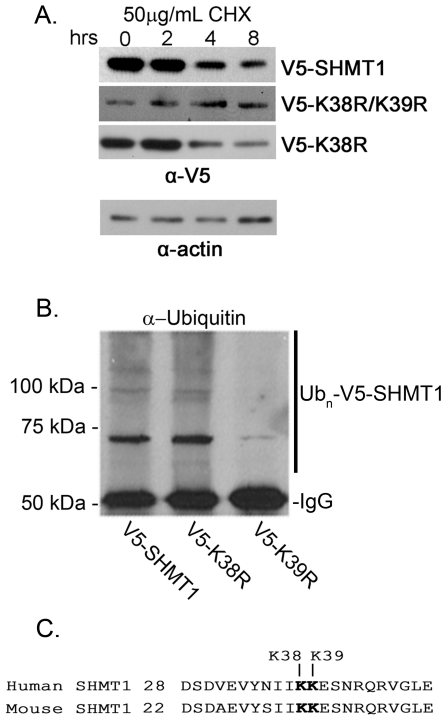

Figure 4.4. SHMT1 K39 is the Ub modification site. HeLa cells were transfected with expression vectors encoding V5 tagged wild type SHMT1, K38R SHMT1, K38R/K39R SHMT1, or K39R SHMT1. Panel A: Total cellular protein extracts (20 μg) were separated by electrophoresis and V5-SHMT1 protein levels determined by immunoblots against V5. V5-wild type SHMT1 and V5-K38R SHMT1 both exhibited a half-life of approximately 4 h. Mutation of both K38R and K39R results in SHMT1 stability. Actin was used as a loading control. Panel B: Ub-V5-SHMT1 was visualized in total cell protein extracts (20 μg) by V5 immunoprecipitation followed by Ub immunoblots. Ub-V5-SHMT1 is reduced in K39R mutants compared to wild type SHMT1 and K38R mutants. Panel C: The conserved SUMO motif (IKKE) is also a site for ubiquitination.

To determine if ubiquitination occurs at this site, expression vectors encoding V5-SHMT1, V5-K38R SHMT1, and V5-K38R/K39R were transfected into HeLa cells. The cells were treated with CHX to determine the role of K38 and K39 in SHMT1 turnover and half-life. V5-SHMT1 and V5-K38R SHMT1 exhibited similar half-lives, whereas V5-K38R/K39R SHMT1 was stable over time (Figure 4.4A). Immunoprecipitation of the V5 tag followed by immunobloting with anti-Ub antibody indicated that mutation of K39 results in a marked reduction of Ub-SHMT (Figure 4.4B). These data demonstrate that K39 is a modification site for ubiquitination and that K39 ubiquitination leads to proteasomal processing.

SHMT1 co-localizes with the 19S cap and 20S core of the proteasome in the nucleus and the cytosol – Immunolocalization and biochemical studies have shown that proteasomes are localized to nuclei and cytosol (10,11). To determine if degradation of SHMT1 occurs within the nucleus and cytoplasm, immunochemistry was performed using HeLa cells treated with either DMSO or Mg132. SHMT1 and the proteosome 20S catalytic core and 19S cap colocalized in both the cytosol and nucleus with discrete puncta formation following Mg132 treatment as compared to control DMSO treatments, indicating that SHMT1 associates with the proteosome in both compartments (Figure 4.5).

Inhibition of nuclear export leads to accumulation of SHMT1 in the nucleus – To determine if SHMT1 is degraded within the nucleus or if it is shuttled to the cytoplasm prior to degradation, HeLa cells were treated with the nuclear export inhibitor leptomycin B (LMB) for 24 h with or without Mg132. Nuclei were isolated and SHMT1 protein levels were quantified by western blot. Nuclear SHMT1 levels increased following LMB treatment, with an accumulation of higher molecular weight immunoreactive bands in both the Mg132 treated and untreated cells (Figure 4.6A and B). Nuclear extracts from Mg132 treated cells exhibited a prominent 75 kDa band that was identified to be a SUMO-2/3 conjugate of SHMT1 (Figure 4.6B, C and D).

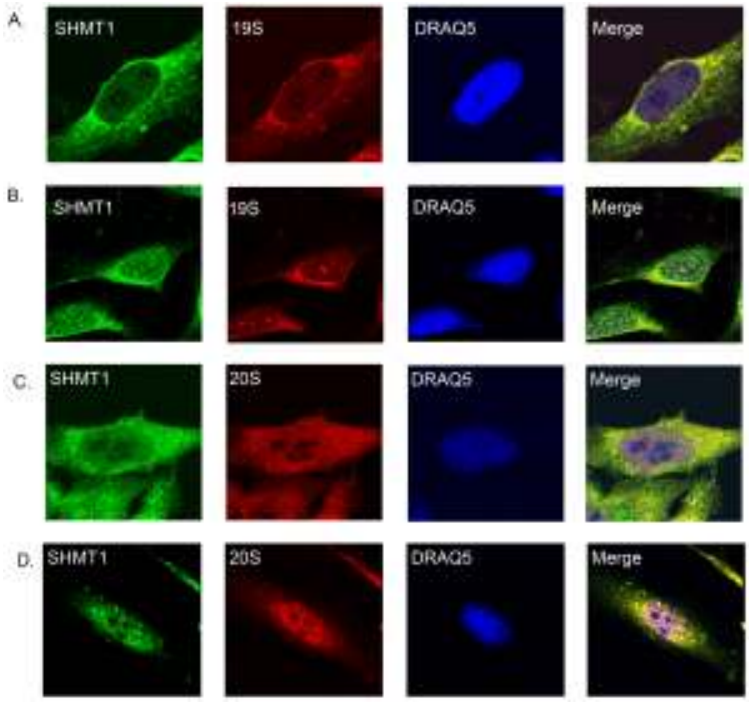

Figure 4.5. SHMT1 co-localizes with the 19S cap and 20S core of the proteasome in the nucleus and the cytosol. Cells were treated with DMSO (A and C) or 50 μM Mg132 (B and D) for 3 hours. Cells were washed and medium was added back and cells were incubated for a 12 h recovery. Immunohistochemistry was performed using antibodies against SHMT1, 20S α + β subunits, and the 19S S7 subunit. DRAQ5 was used for nuclear staining. Cells were then visualized using confocal microscopy. Colocalization of SHMT1 with 19S and 20S are seen in controls most prevalently within the cytosol. Upon treatment with Mg132 and recovery, colocalization of 19S and 20S with SHMT1 is observed within puncta in the nucleus and cytoplasm.

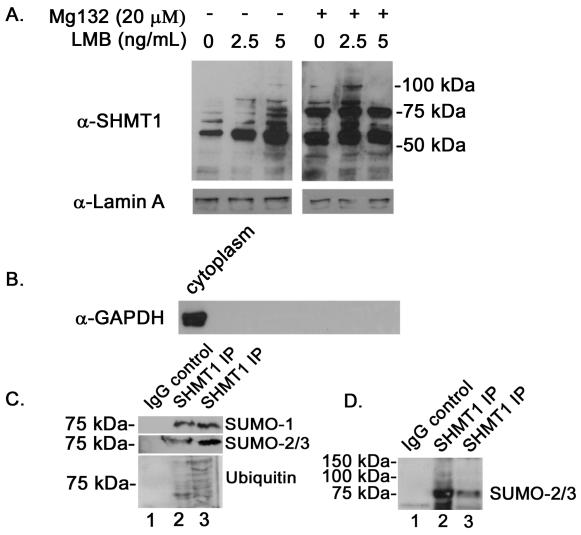

Figure 4.6. Inhibition of nuclear export leads to accumulation of SHMT1 in the nucleus. Panel A: HeLa cells were treated with or without 20 μM Mg132 and varying levels of the nuclear export inhibitor, leptomycin b (LMB) for 24 hours. Nuclei were isolated from cells and lysed using SDS-PAGE loading buffer. SHMT1 immunoblots were completed as described in figure legend 4.2. Lamin A immunoblots were performed to control for loading. Panel B: Nuclear purity was assessed by GAPDH immunoblotting. Panel C: SHMT1 immunoprecipitations were performed using nuclear extracts from cells treated with 2.5 ng/mL LMB (lane 2) or 2.5 ng/mL LMB and 20 μM Mg132 (lane 3) as described in figure 3. Non-immune IgG was used as a negative control for samples treated as in lane 3. Panel D: SHMT1 immunoprecipitations were performed using nuclear extracts from cells treated with 2.5 ng/mL LMB (lane 3) or 2.5 ng/mL LMB and 20 μM Mg132 (lane 2). Non-immune IgG was used as a negative control for samples treated as in lane 2. A darker exposure shows the presence of multiple higher molecular weight SHMT1-SUMO-2/3 conjugates in samples treated with Mg132.

In the LMB treated cells without Mg132, nuclear extracts accumulated higher molecular weight SHMT1 immunoreactive bands consistent with canonical ubiquitination ladders (Figure 4.6A). These were identified as Ub-SHMT1 through immunoprecipitation (Figure 4.6C). An increase in nuclear SUMO-2/3-SHMT1 conjugates and Ub conjugates were observed in the samples treated with LMB and Mg132 (Figure 4.6C and 4.6D). These data demonstrate that nuclear Ub-SHMT1 conjugates accumulate when SHMT1 nuclear export is inhibited, and that mixed SUMO-2/3 and Ub SHMT1 conjugates accumulate when both SHMT1 nuclear export and degradation are impaired, indicating a role for Ub modification in nuclear export, and SUMO-2/3 modification in SHMT1 degradation.

K63 polyubiquitination of SHMT1 is cell cycle and compartment specific – Ubc13 has been reported to interact with SHMT1 (2), which catalyzes the formation of K63 linked polyUb chains and is important for exporting p53 out of the nucleus (12). The cell cycle dependency and compartment specificity of SHMT1 K63 Ub linkages was determined in nuclear and cytosolic fractions of HeLa cells. K63 ubiquitination was present in S and G2/M while absent from G1 in both nuclear and cytosolic fractions. SHMT1 K63 polyubiquitination was extensive in the nuclear fraction (Figure 4.7B) while only bands consistent with di-ubiquitination were observed in the cytosolic fraction (Figure 4.7A). K63 ubiquitination of SHMT1 exhibited a distinct cell cycle profile in both the cytosolic and nuclear fractions compared to ubiquitination in general (Figures 4.7 & 4.1C).

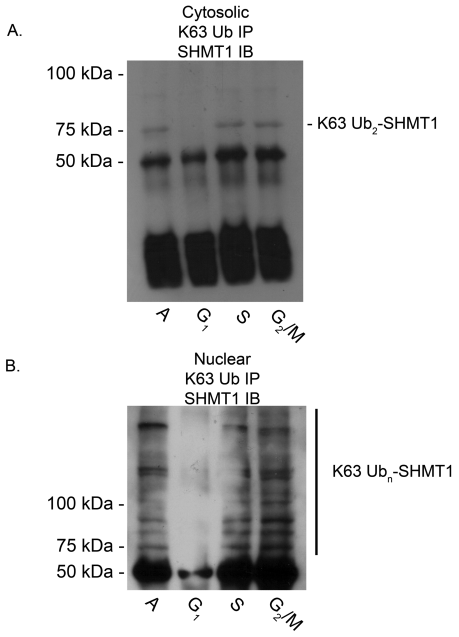

Figure 4.7. K63 polyubiquitination of SHMT1 is cell cycle and compartment specific. HeLa cells were treated with cell cycle blocking agents as reported above. Nuclear and cytosolic fractions were isolated and immunoprecipitation against K63-linkage specific Ub were performed. Antibody protein complexes were isolated from 20 μg of extract protein using protein g conjugated dynabeads. Immunoblots were performed against SHMT1 as described in figure legend 4.2. In the cytosolic fraction, K63 linked diUb was the most prevalent band and was diminished in G1 phase compared to S and G2/M phases. In the nuclear fraction, extensive K63 polyubiquitination was observed in S and G2/M phases. K63 ubiquitination was diminished in G1 phase in the nuclear fraction.

Ubc13 affects SHMT1 nuclear accumulation – To determine if Ubc13 mediates nuclear accumulation and/or SHMT1 half-life within the nucleus, a SHMT1-YFP expressing vector, and either an Ubc13-expressing vector or Ubc13 siRNA were co-expressed in the presence and absence of LMB (Figure 4.8).

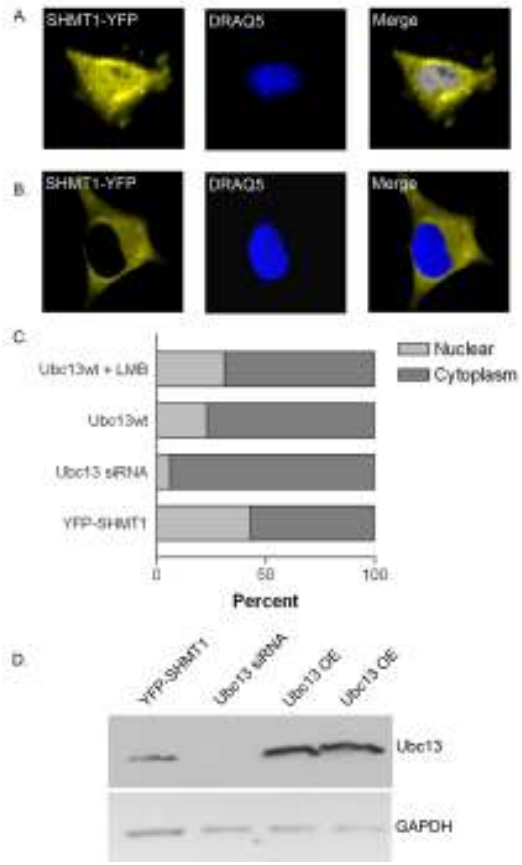

Figure 4.8. Ubc13 affects nuclear accumulation of SHMT1. Expression vectors encoding SHMT1-YFP, Ubc13, or siRNA against Ubc13 were transfected into HeLa cells. Cells were visualized using confocal microscopy with DRAQ5 as the nuclear control. Cells with nuclear SHMT1 (Panel A) versus cytosolic (Panel B) were counted (n = 100) for each of the following treatments: YFP-SHMT1 with endogenous Ubc13 levels; YFP-SHMT1 and Ubc13 siRNA; YFP-SHMT1 and Ubc13 overexpression; and YFP-SHMT1 with Ubc13 overexpression and leptomycin b treatment (LMB). (Panel C) YFP-SHMT1 samples with endogenous Ubc13 levels exhibited highest number of cells exhibiting nuclear SHMT1 (43%). Overexpression of Ubc13 with LMB treatment had intermediate levels (31%) between endogenous Ubc13 and Ubc13 overexpression alone (23%). Treatment with siRNA directed against Ubc13 exhibited the lowest number of cells with nuclear SHMT1 (6%). (Panel D) Immunoblotting was performed on 20 µg of total cell extract to ensure Ubc13 knockdown and over-expression in cells with GAPDH as a loading control.

43% of cells expressing YFP-SHMT1 with endogenous levels of Ubc13 accumulated SHMT1 in the nucleus. Ubc13 over-expression led to fewer cells with nuclear SHMT1 (23%), indicating a role for Ubc13 in nuclear SHMT1 accumulation. Ubc13 overexpression with LMB treatment restored nuclear SHMT1 levels to 31%, which is statistically greater than observed for non-LMB treated samples (t-test, $p<0.0001$, n=100) indicating a role for Ubc13 in facilitating SHMT1 nuclear export. Alternatively, overexpression of Ubc13 may have antagonistic affects on Ubc9 in the cytosol, although LMB would not be expected to restore nuclear SHMT1 if that were the case. Depletion of Ubc13 by siRNA treatment strongly inhibited SHMT1 accumulation in the nucleus with only 6% of cells exhibiting nuclear SHMT1. This may reflect competition between Ubc9 and Ubc13 in the nucleus leading to Sumo2/3 mediated SHMT1 degradation. The effects were not due to cell cycle differences as determined by cell sorting (unpublished data). These data suggest that Ubc13 may be playing a role in both stabilization of SHMT1 within nuclei and export of SHMT1 out of nuclei.

Ubc13 affects cytosolic but not nuclear turnover of SHMT1 – To determine if Ubc13 stabilizes SHMT1 in the nucleus and the cytosol, the effect of Ubc13 expression on SHMT1 half-life was determined (Figure 4.9).

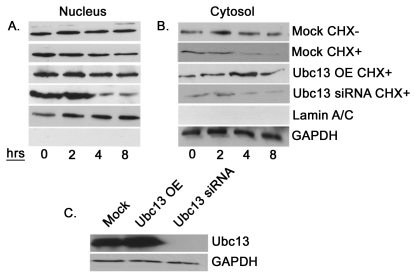

Figure 4.9. Ubc13 effects cytosolic turnover but not nuclear turnover of SHMT1. HeLa cells were subjected to mock, cDNA encoding Ubc13, or Ubc13 siRNA transfections and subjected to 50 µg/mL CHX for the times indicated. Nuclei and cytosol were isolated. A)SHMT1 was stable within the nucleus in all samples except for Ubc13 siRNA treated. B) Cytosolic SHMT1 was less stable within the cytosol. Ubc13 overexpression and knockdown increased half-life of SHMT1 C) To ensure that Ubc13 over-expressed and was knocked down, immunoblotting against Ubc13 on samples treated with cycloheximide for 8 hours was performed. GAPDH was used as a loading control.

SHMT1 was stable in nuclear extracts from cells treated with cycloheximide except for cells treated with Ubc13 siRNA, supporting the hypothesis that Ubc9 and Ubc13 compete for SHMT1 modification leading to either degradation in the nucleus or nuclear export respectively. In cytoplasmic extracts, cells over-expressing Ubc13 exhibited elevated SHMT1 levels and increased SHMT1 stability, indicating that UBC9 mediated SHMT1 K63 modification protects SHMT1 from degradation in the cytoplasm. Ubc13 knockdown led to a decrease in SHMT1 stability in the cytosolic fraction again supporting a role for K63 ubiquitination in stabilizing SHMT1 in the cytoplasm and nucleus.

K48R and K63R ubiquitin mutants affect cytosolic and nuclear SHMT1 turnover. Ubc13 functions in K63 Ub linkages, whereas the major Ub linkage implicated in degradation are K48 modifications. To determine the role of K63 and K48 Ub modifications on SHMT1 stability, K48 and K63 mutant Ub proteins were expressed in cells and their effect on SHMT1 stability determined in the cytoplasmic and nuclear compartments. SHMT1 levels were stable in nuclear extracts from cells transfected with either K48R or wild-type Ub, indicating that K48 linked Ub is not involved in nuclear SHMT1 stability (Figure 4.10A). However, SHMT1 was stable in cytosolic extracts from cells expressing K48R Ub compared to extracts from cells expressing wild type Ub, indicating a role for K48 Ub linkages in SHMT1 turnover in the cytoplasm (Figure 4.10A). In contrast, SHMT1 stability was unaffected in cytoplasmic extracts expressing K63R Ub relative to cytosolic extracts from cells expressing wild type Ub, indicating that SHMT1 K63 Ub modification does not play a role in SHMT1 stability in the cytoplasm. However, SHMT1 stability was decreased in nuclear extracts from cells expressing K63R Ub relative to cytosolic extracts from cells expressing wild type Ub, indicating a protective role for K63 Ub modification of SHMT1 in the nucleus. These data indicate that SHMT1 is degraded via K48 polyubiquitination only in the cytoplasm, whereas K63 Ub modification is necessary for SHMT1 stability in the nucleus.

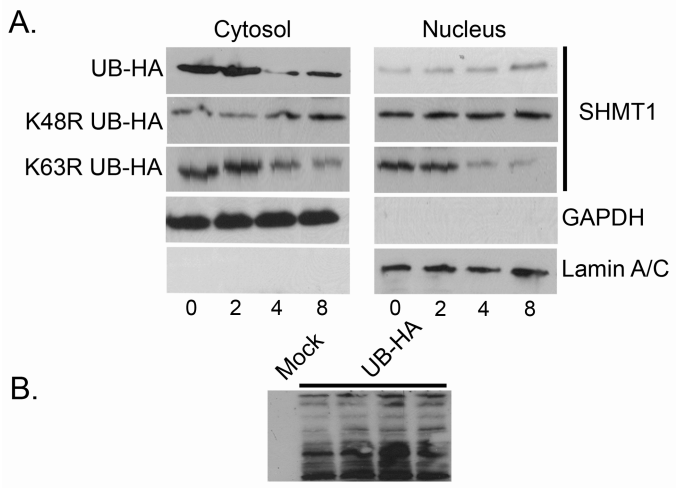

Figure 4.10. Ub K63 modifications enhance SHMT1 stability in the nucleus, whereas Ub K48 modifications decrease SHMT1 stability in the cytoplasm. HeLa cells were transfected with expression vectors encoding HA-Ub, HA-K48R Ub, or HA-K63R Ub. Following transfection, the cells were subjected to 50 μg/mL CHX for the times indicated, and SHMT1 immunoblotting performed on nuclear and cytosolic fractions as described in figure legend 2. Panel A: SHMT1 was stable in nuclear extracts from cells transfected with HA-WT Ub and HA-K48R Ub whereas in HA-K63R Ub transfections decreased SHMT1 stability. In cytosolic fractions, SHMT1 stability was enhanced by transfection of HA-K48R Ub as compared to HA-WT Ub and HA-K63R Ub. Lamin A/C and GAPDH immunoblots were performed to control for nuclear and cytosolic purity and loading. Panel B: A representative figure of HA immunoblotting is shown here to validate expression.

DISCUSSION

Thymidine nucleotide synthesis and pool size is highly regulated, with expansion of the pool occuring during S-phase (13,14). As the need for dTTP diminishes towards mitotic entry; depletion of dTTP pools is a necessity to avoid growth retardation and genetic instability (7). SHMT1 expression has been shown to be rate-limiting *de novo* dTMP synthesis in both cell culture (15) and animal models (16). Previous studies have observed that DHFR is mono-ubiquitinated by MDM2 and that mono-ubiquitination lowers DHFR activity (17). However, ubiquitination of DHFR is not involved in DHFR degradation (17). TYMS degradation has also been studied and has been found to be proteasomal dependent but Ub independent (18-20). Regulation of SHMT1 levels appears to be central to determining *de novo* dTMP synthesis capacity for DNA replication and repair. Here we report that SHMT1 levels are

regulated in an Ub dependent proteasomal manner in both the cytoplasm and in the nucleus. The ubiquitination observed is cell cycle dependent with greater SHMT1 ubiquitination occurring during G1 and G2/M phases.

In this study we demonstrate the interplay of SUMOylation and ubiquitination for the control of SHMT1 levels within the nucleus and cytoplasm. We have previously shown that mutation of the conserved SHMT1 SUMO motif prevents SHMT1 translocation to the nucleus (4). Here we show that mutation of the conserved SUMO site leads to the stabilization of SHMT1 in cycloheximide treated samples and that there is a requirement for K39 for SHMT1 degradation. Co-localization of SHMT1 with the 20S catalytic core and 19S cap of the proteasome within the cytoplasm and nucleus indicates that SHMT1 degradation occurs in both compartments. In the cytoplasm, SHMT1 degradation is facilitated by K48 Ub linkages, whereas in the nucleus K63-linked ubiquitination prevents degradation, potentially by blocking Ubc9-mediated Sumo2/3 modification (Figure 4.11) This finding suggests that K63-linked ubiquitination may occur within the nucleus once SUMO1 modification that is required for nuclear import is removed and leads to the export of SHMT1 from the nucleus to the cytoplasm.

Our proposed model for the interplay between ubiquitination and SUMOylation is as follows: following the SUMO-1 dependent import of SHMT1 within the nucleus, the SUMO-1 moiety can be removed from the SUMO consensus motif of SHMT1 by the action of SUMO proteases (SENPs) (Figure 4.11). Following removal, ubiquitination can occur via Ubc13 creating K63 Ub linkages. Although some K63 linked Ub modifications have been observed to be signals for proteasomal degradation (21), our data does not support that hypothesis for SHMT1. Total cellular SHMT1 protein levels decline during G1 and G2/M phases with a

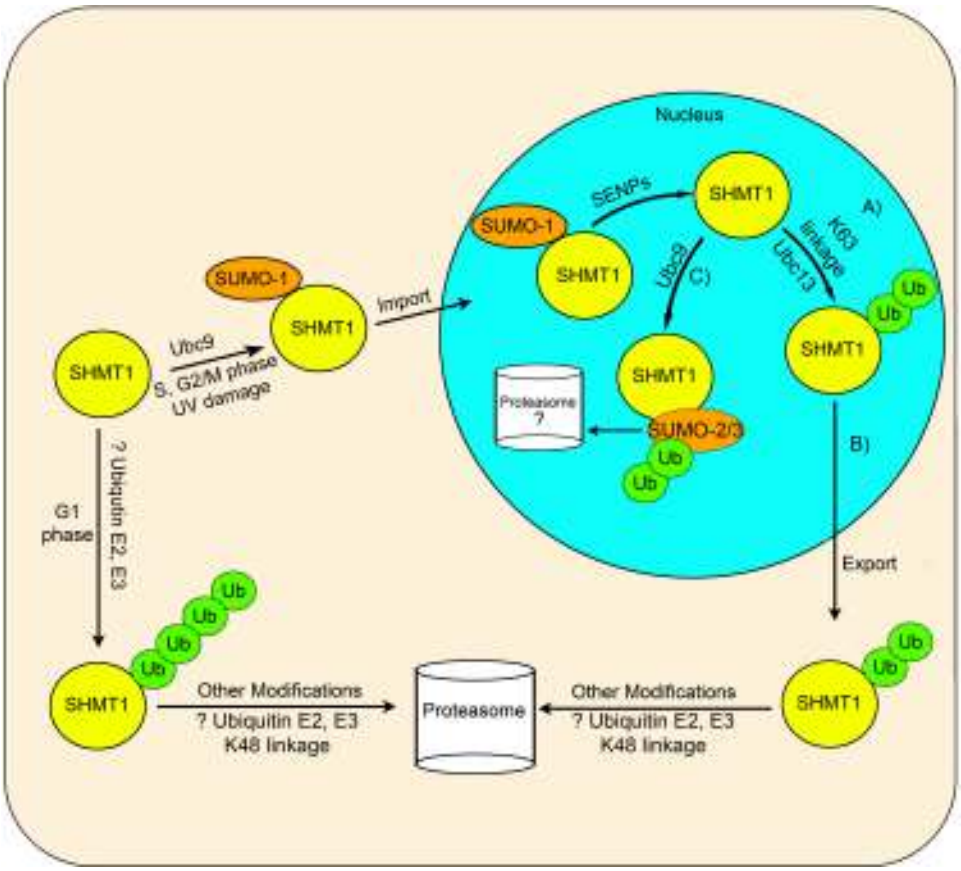

Figure 4.11. Interactions among SHMT1 ubiquitination and SUMOylation. In this model, SUMO-1 is conjugated to SHMT1 by Ubc9 during S, G2/M phases and in response to UV damage which leads to nuclear import. The Ub E2 conjugase Ubc13 acts to A) stabilize SHMT1 within the nucleus and B) signals nuclear export of SHMT1 through K63 specific Ub linkage. Following nuclear export, SHMT1 is degraded via the proteasome in a K48 Ub linkage specific manner by unknown Ub pathway E2s and E3s in the cytoplasm. C) Ubc9 catalyzes the formation of SUMO-2/3 conjugates which may be involved in nuclear SHMT1 degradation as SHMT1 accumulates in the nucleus when nuclear export is blocked and proteasomal degradation is inhibited. Ubiquitination of SHMT1 also increases in the nucleus following proteasome inhibition. Following SUMO-2/3 addition to SHMT1, ubiquitination may occur in mixed SUMO/Ub chains mediating SHMT1 degradation. Degradation of SHMT1 may occur in both nuclear and cytosolic compartments.

concomitant increase in ubiquitination, which reflects predominately K48 linkages in the cytoplasm (Fig 4.2). K63 ubiquitination occurs most during S and G2/M phases but is absent in G1 phase. K63 linked ubiquitination seems to serve a role as a mediator of SHMT1 export, as is the case for p53 protein (22) and also as an important factor in maintaining SHMT1 stability within the nucleus. Alternatively, K63 ubiquitination may act as a way to retain

SHMT1 in the nucleus. More research must be done in order to more fully understand these processes.

SHMT1 is also a substrate for UBC-9 mediated SUMOylation with SUMO-2/3. Here we propose that mixed SUMO-2/3-Ub chains may be acting to mediate the proteasomal degradation of SHMT1 within the nucleus which has been observed previously for other proteins (23). The role of mixed SUMO-2/3-Ub chains seem to be compartment specific to the nucleus. Future work must be done in order to understand what other Ub pathway enzymes are required for the degradation and stability of SHMT1 within the nucleus and cytosol.

REFERENCES

1. Tibbetts, A. S., and Appling, D. R. (2010) Annu Rev Nutr **30**, 57-81
2. Woeller, C. F., Anderson, D. D., Szebenyi, D. M., and Stover, P. J. (2007) J Biol Chem **282**(24), 17623-17631
3. Anderson, D. D., Woeller, C. F., and Stover, P. J. (2007) Clin Chem Lab Med **45**(12), 1760-1763
4. Anderson, D. D., and Stover, P. J. (2009) PLoS One **4**(6), e5839
5. Fox, J. T., Shin, W. K., Caudill, M. A., and Stover, P. J. (2009) J Biol Chem **284**(45), 31097-31108
6. Herbig, K., Chiang, E. P., Lee, L. R., Hills, J., Shane, B., and Stover, P. J. (2002) J Biol Chem **277**(41), 38381-38389
7. Ke, P. Y., Kuo, Y. Y., Hu, C. M., and Chang, Z. F. (2005) Genes Dev **19**(16), 1920-1933
8. Samsonoff, W. A., Reston, J., McKee, M., O'Connor, B., Galivan, J., Maley, G., and Maley, F. (1997) J Biol Chem **272**(20), 13281-13285
9. Ulrich, H. D. (2009) DNA Repair (Amst) **8**(4), 461-469
10. Lafarga, M., Berciano, M. T., Pena, E., Mayo, I., Castano, J. G., Bohmann, D., Rodrigues, J. P., Tavanez, J. P., and Carmo-Fonseca, M. (2002) Mol Biol Cell **13**(8), 2771-2782
11. Brooks, P., Fuertes, G., Murray, R. Z., Bose, S., Knecht, E., Rechsteiner, M. C., Hendil, K. B., Tanaka, K., Dyson, J., and Rivett, J. (2000) Biochem J **346 Pt 1**, 155-161
12. Laine, A., Topisirovic, I., Zhai, D. Y., Reed, J. C., Borden, K. L. B., and Ronai, Z. (2006) Molecular and Cellular Biology **26**(23), 8901-8913
13. Reichard, P. (1988) Annu Rev Biochem **57**, 349-374

14. Spyrou, G., and Reichard, P. (1988) Mutat Res **200**(1-2), 37-43

15. Oppenheim, E. W., Adelman, C., Liu, X., and Stover, P. J. (2001) J Biol Chem **276**(23), 19855-19861

16. MacFarlane, A. J., Liu, X., Perry, C. A., Flodby, P., Allen, R. H., Stabler, S. P., and Stover, P. J. (2008) J Biol Chem **283**(38), 25846-25853

17. Maguire, M., Nield, P. C., Devling, T., Jenkins, R. E., Park, B. K., Polanski, R., Vlatkovic, N., and Boyd, M. T. (2008) Cancer Res **68**(9), 3232-3242

18. Melo, S. P., Yoshida, A., and Berger, F. G. (2010) Biochem J **432**(1), 217-226

19. Pena, M. M., Melo, S. P., Xing, Y. Y., White, K., Barbour, K. W., and Berger, F. G. (2009) J Biol Chem **284**(46), 31597-31607

20. Pena, M. M., Xing, Y. Y., Koli, S., and Berger, F. G. (2006) Biochem J **394**(Pt 1), 355-363

21. Saeki, Y., Kudo, T., Sone, T., Kikuchi, Y., Yokosawa, H., Toh-e, A., and Tanaka, K. (2009) Embo J **28**(4), 359-371

22. Laine, A., Topisirovic, I., Zhai, D., Reed, J. C., Borden, K. L., and Ronai, Z. (2006) Mol Cell Biol **26**(23), 8901-8913

23. Schimmel, J., Larsen, K. M., Matic, I., van Hagen, M., Cox, J., Mann, M., Andersen, J. S., and Vertegaal, A. C. (2008) Mol Cell Proteomics **7**(11), 2107-2122

CHAPTER 5

SHMT1 and SHMT2 anchor the nuclear de novo thymidylate synthesis pathway to the nuclear lamina for DNA replication and repair

Introduction

Regulation of cellular dTTP synthesis is essential for DNA replication and genome stability in the nucleus (1) and mitochondria (2). Depressed *de novo* thymidylate synthesis, resulting from folate deficiency or anti-folates results in deoxyuridine misincorporation into nuclear DNA leading to genome instability (3). Tetrahydrofolate (THF) is a metabolic cofactor that carries and activates single carbons for the synthesis of purine and thymidine nucleotides, and for homocysteine remethylation to methionine (4). Folate-mediated one-carbon metabolism is compartmentalized in the mitochondria, nucleus, and cytoplasm of eukaryotic cells (5). The enzymes that constitute the *de novo* thymidylate pathway include SHMT1, SHMT2α, thymidylate synthase (TYMS), and dihydrofolate reductase (DHFR). MethyleneTHF generated by SHMT is the one-carbon donor for the TYMS catalyzed conversion of dUMP to thymidylate generating dihydrofolate (DHF). DHFR catalyzes the NADPH-dependent reduction of DHF to regenerate THF for subsequent cycles of *de novo* thymidylate synthesis (Figure 1). SHMT1, TYMS, and DHFR have been localized to the nucleus, and their translocation is mediated by a post-translational modification by the small ubiquitin-like modifier (SUMO) (6,7). SHMT1 nuclear translocation is cell cycle dependent and occurs during the S and G2/M phases and in response to UV damage (7-9). Intact purified nuclei from mouse liver exhibit *de novo* thymidylate synthesis activity, whereas nuclei disrupted by sonication lack this activity indicating that multienzyme complex formation may be required for the pathway to function (6).

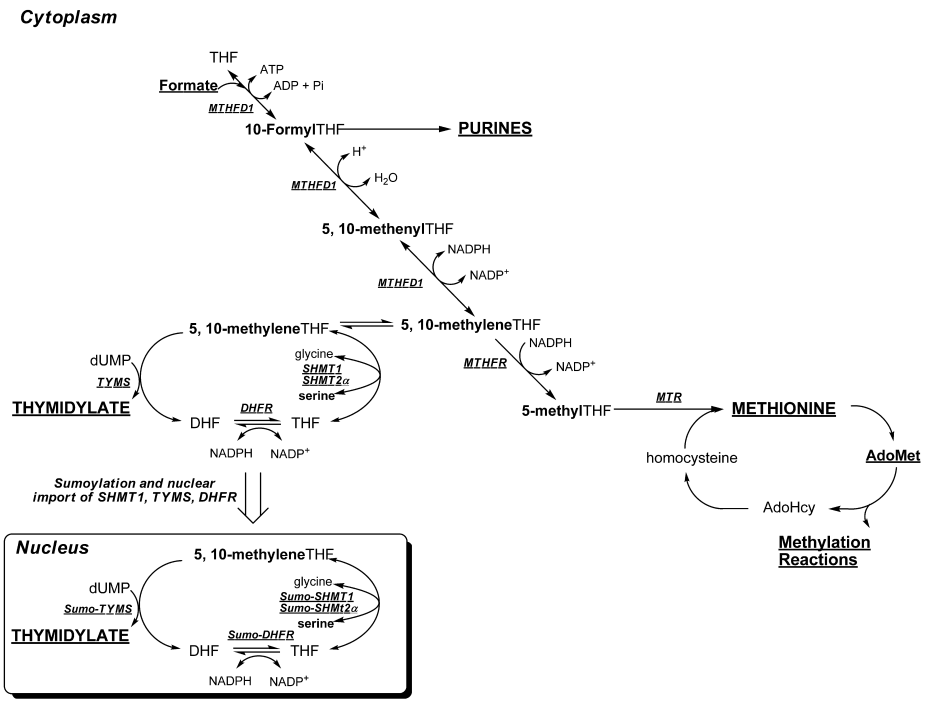

Figure 5.1. Folate Mediated One-carbon metabolism**.** Schematic of folate-mediated one-carbon metabolism in the cytoplasm and nucleus. One-carbon metabolism is required for the *de novo* synthesis of purines and thymidylate, and for the remethylation of homocysteine to methionine. The de novo thymidylate pathway is sumoylated and translocates to the nucleus during S-phase. MTHFD1, Methylenetetrahydrofolate Dehydrogenase; MTR, Methionine Syntase; MTHFR, Methylenetetrahydrofolate Reductase; SHMT1, Cytoplasmic Serine Hydroxymethyltransferase; SHMT2α, Serine Hydroxymethyltransferase 2α; TYMS, Thymidylate Synthase; DHFR, Dihydrofolate Reductase.

Previous studies in cell culture and mouse models have shown that SHMT1 expression determines *de novo* thymidylate synthesis activity, indicating that this enzyme is limiting for *de novo* thymidylate synthesis *in vivo* (10,11). In mammals, there are two SHMT isozymes encoded by distinct genes (12-14). *SHMT1* encodes the cytoplasmic/nuclear isozyme (SHMT1) and *SHMT2* encodes mitochondrial (SHMT2) and cytoplasmic/nuclear (SHMT2α) isoform through alternative promoter use (6,12-14). The primary SHMT2 transcript encodes a mitochondrial leader sequence derived from exon 1 of the *SHMT2* gene. The SHMT2 gene contains a second promoter within intron 1 that generates a second transcript that lacks exon 1 but contains a conserved initiator methionine within Exon 2 (6). This second transcript

encodes SHMT2α, a cytoplasmic/nuclear SHMT isozyme that provides functional redundancy within the *de novo* thymidylate synthesis pathway. SHMT2α accounts for 25% of *de novo* thymidylate biosynthesis activity in purified mouse liver (6).

Recent evidence indicates that the formation of a multi-enzyme metabolic complex is required for *de novo* purine nucleotide biosynthesis in the cytoplasm, referred to as a purinosome. The complex includes the folate utilizing enzymes aminoimidazolecarboximide ribonucleotide formyltransferase (AICARFT), glycinamide ribonucleotide formyltransferase (GARFT), and 5,10-methenylTHF synthetase (MTHFS) (15,16). Formation of the purinosome is regulated by cell cycle, purine levels, protein kinases (17), by microtubule networks (18) and by sumoylation (16), with disruption of microtubule networks resulting in the suppression of the rate of *de novo* purine biosynthesis. Multi-enzyme complexes containing some components of the *de novo* thymidylate cycle, including ribonucleotide reductase, TYMS, and DHFR, have been identified in nuclear extracts (19,20).

Previous studies have identified SHMT1 as an interacting partner with proliferating cell nuclear antigen (PCNA), indicating that SHMT1 and the *de novo* thymidylate pathway may localize to sites of DNA synthesis (8,21). PCNA is a DNA replication and repair processivity factor which acts as a "sliding clamp" and crucial factor to localize proteins to replication forks and repair foci (22,23). *Shmt1*$^{+/-}$ mice accumulate uracil within nuclear DNA (11) and increased sensitivity to neural tube defects (24) and intestinal cancer (25). This study investigated the presence of a nuclear multi-enzyme complex that included the *de novo* thymidylate pathway, and its association with the DNA replication machinery. The results of this study demonstrate that the *de novo* thymidylate synthesis pathway is associated with nuclear lamina, and that SHMT1 or SHMT2α serve essential roles as scaffold proteins for complex formation. Furthermore, this metabolic complex is enriched at sites of DNA

replication initiation, indicating that *de novo* thymidine nucleotide synthesis occurs at the sites of DNA synthesis.

Results

SHMT1, SHMT2α, DHFR and TYMS are present in nuclei during S and G2/M phases.

SHMT1, SHMT2α, TYMS and DHFR have been localized previously to the nucleus and cytoplasm of human and mouse cell lines (2,6,8,16). Nuclear localization of SHMT1 and SHMT2α in mouse embryonic fibroblasts (MEFS) and human cell lines (6,8) is restricted to the S and G2/M phases of the cell cycle and in response to UV damage (9). In this study, the nuclear localization of TYMS and DHFR was determined as a function of cell cycle. As seen previously for SHMT1, DHFR (Figure 5.2) and TYMS (Figure 5.3) localized to the nucleus during S and G2/M phases, but not in G1 phase. These data confirm all the enzymes necessary for *de novo* thymidylate biosynthesis are present within the nucleus during S and G2/M phases. When DNA replication and repair are occurring respectively.

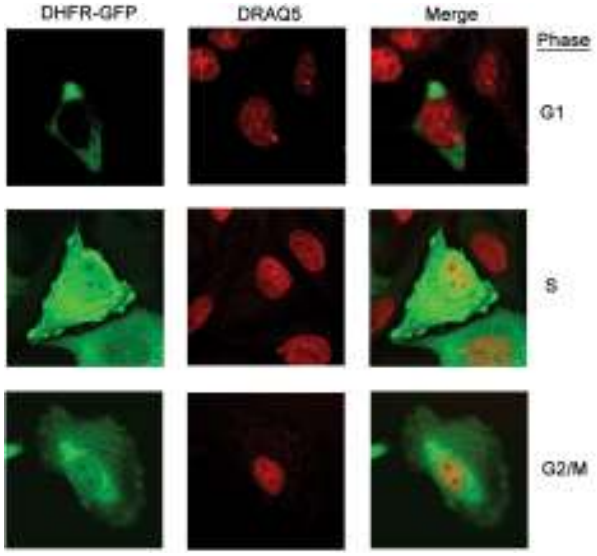

Figure 5.2. DHFR nuclear localization is cell cycle dependent. cDNAs encoding GFP-DHFR were transfected into cells and blocked in G1 (30 uM lovastatin), S phase (1 mM hydroxyurea), and G2/M (100 ng/mL nocodazole) phases of the cell cycle. DRAQ5 was used as the nuclear stain and cells were visualized with confocal microscopy. DHFR is present in nuclei during S and G2/M phases of the cell cycle.

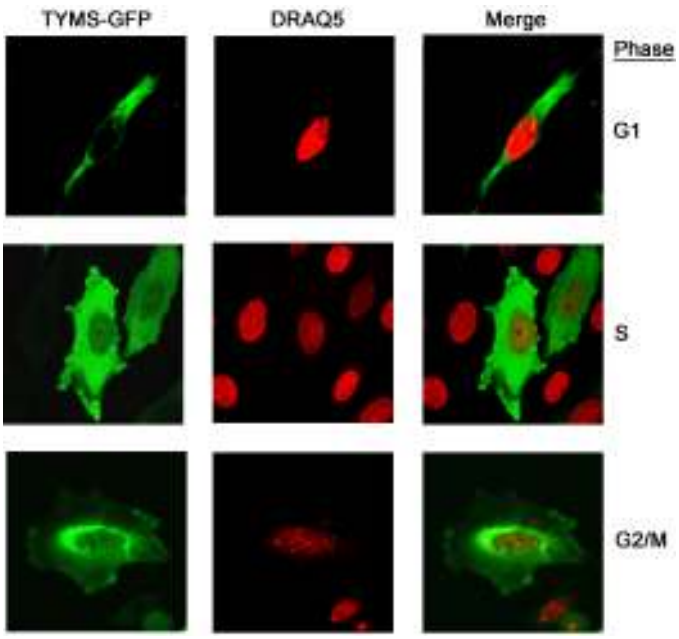

Figure 5.3. TYMS nuclear localization is cell cycle dependent. cDNAs encoding GFP-TYMS were transfected into cells and blocked in G1 (30 uM lovastatin), S phase (1 mM hydroxyurea), and G2/M (100 ng/mL nocodazole) phases of the cell cycle. DRAQ5 was used as the nuclear stain and cells were visualized with confocal microscopy. TYMS is present in nuclei during S and G2/M phases of the cell cycle.

Identification of SHMT1-interacting proteins in nuclear extracts.

Intact purified nuclei from mouse liver can convert tritium-labeled serine and dUMP to tritium-labeled thymidylate (Figure 1), but this activity is lost in sonicated nuclei, indicating that nuclear integrity and multi-enzyme complex formation may be necessary for *de novo* thymidylate synthesis (6). To determine if the *de novo* thymidylate biosynthesis pathway is present in nuclei within a multi-enzyme complex, SHMT1 tandem affinity purification and SHMT1 co-precipitation experiments were performed on benzonase-treated nuclear extracts isolated from S-phase cells and cells treated with UV (Figure 5.4). Over 833 proteins were identified as SHMT1-interacting proteins. The list was refined by excluding proteins with less than 3 peptides identified, and the remaining proteins were grouped by gene ontology term enrichment using the bioinformatics tool DAVID (Table 5.1). Multiple proteins involved in nucleotide metabolism, DNA replication, and repair were identified, as well as 80 lamin

interacting proteins. The majority of the identified proteins known to be involved in DNA replication and repair, as well as lamin interacting proteins, were found in both S-phase and UV treated samples, although some of these interactions were identified only in one of those two exposures (Table 5.1).

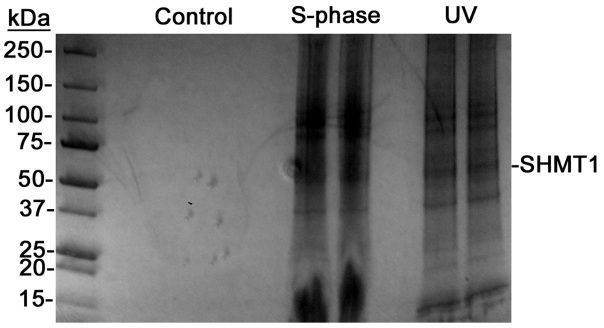

Figure 5.4. Tandem affinity purification of SHMT1. pCMV-FLAG-SHMT1-MAT-Tag-1 (S-phase and UV) and pCMV-FLAG-MAT-Tag-1 empty vector (control) were transfected into HeLa cells. Cells were treated with hydroxyurea (1 mM) for S-phase or exposed to 10 mJ/cm^2 UV. Following treatment, cells were incubated for 24 hours. Nuclei were isolated, treated with benzonase and tandem affinity purified using FLAG and Nickel resins. The lanes were excised and peptide sequences were determined using MS/MS.

Function	Protein Identification	S-phase	UV	Both
DNA repair and replication	APEX1			✓
	LIG3			✓
	LIG4		✓	
	MNAT1	✓		
	NTHL1			✓
	PCNA	✓		
	POLD3		✓	
	POLE		✓	
	PRIM1			✓
	PRIM2		✓	
	RFC1			✓
	XAB2			✓
Cell cycle	RAD21	✓		
	SKP1	✓		
	ANAPC5			✓
	ATR		✓	
	CDC27		✓	
	CUL1			✓
	CCNB1	✓		
	CCNH	✓		
	CDK4	✓		
	ATM		✓	
	STAG1			✓
	YWHAB			✓
Lamin Binding Proteins	LMNA			✓
	LMNB1			✓
	LMNB2	✓		
	DNAJA2	✓		
	BAT1	✓		
	IMO7			✓
	LIMA1			✓
	MED10	✓		
	MED14			✓
	MED19			✓
	MED22	✓		
	MED4	✓		

Table 5.1. Subsets of proteins found using tandem affinity purification and MS/MS.

Validation of SHMT1 interacting partners.

DNA replication occurs on nucleoskeletal structures (26) and disruption of the nuclear lamina results in DNA replication arrests (27,28). Several proteins involved in DNA replication are lamin-binding proteins including PCNA, which acts as a processivity factor for DNA replication (29). SHMT1 has been identified previously as a PCNA interacting partner (8), and this interaction was confirmed in this tandem affinity purification experiment (Figure 5.4, Table 5.1). To validate SHMT1 as a lamin interacting partner, co-immunoprecipitation experiments using benzonase-treated nuclear extracts were performed with antibodies against either Lamin A/C or Lamin B1. SHMT1 co-precipitated with Lamin A/C and Lamin B1 antibodies under stringent (650 mM NaCl) and less stringent conditions (150 mM NaCl) (Figure 5.5A). Neither TYMS or DHFR co-precipitated with lamin proteins under these conditions.

Other SHMT1 interacting partners identified in table 1 were validated by co-immunoprecipitation followed by immunoblotting against the interacting protein. SHMT1, TYMS, and DHFR all co-precipitated with PCNA in nuclear extracts (Figure S4A, B, C), but not in cytoplasmic extracts (Figure 5.6A, and B). Lysine demethylase 1 (KDM1), which has been recently identified as a folate binding protein (30), immunoprecipitated with anti-SHMT1 antibodies (Figure 5.6D). Other proteins involved in DNA replication and repair including DNA polymerases δ and ε (POLD and POLE respectively), replication factor C activator 1 (RFC1), and uracil DNA glycosylase 2 (UNG2) (Figure 5.6E) all co-immunoprecipitated with SHMT1. In total, 8 validations were performed and no false positives were identified.

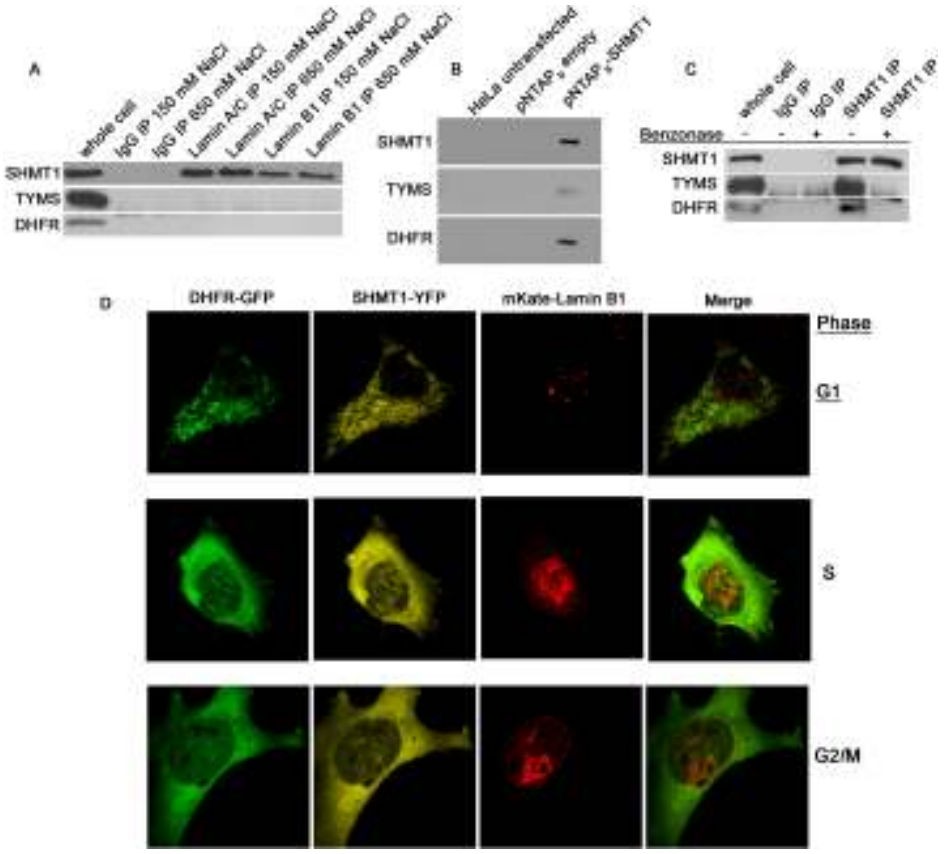

Figure 5.5. SHMT1 is a nuclear lamin associated protein**.** A) Both Lamin A/C and Lamin B1 co-immunoprecipitations from benzonase-treated nuclar extracts contained SHMT1 even in high salt conditions (650 mM NaCl), whereas neither TYMS or DHFR immumoprecipitated even under low salt conditions (150 mM NaCl). B) pNTAPb-SHMT1 and pNTAPb empty vectors were transfected into HeLa cells and tandem affinity purification was performed using streptavidin and calmodulin resins. SHMT1, TYMS, and DHFR were detected in pNTAPb-SHMT1 transfections in samples that were not treated with nucleases. C) The DNA dependence of SHMT1, TYMS, and DHFR interactions were determined by SHMT1 immunoprecipitation in purified nuclear extracts treated with or without benzonase. TYMS and DHFR only immunoprecipitated with SHMT1 in samples lacking benzonase treatment. D) The interaction of SHMT1, laminB1 and DHFR was investigated by confocal microscopy following transfection of cDNAs encoding GFP-DHFR, SHMT1-YFP, and mKate-LaminB1 fusion proteins in cells blocked in G1 (30 uM lovastatin), S phase (1 mM hydroxyurea), and G2/M (100 ng/mL nocodazole) phases of the cell cycle. Co-localization of DHFR and SHMT1 with LaminB1 is concomitant with nuclear localization of DHFR and SHMT1 during S and G2/M, but not during G1 phases of the cell cycle.

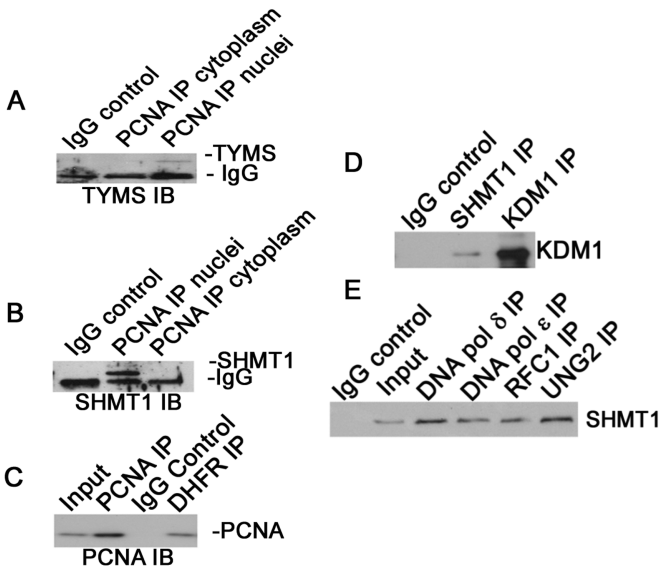

Figure 5.6. Further validation of SHMT1 interacting partners. Nuclear (A,B, C, and D) and cytosolic fractions (A and B) of HeLa cells were isolated and subjected to immunoprecipitations. A) TYMS and B) SHMT1 co-precipitated with PCNA only in nuclear fractions. C) Nuclear fractions were subjected to PCNA, control, or DHFR immunoprecipitations. PCNA co-precipitates with DHFR, but not in control IgG. D) SHMT1 co-immunoprecipitates with KDM1 but not in IgG controls. E) SHMT1 co-immunoprecipitates with DNA polymerases δ and ε, RFC1, and UNG2, but not in IgG controls.

SHMT1 interaction with TYMS and DHFR is DNA dependent.

Neither TYMS nor DHFR were identified as SHMT1- or lamin-interacting proteins by tandem affinity purification. The ability of nuclear SHMT1 to interact with TYMS and DHFR in the absence of DNA digestion was determined by co-precipitation with SHMT1 in small scale tandem affinity purification (Figure 5.5B) and SHMT1 immunoprecipitation (Figure 5.5C). In the tandem affinity purification, both TYMS and DHFR co-precipitated with SHMT1 in the absence of benzonase treatment (Figure 5.5B). However, neither TYMS nor DHFR co-precipitated with SHMT1 in nuclear extracts treated with benzonase, whereas in the absence of benzonase treatment, co-immunoprecipitates contained TYMS and DHFR (Figure 5.5C).

Co-localization of the de novo thymidylate biosynthesis pathway with Lamin B1.

The co-localization of the *de novo* thymidylate biosynthesis pathway with the nuclear lamina was investigated by confocal microscopy. HeLa cells transfected with pCMV6-AC-DHFR-GFP, phiYFP-N-SHMT1, and mKate2-LaminB1 expression plasmids exhibited co-localization of Lamin B1, SHMT1, and DHFR fusion proteins in filament-like linear structures and clusters in S and G2/M phases of the cell cycle (Figure 5.5D). To control for potential artifacts resulting from Lamin B1 fusion protein expression, confocal microscopy was performed on HeLa cells following transfection of pCMV6-AC-DHFR-GFP (Figure 5.7A), pCMV6-AC-TYMS-GFP (Figure 5.7B and 5.7C), or phiYFP-N-SHMT1 (Figure 5.7C) plasmids.

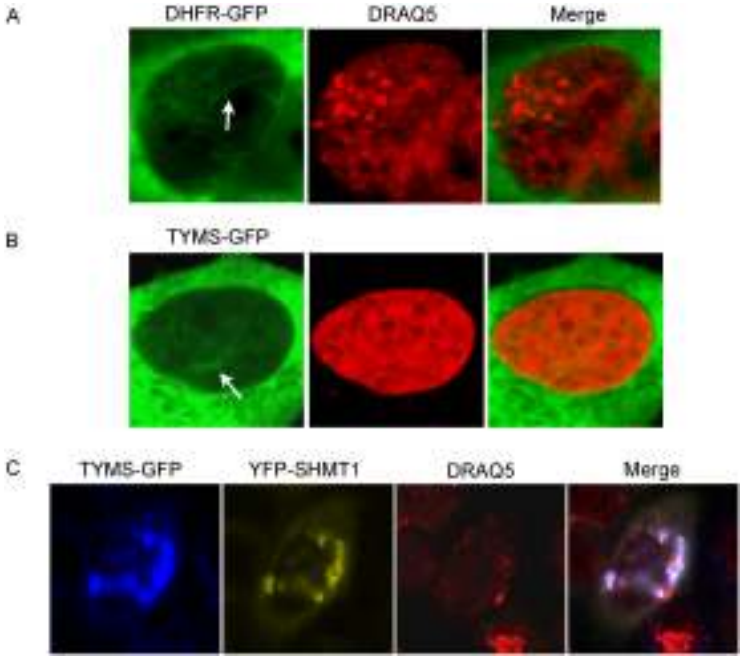

Figure 5.7. TYMS, DHFR, and SHMT1 localize to linear structures within nuclei regardless of LaminB1 over-expression. cDNAs encoding A) GFP-DHFR, B) and C) GFP-TYMS, and C) YFP-SHMT1 were transfected into HeLa cells. DRAQ5 was used as the nuclear stain to control for LaminB1 over-expression causing aggregation. Cells were visualized with confocal microscopy. Over-expression of LaminB1 in cells is not a requirement for visualization of linear structures within nuclei. DHFR, TYMS, and SHMT1 all form linear structures (white arrows) within nuclei.

All three fusion proteins, which constitute the *de novo* thymidylate biosynthesis cycle, co-localized as linear structures within nuclei demonstrating that the formation of these structures was not of the result of Lamin B1 over expression.

Formation of the thymidylate biosynthesis complex is nucleotide independent.

Previous studies have demonstrated that the assembly of the purinosome, a cytoplasmic multi-enzyme complex comprised of the *de novo* purine biosynthesis enzymes, is regulated by levels of purines within the cell (16,31). The effect of nucleotides on multi-enzyme complex formation of the *de novo* thymidylate biosynthesis pathway in nuclei was determined in HeLa cells grown in media lacking all nucleotides (DMEM), lacking deoxyuridine (dU), lacking thymidine (dT), or media replete with nucleotides (αMEM) following transfection with the plasmids pCMV6-AC-TYMS-GFP, phiYFP-N-SHMT1, and mKate2-LaminB1 (Figure 5.8). The presence or absence of nucleosides in the culture media did not affect the co-localization of SHMT1, TYMS, and Lamin B1 as determined by confocal microscopy, demonstrating that formation of the observed linear structures is independent of nucleoside availability.

SHMT1 and SHMT2α are required for DHFR, TYMS and Lamin B1 co-localization.

The lamin-binding property of SHMT1 and the lack of interaction among TYMS and DHFR and lamins suggested that SHMT1 and/or SHMT2α may function as scaffold proteins required for DHFR and TYMS localization to the lamina and assembly of the *de novo* thymidylate synthesis pathway complex. Therefore, the co-localization of TYMS and DHFR with nuclear lamins was investigated in the absence of SHMT. DHFR-GFP and mKate-LaminB1 (Figure 5.9A) or TYMS-GFP and mKate-LaminB1 (Figure 5.10A) co-localized in HeLa cells transfected with scrambled siRNA in 95% of the observed cells, but was reduced to 50% and 75% respectively of cells treated with SHMT2 siRNA. Lamin B1 and DHFR or TYMS co-localizing structures were observed in only 5% and 14% respectively of cells treated with SHMT1 siRNA, and were absent in SHMT1 and SHMT2 siRNA treated samples.

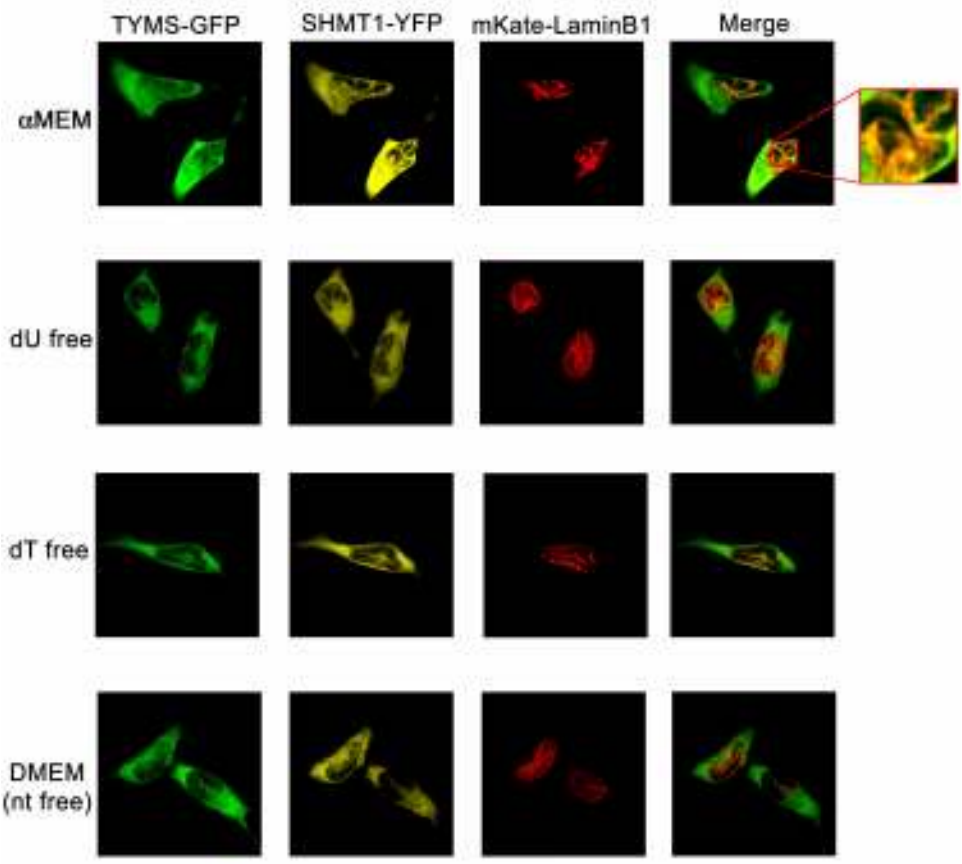

Figure 5.8. SHMT1 and TYMS form linear lamin B1 co-localizing structures in a non-substrate specific manner. The cDNAs encoding YFP-SHMT1, TYMS-GFP, and mKate-LaminB1 fusion proteins were transfected into cells grown in media containing nucleotides (α-MEM), no nucleotides (DMEM), and α-mem lacking either deoxyuridine (dU) or thymidine (dT) and visualized with confocal microscopy. The co-localization of SHMT1 and TYMS with LaminB1 was independent of nucleotides in the culture medium.

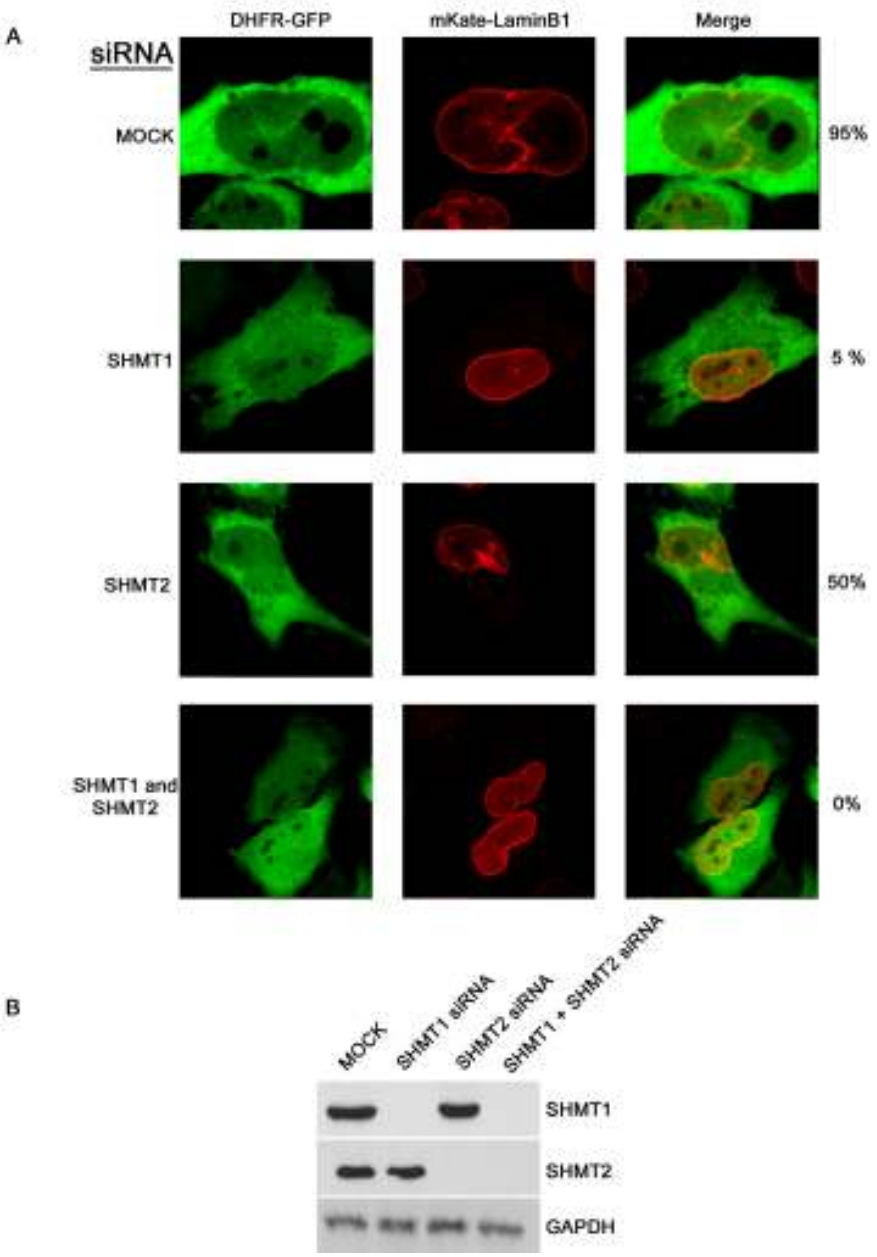

Figure 5.9. SHMT1 and SHMT2 are required for DHFR and Lamin B1 co-localization. A) cDNAs encoding GFP-DHFR, mKate-Lamin B1, and siRNAs including scrambled (mock) SHMT1, SHMT2, or both SHMT1 and SHMT2 were transfected into HeLa cells. Cells were blocked in S-phase using hydroxyurea (2 mM) and visualized with confocal microscopy. For each siRNA treatment, 100 cells were counted. The presence of DHFR and Lamin B1 co-localizing structures occurred in 95%, 5%, 50%, and 0% of cells transfected with scrambled, SHMT1, SHMT2, and both SHMT1 and SHMT2 siRNAs respectively. B) Immunoblotting was performed on siRNA treated samples to ensure knockdown of SHMT1 and SHMT2. GAPDH was used as a loading control.

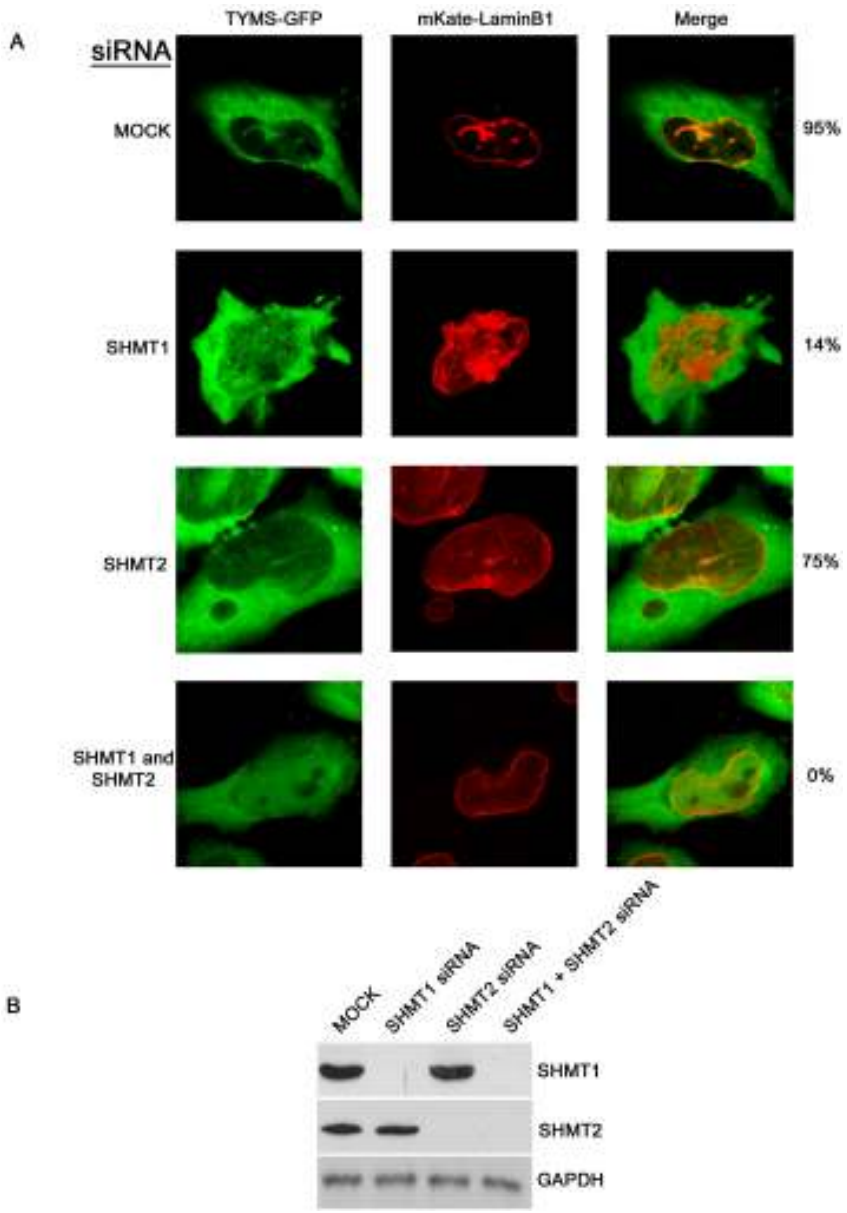

Figure 5.10. SHMT1 and SHMT2 are required for TYMS and Lamin B1 co-localization. A) cDNAs encoding GFP-TYMS, mKate-Lamin B1 fusion proteins and siRNAs including scrambled (mock) SHMT1, SHMT2, or both SHMT1 and SHMT2 were transfected into HeLa cells. Cells were blocked in S-phase using hydroxyurea (2 mM) and visualized with confocal microscopy. For each siRNA treatment, 100 cells were counted. The presence of DHFR and Lamin B1 co-localizing structures occurred in 95%, 14%, 75%, and 0% of cells transfected with scrambled, SHMT1, SHMT2, and both SHMT1 and SHMT2 siRNAs respectively. B) Immunoblotting was performed on siRNA treated samples to ensure knockdown of SHMT1 and SHMT2. GAPDH was visualized as a loading control.

Immunoblotting was performed against SHMT1 and SHMT2 to ensure that the knockdown of those enzymes had occurred (Figures 5.9B and 5.10B). These data demonstrate that SHMT1 or SHMT2α function as scaffolds that are required for TYMS and DHFR co-localization with Lamin B1.

TYMS, DHFR, and SHMT2 do not affect SHMT1 and Lamin B1 co-localization.

The effect of TYMS, DHFR, and SHMT2 on SHMT1 co-localization with Lamin B1 was investigated in HeLa cells expressing SHMT1-YFP and mKate-LaminB1 (Figure 5.11A). Lamin B1 and SHMT1 co-localized independent of TYMS, DHFR or SHMT2 expression which was reduced by siRNA treatment. Immunoblotting was performed against TYMS, DHFR, and SHMT2 to ensure that the knockdown of those enzymes had occurred (Figure 5.11B). These data demonstrate that SHMT1 is essential for the *de novo* thymidylate synthesis pathway complex formation, and that SHMT1 anchors the *de novo* thymidylate pathway to Lamin B1.

SHMT2α functions as a scaffold protein independent of SHMT1

Previous studies have demonstrated that SHMT1 and SHMT2α are functionally redundant in *de novo* thymidylate synthesis (6). The dependency of the SHMT2α-lamin interaction on SHMT1, TYMS and DHFR was investigated in HeLa cells expressing SHMT2α-RFP and mKate-LaminB1 fision proteins (Figure 5.12A). SHMT2α and Lamin B1 co-localized independent of TYMS, DHFR and SHMT1 expression which was reduced by siRNA treatment. Immunoblotting was performed against TYMS, DHFR, and SHMT1 to ensure that the knockdown of those enzymes had occurred (Figure 5.12B). These data demonstrate that SHMT2α co-localizes with Lamin B1 even in the absence of SHMT1, further supporting the functional redundancy of SHMT2α and SHMT1 in nuclear *de novo* thymidylate synthesis.

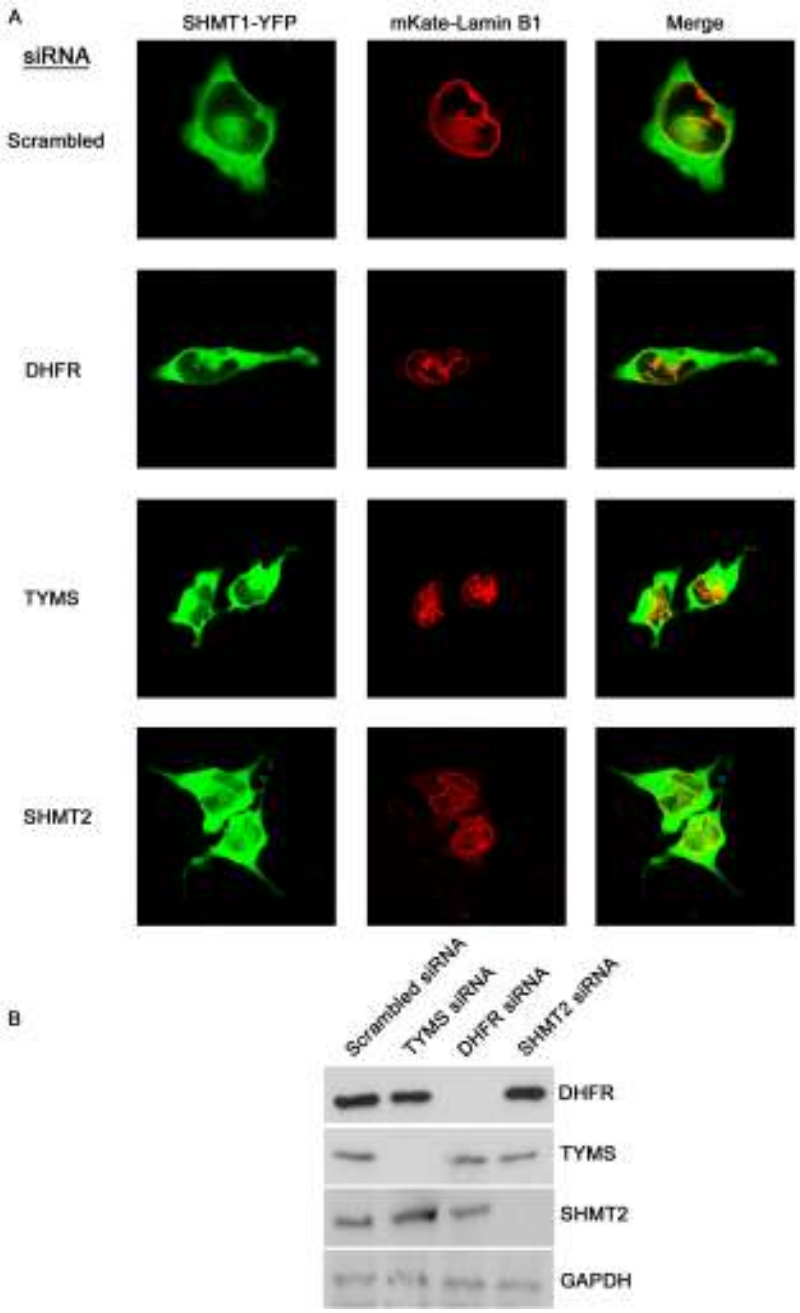

Figure 5.11. TYMS, DHFR, and SHMT2 are not requirements for SHMT1 and Lamin B1 co-localization. A) cDNAs encoding SHMT1-YFP, mKate-Lamin B1, and siRNAs including scrambled, DHFR,TYMS, or SHMT2 were transfected into HeLa cells. The formation of Lamin B1 and SHMT1 co-localizing structures was not inhibited by knockdown of DHFR, TYMS, or SHMT2. B) Immunoblotting was performed on siRNA treated samples to ensure knockdown of DHFR, TYMS and SHMT2. GAPDH was used as a loading control.

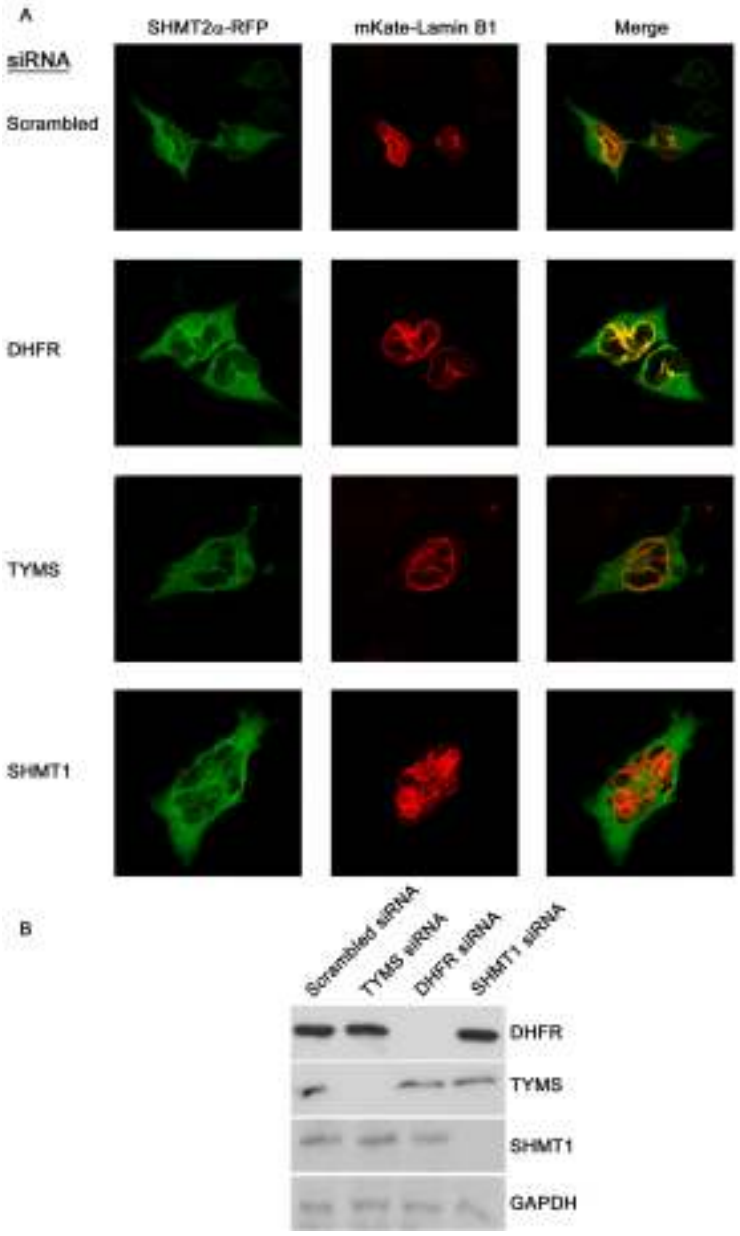

Figure 5.12. TYMS, DHFR, and SHMT1 are not requirements for SHMT2α and Lamin B1 co-localization. cDNAs encoding SHMT2α-RFP, mKate-Lamin B1, and siRNAs including scrambled, DHFR,TYMS, or SHMT1 were transfected into HeLa cells. DHFR, TYMS, and SHMT1 were not required for SHMT2α and Lamin B1 co-localization. B) Immunoblotting was performed on siRNA treated samples to ensure knockdown of DHFR, TYMS and SHMT1. GAPDH was used as a loading control.

The SHMT1 scaffold function can determine de novo thymidylate synthesis capacity.

Previous studies in SHMT1-deficient mice (11) and cell culture models (10,32) have demonstrated strong correlations between SHMT expression and *de novo* thymidylate synthesis capacity, although enzyme kinetic studies do not support that SHMT is catalytically rate-limiting in the *de novo* thymidylate biosynthesis pathway (33). To distinguish between the catalytic and scaffold contributions by SHMT1 to nuclear *de novo* thymidylate biosynthesis, a dominant negative SHMT1 protein (DN2-SHMT1) was expressed in SH-SY5Y cells that express endogenous SHMT1, and its effect on *de novo* thymidylate synthesis determined. SHMT is a tetramer, best described as a dimer of obligate dimers, in which amino acid residues from each monomer in the obligate dimer contribute to both active sites in the dimer (34,35). Previously, we have described the generation of a DN2-SHMT1 protein (Y82A/Y83F/K257Q) that dimerizes with wild type SHMT1 creating a stable protein that lacks catalytic activity in both active sites of the dimer (35). Y82 is required for hydrophobic stacking with the *p*-aminobenzoylglutamate moiety of tetrahydrofolate, and the Y82A mutation eliminates folate binding. The hydroxyl group of Y83 and K257 are required for SHMT1 catalytic activity. Transfection of dominant negative mutants into cells containing endogenous SHMT1 would result in a statistical mixture of active and inactive SHMT1 tetramers, while decreasing the specific activity of SHMT1 in the cell. Co-expression of YFP-DN2-SHMT1 and mKate-LaminB fusion proteins resulted in the formation of linear structures SHMT1-laminB structures that were indistinguishable from structures resulting from coexpression of wild-type YFP-SHMT1 and mKATE-LaminB1 coexpression (Figure 5.13A), indicating that the mutations required to generate DN2-SHMT1 did not impair its lamin binding activity. To determine the effect of DN2-SHMT1 expression on SHMT1 activity with respect to *de novo* thymidine biosynthesis and homocysteine remethylation, metabolic isotope tracer experiments were performed using [L-$^{2}H_{3}$]-serine and SH-SY5Y cells that express

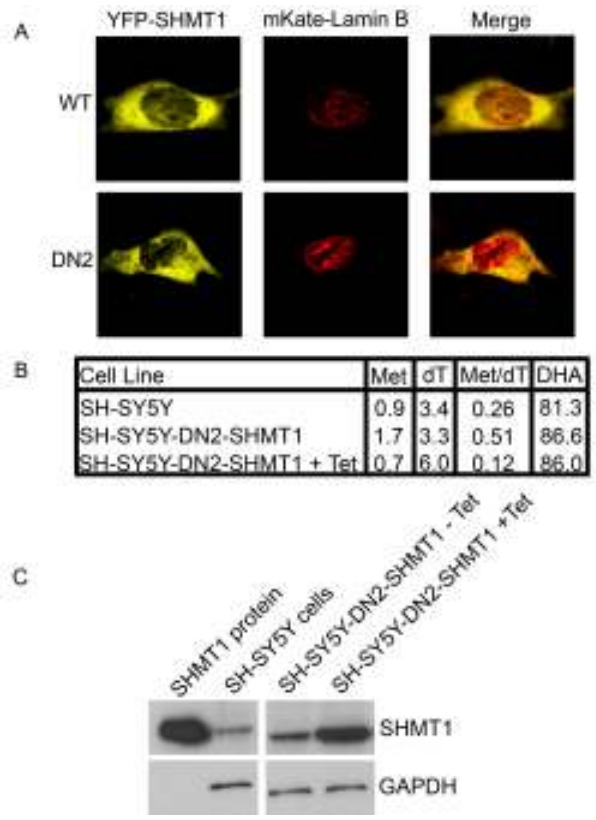

Cell Line	Met	dT	Met/dT	DHA
SH-SY5Y	0.9	3.4	0.26	81.3
SH-SY5Y-DN2-SHMT1	1.7	3.3	0.51	86.6
SH-SY5Y-DN2-SHMT1 + Tet	0.7	6.0	0.12	86.0

Figure 5.13. Dominant negative SHMT1 (DN2-SHMT1) localizes with Lamin B1 and enhances SHMT1 activity in de novo thymidylate biosynthesis. A) cDNAs encoding mKate-Lamin B1 and either YFP-SHMT1 or YFP-DN2-SHMT1 fusion proteins were expressed in HeLa cells and co-localization of the proteins determined by confocal microscopy. Both SHMT and DN2-SHMT1 colocalize with Lamin B1. B) The effect of tetracycline (tet)-inducible expression of DN2-SHMT1 on SHMT1 activity in *de novo* thymidylate biosynthesis was determined in SH-SY5Y cells. Cellular protein and DNA were isolated from cells cultured for 8 days in defined medium containing L-[2,3,3-$^2H_3$]serine. Isotopic enrichment of l-[2,3,3-$^2H_3$]serine into cellular protein pools was determined by the detection of labeled methionine (Met) and dehydroalanine (DHA). DHA is formed from serine during the assay. Enrichment of [2,3,3-$^2H_3$]serine in thymidine (dT) was determined by analysis of nuclear DNA. All values are expressed as the percent of L-[2,3,3-$^2H_3$]serine-derived carbons that contain two deuterium atoms (CD2) in the target compound (or the ratio of carbons containing two deuterium atoms in the target compound divided by the total number of carbons that contain one or two deuterium atoms × 100). Two independent experiments were performed with duplicate measurements for each sample, and identical values were obtained within each experiment. The results from one experiment are shown. The data demonstrate that tet-inducible expression of DN2-SHMT1 decreased SHMT1 specific activity in homocysteine remethylation to methionine in the cytoplasm by 60%, whereas DN2-SHMT1 expression enhances SHMT1 specific activity in de novo thymidylate biosynthesis by 45% C) Immunoblotting was performed on SH-SY5Y-DN2-SHMT1 cells in a tet inducible system. The SH-SY5Y-DN2-SHMT1 cells exhibited increased levels of total SHMT1 in response to tetracycline. These cells were used for isotopic tracer studies. GAPDH was used as a loading control.

DN2-SHMT1 from a tet-inducible promoter (36). In this assay, methylene-THF generated from [L-$^2H_3$]-serine by SHMT1 is incorporated into methionine or thymidine and retains the two deuterium atoms (CD_2) present on the hydroxymethyl group of serine. Alternatively, if [L-$^2H_3$]-serine enters the mitochondria, the hydroxymethyl group will be released from mitochondria as formate containing a single deuterium atom (CD_1) and enters the methylene-THF pool with one deuterium atom (CD1). CD2 -methyleneTHF can also be converted to CD1 methylene-THF through its reversible conversion to methenyl-THF through the activity of MTHFD1, which was identified to interact with SHMT1 in the nucleus both during S-phase and in response to UV. The effect of DN2-SHMT1 expression on CD2 enrichment in thymidine in DNA, and serine and methionine in cellular protein, was determined following culture of SH-SY5Y with [L-$^2H_3$]-serine for 8 days. Figure 5.13B shows that 81.3–86.6% of the isotopically labeled serine used for protein synthesis was unmetabolized as it retained both deuteriums on the C3 carbon in SY-SY5Y cells, and SH-SY5Y-DN2-SHMT1 cells in the presence and absence of tetracycline (Figure 1). If the methionine and thymidylate one-carbon units were only derived from SHMT1, the mass +2 species of these metabolites should be ~80% of the labeled species. Expression of DN2-SHMT1 suppressed CD2 incorporation into methionine by 60%, consistent with a loss of SHMT1 specific activity in the cytoplasm. Interestingly, CD2 incorporation into thymidine within nuclear DNA was increased by 45%, indicating that DN2-SHMT1 expression increased the flux of SHMT1-derived one-carbons into thymidylate. These results demonstrate that the lamin-binding activity and scaffold function of SHMT1 contributes more than its catalytic activity to *de novo* thymidylate biosynthesis in this cell line (Figure 5.13B).

De novo thymidylate pathway is associated with episomal DNA.

The interaction of SHMT1 and the *de novo* thymidylate cycle with proteins involved in DNA replication and repair including UNG2, RFC1, PCNA, and DNA polymerases δ and ε (Table

1, Figure 5.6E) indicates that the thymidylate biosynthesis pathway may function at the replication fork. During DNA replication initiation, RFC interacts with DNA at the primer-template junction and loads PCNA onto the DNA template which allows for the processive replication of DNA by DNA polymerases δ and ε (22). Mammalian origins of replication are not well characterized; therefore a model system of episomally replicating DNA was employed to determine if the *de novo* thymidylate biosynthesis pathway is present at the replication fork. HeLa cells were transfected with the pBABE-Puro SV40 LT plasmid which contains both the SV40 LT antigen cDNA as well as the SV40 origin of replication. The SV40 LT antigen is sufficient for replication initiation at the SV40 origin of replication (37) and has also been shown to induce S-phase (38). Tandem ChIP experiments using antibodies directed against PCNA followed by IgG, SHMT1, TYMS, or DHFR showed that all three enzymes required for *de novo* thymidylate synthesis are present on DNA, with the greatest occupancy observed at the SV40 origin of replication (Figure 5.14C). Because of the bi-directional nature of DNA replication, regions either upstream or downstream of the SV40 origin of replication were also probed. The required enzymes for *de novo* thymidylate biosynthesis were present within the SV40 LT antigen coding region (Figure 5.14A) and also within a randomly chosen area of the vector referred to as pBABE-Puro vector (Figure 5.14B). These data demonstrate that *de novo* thymidylate biosynthesis localizes to replication forks and suggests the processive synthesis and incorporation of dTTP into DNA during replication.

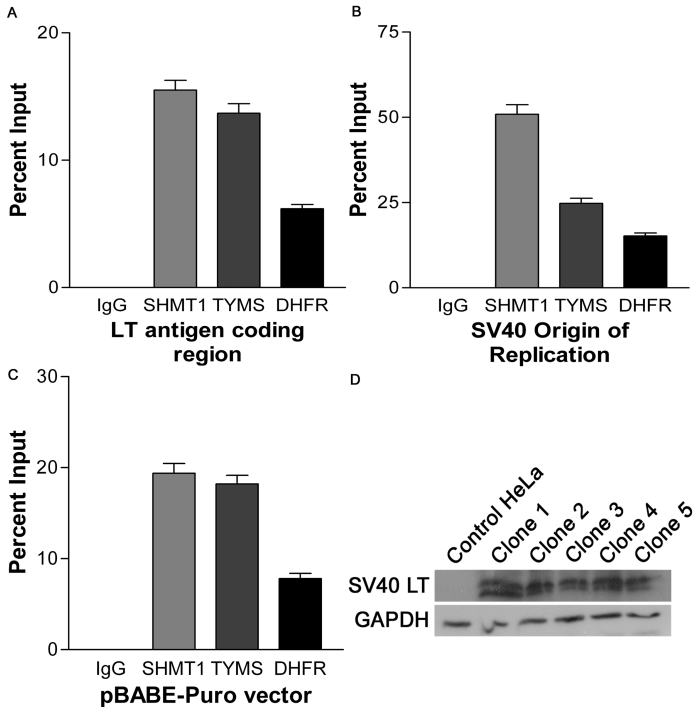

Figure 5.14. The *de novo* dTMP synthesis pathway is associated with episomal DNA in tandem chromatin immunoprecipitations. HeLa cells were transfected with pBABE-Puro-SV40 LT vector and selected for using puromycin. Clones were isolated and immunoblots performed against SV40 large T antigen (SV40 LT) to ensure clones were expressing SV40 LT (D). Tandem ChIP assays were performed as described in experimental procedures using antibodies directed against PCNA and then antibodies directed against non-immune IgG, SHMT1, TYMS, or DHFR. Regions of the pBABE-Puro-SV40 LT vector were probed for using real-time PCR (A,B, and C). All three enzymes precipitated regions of the vector including the A) LT antigen coding region , B) SV40 origin of replication, and C) downstream region of the SV40 origin. Highest occupancy occurred around the SV40 origin.

Discussion

Previous studies of cell culture and mouse models has indicated that SHMT1 expression is limiting for *de novo* thymidylate synthesis. Reduced SHMT1 expression in MCF-7 cells revealed a decrease in cellular *de novo* thymidylate synthesis whereas increases in SHMT1 expression in MCF-7 and SH-SY5Y cells increases cellular thymidylate synthesis (10). Uracil accumulation in DNA is a proxy for thymidylate synthesis capacity, and *Shmt1*$^{+/-}$ mice exhibit elevated uracil levels in liver DNA compared to wild-type littermates (11), demonstrating a key role of this enzyme in determining cellular thymidylate synthesis capacity. *De novo* thymidylate synthesis occurs in isolated intact nuclei, and SHMT1 and SHMT2α are present in the nucleus during S and G2/M phases (6). Here we show the localization of TYMS and DHFR to the nucleus during S and G2/M phases, supporting a role for nuclear *de novo* thymidylate synthesis during DNA replication and repair.

Previous studies have shown that *de novo* thymidylate synthesis activity in isolated nuclei is impaired following sonication, indicating a role for nuclear architecture in thymidylate synthesis (6). The results of this study provide a mechanism for this observation, by demonstrating that SHMT1 and SHMT2α are lamin binding proteins that serve as scaffold proteins required for assembly of the *de novo* thymidylate synthesis pathway into a multi-enzyme complex in the nucleus. Metabolic tracer studies in cells expressing a dominant negative form of SHMT1 demonstrate that the SHMT1 scaffold function can make a greater contribution to SHMT1 activity for de novo thymidylate synthesis than its catalytic activity. Increased uracil misincorporation in DNA along with increased risk of intestinal cancer (25) and neural tube defects (24) in *Shmt1*$^{+/-}$ mice show although there is redundancy within the *de novo* thymidylate synthesis pathway due to both SHMT2α activity and scaffold function within nuclei, the pathway is sensitive to lack of SHMT1. Furthermore, the dominant negative SHMT1 cell lines reduced methionine synthesis which is indicative of cytoplasmic

folate-mediated one-carbon metabolism but enhanced thymidylate synthesis. If *de novo* thymidylate synthesis was cytoplasmic, it would be expected to also be reduced in dominant negative SHMT1 cell lines, which was not the case. These data support that *de novo* thymidylate synthesis occurs in the compartments in which DNA is synthesized (2,6) and not in the cytosol.

The nuclear lamina has been observed to play an important role in tethering DNA to the nuclear periphery during replication and repair. The formation of *de novo* thymidylate multi-enzyme complexes and lamin associated structures demonstrated in this study is dependent on cell cycle, occurring during the S and G2/M phases when DNA replication occurs, and is independent of nucleotide availability. These data support a role for SHMT1 in anchoring *de novo* thymidylate synthesis to the nuclear lamina and this scaffold function likely accounts for its role as a limiting factor for *de novo* thymidylate biosynthesis in cell culture and mouse models (10,11,32). The results of this study also indicate that *de novo* thymidylate biosynthesis occurs at the sites of DNA synthesis and is associated with the DNA replication machinery. SHMT1 was shown to interact with PCNA, RFC1 and the DNA polymerases δ and ε, and PCNA interacts with SHMT1, TYMS, and DHFR, and has previously been identified as a lamin binding protein (29). SHMT1, TYMS and DHFR proteins are associated with replicating DNA, and enriched at sites of DNA replication initiation. These data indicate that *de novo* thymidylate biosynthesis is occurring at replication forks. *De novo* thymidylate biosynthesis is unique from the biosynthesis of other deoxyribonucleotides in its compartmentation to the nucleus at replication forks. Thymidine deoxyribonucleotides are also unique in that they are not essential during DNA replication, as dUTP can be incorporated into DNA in lieu of dTTP. The presence of the *de novo* thymidylate biosynthesis at the replication fork may permit regulation of dUTP incorporation into DNA, which may function to regulate transcriptional networks and biological pathways, as has been demonstrated in

Drosophila (39,40), and may account for the sensitivity of $SHMT^{+/-}$ mice to neural tube closure defects (24) and intestinal cancers (25).

Materials and Methods

Cell Lines and Media— HeLa cells were obtained and cultured as previously reported (6). Cells were grown in α-MEM or DMEM (Hyclone) supplemented with 10% fetal bovine serum (Hyclone) and penicillin/streptomycin (Mediatech) at 37° C and 5% CO_2. For all experiments, α-MEM (Hyclone) lacking nucleotides was used and supplemented with 10% dialyzed and charcoal treated fetal bovine serum and penicillin/streptomycin (Mediatech) with and without deoxyribonucleosides (10 mg/L). Cells were maintained in these medias at 37° C and 5% CO_2 for 2 passages over 1 week prior to transfection. The SH-SY5Y human neuroblastoma cell line has been described previously (41). Cells were cultured in αMEM with 10% dialyzed fetal bovine serum for all experiments. DN2-SHMT1 expression was induced in cell lines by the addition of 1 μg/ml tetracycline for a minimum of 4 days prior to experimentation as previously described for SH-SY5Y-FDH cells lines (36).

Generation of Human DN2-SHMT1-expressing Cell Lines—Generation of the pet28a-DN2-SHMT1 cDNA was described previously (35). This vector was treated with *Kpn1* and *BamHI* (New England Biolabs) to isolated DN2-SHMT1 cDNA as was the pcDNA4/TO/*myc*-His C vector (Invitrogen). Following isolation of the restriction fragments through gel purification using the QIAquick Gel Extraction Kit (Qiagen), DN2-SHMT1 cDNA was ligated into the pcDNA4/TO/*myc*-His C vector using T4 DNA ligase (Invitrogen) generating pcDNA4-DN2-SHMT1. Stable SH-SY5Y cell lines expressing pcDNA6/TR vector (Invitrogen) and pcDNA4-DN2-SHMT1 were generated. SH-SY5Y cells were electroporated with 20 μg of plasmid DNA (pcDNA4-DN2-SHMT1 and pcDNA6/TR vector) at 0.22 kV and 950 microfarads (Bio-Rad Gene-Pulser), then cultured with αMEM for 48 h. The medium was replaced with αMEM containing blasticidin (10 μg/ml) and Zeocin (100 μg/ml, Invitrogen) to

select for stable integrants. Individual colonies resistant to Zeocin treatment were selected and expanded using αMEM containing blasticidin and Zeocin, and clonal lines expressing human DN2-SHMT1 protein were screened by Western blot analyses.

Vectors and transfection procedures – pCMV6-AC-DHFR-GFP, pCMV6-AC-TYMS-GFP, phiYFP-SHMT1, and TagRFP-N-SHMT2α were previously described (6). PmKate2-LaminB1 was purchased from Evrogen. The pBABE-puro SV40 LT vector was deposited in Addgene by Dr. Thomas Roberts and purchased from Addgene (Addgene plasmid 13970). $pNTAP_B$ and pCMV-FLAG-MAT-Tag-1 were obtained from Stratagene and Sigma respectively. PCR was used to create adapters on SHMT1 cDNA for ligation. The forward primers for both $pNTAP_B$-SHMT1 and pCMV-FLAG-SHMT1-MAT-Tag-1 was 5'-ATAT**AAGCTT**ATGACGATGCCAGTCAAC-3' where the bold text indicates a HindIII (New England Biolabs Inc.) site. The reverse primer for $pNTAP_B$-SHMT1 was 5'-ATAT**CTCGAG**GAAGTCAGGCAGGCCAGG-3' where the bold text indicates a XhoI (New England Biolabs Inc.) site. The reverse primer for pCMV-FLAG-SHMT1-MAT-Tag-1 was 5'-ATAT**AGATCT**GAAGTCAGGCAGGCCAGG-3' where the bold text indicates a BglII (New England Biolabs Inc.) restriction site. PCR reactions were completed as follows: 95°C for 45 s, 55°C for 45 s, and 72°C for 2 min. Following PCR, products were gel purified using the QIAquick Gel extraction kit (Qiagen). Vectors and PCR products were restriction digested with their respective restriction enzymes as per manufacturer's protocol. Ligation was completed using T4 DNA ligase (Invitrogen) as per manufacturer's protocol. All transfection procedures were completed using Kit R (Lonza) for a Nucleofector II (Lonza) as per manufacturer's instructions.

Confocal microscopy – Following nucleofection, cells were incubated at 37° under 5% CO_2 for 24 hours. For visualization of nuclei in cells not transfected with pmKate2-Lamin B1, DRAQ5 (Alexis Biochemicals) was used per manufacturer's instruction. Confocal

fluorescence microscopy (Leica TCS SP2 system) was used to image all cells at the Cornell Microscope and Imaging Facility.

Cell Cycle Synchronization and Analysis—HeLa cells at 60% confluence were arrested at various cell cycle stages using 30 μM lovastatin (Sigma) (for G1 phase), 2 mM hydroxyurea (Sigma) (for S phase), or 100 ng/mL nocodazole (Sigma) (for G2/M phase) following transfection. Preparation for fluorescence activated cell sorting (FACS) was performed as previously described (8). FACS analysis was performed by Biomedical Sciences Flow Cytometry Core Laboratory at Cornell University.

Immunoblotting – SHMT1, SHMT2, TYMS, DHFR, and GAPDH immunoblots were performed as described previously (6,7). Antibodies directed towards PCNA and the SV40 LT antigen were purchased from Abcam. Mouse anti-PCNA and Mouse anti-SV40 Large T antigen were diluted in 5% non-fat dry milk (Carnation) containing 1% NP40 (US Biologicals) at a concentration of 1 μg/mL and 1:1000 respectively. Goat anti-mouse HRP (Pierce) secondary antibodies were used at a dilution of 1:10,000. SuperSignal West Pico Chemiluminescent substrate was used for visualization (Pierce).

Immunoprecipitation – Immunoprecipitation was conducted using the Dynabeads Protein G Immunoprecipitation Kit (Invitrogen). For whole cell immunoprecipitation, HeLa cells were lysed using mammalian protein extraction reagent (Pierce) supplemented with 2 mM β-mercaptoethanol (Calbiochem), 0.1 mM EDTA (Fisher Scientific), 1 mM PMSF (Alexis Biochemicals), and 1:1000 Protease Inhibitor Cocktail (Sigma). For immunoprecipitations from nuclear and cytosolic extracts, nuclei were purified using the Active Motif Nuclear extract kit per manufacturer's protocol. Antibodies directed toward the following proteins were purchased from Abcam: DNA polymerase δ, UNG2, PCNA, and DHFR. Lamin A/C, Lamin B1, DNA polymerase ε, KDM1 and RFC1 antibodies were purchased from Santa Cruz Biotechnology. Non-immune IgG was purchased from Pierce. SHMT1 antibody was obtained

as previously described (8). 1 mg of total protein per sample was incubated with 5 μg of antibody overnight at 4°C. The beads were collected and washed four times with PBS/0.1% Tween 20 (Fisher). For Lamin A/C and Lamin B1 immunoprecipitations, washes contained either 150 mM NaCl or 650 mM NaCl in PBS/0.1% Tween 20. For all immunoprecipitations, 40 μls of SDS-PAGE sample buffer were added to the beads to elute with heating at 100°C.

SHMT1 tandem affinity purification – $pNTAP_B$-SHMT1 was transfected into HeLa cells as described above. For the isolation of TAP tagged SHMT1 and co-eluting proteins, the Interplay mammalian TAP system kit (Stratagene) was used according to manufacturer's protocol. For isolation of FLAG-SHMT1-MAT and co-eluting proteins for peptide sequencing, pCMV-FLAG-SHMT1-MAT-Tag-1 was transfected as described above. Approximately 4 x 10^8 HeLa cells were used per group. The groups were: empty pCMV-FLAG-MAT-Tag-1 control, and pCMV-FLAG-SHMT1-MAT-Tag-1 S-phase synchronized cells and UV treated cells. UV treatment was accomplished as previously reported (9). 24 h following treatments, cells were washed with 20 mLs PBS/1 mM PMSF three times. Cells were scraped into 5 mLs of PBS/1 mM PMSF and collected in 50 mL conical tubes (Corning). Cells were pelleted at 1000 rpm for 5 min and resuspended in 15 mLs swelling buffer (25mM HEPES (Fisher) pH 7.8, 1.5mM $MgCl_2$ (Fisher), 10mM KCl (Fisher), 0.1% NP40 (US Biologicals), 1.0mM PMSF (Alexis Biochemicals), 1:100 Protease inhibitor (Sigma)) and incubated on ice for 10 min. Cells were homogenized with 25 strokes of a B-type dounce homogenizer and checked for cell lysis using trypan blue (Fisher) exclusion. The homogenate was then filtered through a 70um mesh (BD Bioscience) and centrifuged at 4000 rpm for 5 min to collect nuclei. Nuclei were washed with swelling buffer 2X followed by centrifugation. Nuclei were then resuspended in 1 mL ice-cold sodium phosphate (Fisher) pH 8.0/ 75 mM NaCl/ 1mM PMSF/ 1:100 protease inhibitor for histidine tag isolation (Sigma). $MgCl_2$ was added to a concentration of 2 mM. Benzonase (Sigma) was added at a concentration of 250

U/mL sample for removal of DNA and incubated for 30 minutes on ice. Following benzonase treatment, samples were centrifuged at 14,000 rpm for 15 minutes. The supernatant was collected and FLAG-SHMT1-MAT and co-eluting proteins were purified using Invitrogen His-TALON magnetic beads per manufacturer's instructions. Following elution, the eluates were combined and diluted with 1 volume 100 mM Tris pH 7.4 and 2 mM EDTA and 1:100 protease inhibitor cocktail for FLAG immunoprecipitation using FLAG affinity gel (Sigma) per manufacturer's instruction. The eluate from the FLAG immunoprecipitation was then subjected to protein precipitation using the ND Protein Precipitation Kit (National Diagnostics) per manufacturer's protocol. The protein pellet was resuspended in 20 uL of 20 mM Tris pH 7.5 and 20 uL 2X SDS-PAGE loading buffer (Biorad) and heated at 95° for 10 minutes.

Mass Spectrometry – Tandem affinity purified samples from S-phase blocked and UV treated cells were run on a 12% polyacrylamide gel and was stained with Novex colloidal blue staining reagent (Invitrogen). The lanes were excised and great care was taken to avoid sample contamination. Excised lanes were cut into 9 fractions of approximately 7 mm by 5 mm areas and sent to the Harvard Microchemistry Facility for peptide digestion, purification, and sequencing. Each excised fraction was reduced, carboxyamidomethylated and digested with trypsin. Peptide identification of each digestion mixture was performed by microcapillary reversed-phase HPLC nanoelectrospray tandem mass spectrometry (μLC-MS/MS) on an LTQ-Orbitrap Velos or XL mass spectrometer (ThermoFisher Scientific, San Jose, MA). The Orbitrap repetitively surveyed an *m*/*z* range from 395 to 1600, while data-dependent MS/MS spectra on the twenty (Velos) or ten (XL) most abundant ions in each survey scan were acquired in the linear ion trap. MS/MS spectra were acquired with relative collision energy of 30%, 2.5-Da isolation width, and recurring ions dynamically excluded for 60 s. Preliminary sequencing of peptides was facilitated with the SEQUEST algorithm with a 30 ppm mass

tolerance against a species specific (human) subset of the UniProt Knowledgebase. With a custom version of the Harvard Proteomics Browser Suite (ThermoFisher Scientific, San Jose CA), peptide spectrum matches (PSMs) were accepted with mass error < 2.5ppm and score thresholds to attain an estimated false discovery rate (FDR) of ~1% using a reverse decoy database strategy. Gene ontology term enrichment was performed using DAVID with the total set of proteins with a peptide count $\geq$ 3 and greater than 1 ratio of experimental group peptide counts to control group peptide counts (42,43).

Metabolic isotope tracer studies- Metabolic isotope tracer studies were completed as previously described (32). Cells were plated in 100-mm plates at 50% confluence in treatment media (10 g/liter HyQ αMEM-modified (HyClone), 2.5 g/liter $NaHCO_3$, 11.2% (v/v) dialyzed fetal bovine serum, 0.05 μm 5-formyl-THF, 10 μm methionine, 1 mg/liter pyridoxine, glycine at 0.2 mM, 26 mg/liter L-[5,5,5-$^2H_3$]leucine, but lacking ribo- and deoxyribonucleosides, hypoxanthine, thymidine and serine]. Media were supplemented with L-[2,3,3-$^2H_3$]serine (250 μm) and were refreshed every 2-3 days. Cells were cultured for 8 days with 2-4 doublings. Media were removed and cells washed in 2 ml of ice-cold phosphate-buffered saline. Cells were pelleted and whole cell pellets were lysed with 600 μl of 5% trichloroacetic acid for protein isolation. Total cellular protein was pelleted by centrifugation at 4000 × *g* for 30 min at 4 °C. Protein pellets were suspended in 6 N HCl (100 μl) in vacuum hydrolysis tubes and heated at 100 °C for 20 h. The amino acids were purified by cation exchange chromatography (44-46). Amino acids were converted to heptafluorobutyryl *n*-propyl ester derivatives (45) and were separated on an HP-5MS column (30 m × 0.25 mm). Isotopic enrichment was determined in electron capture negative ionization mode by gas chromatography-mass spectrometry using a model 6890 gas chromatograph and model 5973 mass spectrometer (Hewlett-Packard Corp., Palo Alto, CA). Selected ion monitoring was conducted at a mass-to-

charge ratio *m*/*z* 519–523 for serine, *m*/*z* 305–308 for dehydroalanine (DHA), *m*/*z* 349–353 for leucine, and *m*/*z* 367–370 for methionine.

Total genomic DNA was isolated using a QIAamp DNA Blood Mini kit (Qiagen). DNA samples were dried under nitrogen and suspended in formic acid (1 ml) and hydrolyzed at 150 °C for 45 min in vacuum hydrolysis tubes. After drying at 55 °C under nitrogen, derivitization was performed by dissolving the bases in 0.2 ml of a 1:1 mixture of *N*,*O-bis*-[trimethylsilyl]trifluoroacetamide/1% trimethylchlorosilane (Pierce) and acetonitrile, and heated at 140 °C for 30 min. The trimethylsilane-base derivatives were separated on a HP-5MS column. Isotopic enrichment was determined in positive ionization mode by gas chromatography-mass spectrometry using a model 6890 gas chromatograph and model 5973 mass spectrometer (Hewlett-Packard Corp., Palo Alto, CA). Selected ion monitoring was conducted at a mass-to-charge ratio *m*/*z* 255–257 for thymine.

Tandem Chromatin Immunoprecipitation – Clones 1,2, and 3 of pBABE-Puro SV40 LT expressing HeLa cells that were selected using puromycin were used for this experiment. Approximately 2 x 10^8 cells were used per clone. Each plate was washed 3 times with ice-cold PBS. The bifunctional cross-linker Dimethyl 3,3´-dithiobispropionimidate (DTBP) (Pierce) was resuspended at a concentration of 5 mM in PBS pH 8.0. 20 mL per plate was added and cells were incubated at 4° for 30 minutes. Cells were then washed 2 X with PBS. 20 mLs ice-cold quenching buffer (100 mM Tris pH 8.0, 150 mM NaCl) was added per plate and incubated for 10 minutes at 4°. Each plate was washed 3 X with room temperature PBS. A 1% formaldehyde (Fisher) solution in PBS was added to each plate and incubated at room temperature for 10 minutes. To quench formaldehyde crosslinking, 3 mLs of 1.375 M glycine (Fisher) were added. Plates were washed 3 times with ice-cold PBS supplemented with 0.5 mM PMSF. Cells were scraped into 5 mL ice cold PBS containing 0.5 mM PMSF and centrifuged at 1000 rpm for 5 minutes at 4°. The pelleted cells were resuspended in 10

volumes of swelling buffer and then subjected to dounce homogenization and centrifugation as reported above. Pelleted nuclei were resuspended in 5 mL sonication buffer (50mM Hepes pH 7.9, 140 mM NaCl, 1 mM EDTA, 1% Triton X-100, 0.1% Na-deoxycholate, 0.1% SDS, 0.5 mM PMSF, and 1:1000 protease inhibitor cocktail). Nuclei were sonicated using a 3mm microtip probe on a Branson Sonifier 150 at 80% with 10 second pulses 10 times with 1 minute rests on ice between pulses. Sonicated nuclei were centrifuged at 14,000 rpm for 15 minutes at 4° and the supernatant supplemented with 1μg/mL sonicated salmon sperm DNA (Invitrogen) and bovine serum albumin (Sigma) at 1 mg/mL. The lysate was precleared using 50 μL Invitrogen Protein G Dynabeads for 2 hours at 4° and beads collected on a magnet and the supernatant removed. Samples were divided into 1 mL aliquots for immunoprecipitation. 5 μg PCNA (Abcam) antibody was incubated 12 hours per 1 mL aliquot at 4°. 50 μL Invitrogen Protein G Dynabeads were added and incubated for 1 hour at 4°. The beads were collected on a magnet and washed twice with 1 mL sonication buffer. The beads were washed twice with 1 mL sonication buffer containing 500 mM NaCl and then twice with 1 mL 20mM Tris, pH 8.0, 1mM EDTA, 250mM LiCl, 0.5% NP-40, 0.5% Na-deoxycholate, 0.5 mM PMSF, and Protease inhibitor cocktail. Two more washes were performed with 1 mL TE buffer. 50 μLs of 10 mM DTT was then added to the beads and incubated at 37° for 30 min. The eluate was removed and that step was repeated. The eluates were then combined and diluted 40 times with sonication buffer. 10% of the sample was kept for input. The sample was then aliquoted into 1 mL fractions for TYMS, DHFR, SHMT1, and IgG control immunoprecipitations. 5 μg of each antibody was used and samples were incubated 12 hours at 4°. 50 μL of Invitrogen Protein G Dynabeads were then added and incubated for 1 hour at 4°. Washes were performed as above. To elute, 200 μL 50mM Tris, pH 8.0, 1mM EDTA, 1% SDS, and 50mM NaHCO3 was added and beads were heated to 65° for 10 minutes. This step was repeated and eluates combined giving 400 μL final volume. The input and samples were then treated with 21 μL 4

M NaCl and incubated for 12 hours at 65°. 2 µL RNase A (5 mg/mL) (Rockland Immunochemicals, Inc.) was added to each sample followed by incubation at 37° for 1 hour. EDTA was then added to a concentration of 5 mM. 2 µL Proteinase K (10 mg/mL) (Rockland Immunochemicals, Inc.) was then added and samples were incubated for 2 hours at 42°. Samples were extracted with phenol/chloroform/isoamylalcohol (Sigma) once and then with chloroform/isoamylalcohol (Sigma) once. 1 µL glycogen (Sigma) (20 mg/mL) was added followed by addition of 40 µL 3 M Na-acetate (Fisher) and 1 mL 100% ethanol (Pharmco-AAPER). Samples were vortexed and precipitated for 12 hours at -20° followed by centrifugation at 14,000 rpm for 30 minutes and pellets were washed with 75% ethanol. Centrifugation was repeated and the pellet was allowed to dry at room temperature. Samples were then resuspended in 100 µL 10 mM Tris pH 7.5 for real-time PCR analysis.

Real-time PCR – Forward and reverse primers used for real-time PCR surrounding the SV40 origin of replication were 5'-CAGCAGGCAGAAGTATGCAAAGCA-3' and 5'-TACTTCTGGAATAGCTCAGAGGCCGA-3'respectively. For the pBABE-Puro vector region the forward and reverse primers were 5'-ACAGAGTTCTTGAAGTGGTGGCCT-3' and 5'-TGGTTTGTTTGCCGGATCAAGAGC-3' respectively. For the large t-antigen insert, the forward and reverse primers were 5'-ACTCCACACAGGCATAGAGTGTCT-3' and 5'-CCCACCTGGCAAACTTTCCTCAAT-3' respectively. Real-time PCR analysis was performed using Quantifast SYBR green PCR kit (Qiagen). PCR products were quantified using an Applied Biosystems 7500 real-time PCR system.

REFERENCES

1. Samsonoff, W. A., Reston, J., McKee, M., O'Connor, B., Galivan, J., Maley, G., and Maley, F. (1997) *J Biol Chem* **272**(20), 13281-13285
2. Anderson, D. D., Quintero, C. M., and Stover, P. J. (2011) *Proc Natl Acad Sci U S A*, published ahead of print
3. Blount, B. C., Mack, M. M., Wehr, C. M., MacGregor, J. T., Hiatt, R. A., Wang, G., Wickramasinghe, S. N., Everson, R. B., and Ames, B. N. (1997) *Proc Natl Acad Sci U S A* **94**(7), 3290-3295
4. Fox, J. T., and Stover, P. J. (2008) *Vitam Horm* **79**, 1-44
5. Tibbetts, A. S., and Appling, D. R. (2010) *Annu Rev Nutr* **30**, 57-81
6. Anderson, D. D., and Stover, P. J. (2009) *PLoS One* **4**(6), e5839
7. Anderson, D. D., Woeller, C. F., and Stover, P. J. (2007) *Clin Chem Lab Med* **45**(12), 1760-1763
8. Woeller, C. F., Anderson, D. D., Szebenyi, D. M., and Stover, P. J. (2007) *J Biol Chem* **282**(24), 17623-17631
9. Fox, J. T., Shin, W. K., Caudill, M. A., and Stover, P. J. (2009) *J Biol Chem* **284**(45), 31097-31108
10. Oppenheim, E. W., Adelman, C., Liu, X., and Stover, P. J. (2001) *J Biol Chem* **276**(23), 19855-19861
11. MacFarlane, A. J., Liu, X., Perry, C. A., Flodby, P., Allen, R. H., Stabler, S. P., and Stover, P. J. (2008) *J Biol Chem* **283**(38), 25846-25853
12. Garrow, T. A., Brenner, A. A., Whitehead, V. M., Chen, X. N., Duncan, R. G., Korenberg, J. R., and Shane, B. (1993) *J Biol Chem* **268**(16), 11910-11916

13. Stover, P. J., Chen, L. H., Suh, J. R., Stover, D. M., Keyomarsi, K., and Shane, B. (1997) *J Biol Chem* **272**(3), 1842-1848

14. Girgis, S., Nasrallah, I. M., Suh, J. R., Oppenheim, E., Zanetti, K. A., Mastri, M. G., and Stover, P. J. (1998) *Gene* **210**(2), 315-324

15. An, S., Kumar, R., Sheets, E. D., and Benkovic, S. J. (2008) *Science* **320**(5872), 103-106

16. Field, M. S., Anderson, D. D., and Stover, P. J. (2011) *Frontiers in Genetics* **2**(36), 1-13

17. An, S., Kyoung, M., Allen, J. J., Shokat, K. M., and Benkovic, S. J. (2010) *J Biol Chem* **285**(15), 11093-11099

18. An, S., Deng, Y., Tomsho, J. W., Kyoung, M., and Benkovic, S. J. (2010) *Proc Natl Acad Sci U S A* **107**(29), 12872-12876

19. Prem veer Reddy, G., and Pardee, A. B. (1980) *Proc Natl Acad Sci U S A* **77**(6), 3312-3316

20. Noguchi, H., Prem veer Reddy, G., and Pardee, A. B. (1983) *Cell* **32**(2), 443-451

21. Li, S., Armstrong, C. M., Bertin, N., Ge, H., Milstein, S., Boxem, M., Vidalain, P. O., Han, J. D., Chesneau, A., Hao, T., Goldberg, D. S., Li, N., Martinez, M., Rual, J. F., Lamesch, P., Xu, L., Tewari, M., Wong, S. L., Zhang, L. V., Berriz, G. F., Jacotot, L., Vaglio, P., Reboul, J., Hirozane-Kishikawa, T., Li, Q., Gabel, H. W., Elewa, A., Baumgartner, B., Rose, D. J., Yu, H., Bosak, S., Sequerra, R., Fraser, A., Mango, S. E., Saxton, W. M., Strome, S., Van Den Heuvel, S., Piano, F., Vandenhaute, J., Sardet, C., Gerstein, M., Doucette-Stamm, L., Gunsalus, K. C., Harper, J. W., Cusick, M. E., Roth, F. P., Hill, D. E., and Vidal, M. (2004) *Science* **303**(5657), 540-543

22. Moldovan, G. L., Pfander, B., and Jentsch, S. (2007) *Cell* **129**(4), 665-679

23. Ulrich, H. D. (2009) *DNA Repair (Amst)* **8**(4), 461-469

24. Beaudin, A. E., Abarinov, E. V., Noden, D. M., Perry, C. A., Chu, S., Stabler, S. P., Allen, R. H., and Stover, P. J. (2011) *Am J Clin Nutr* **93**(4), 789-798

25. Macfarlane, A. J., Perry, C. A., McEntee, M. F., Lin, D. M., and Stover, P. J. (2011) *Cancer Res* **71**(6), 2098-2107

26. Hozak, P., Hassan, A. B., Jackson, D. A., and Cook, P. R. (1993) *Cell* **73**(2), 361-373

27. Spann, T. P., Moir, R. D., Goldman, A. E., Stick, R., and Goldman, R. D. (1997) *J Cell Biol* **136**(6), 1201-1212

28. Moir, R. D., Spann, T. P., Herrmann, H., and Goldman, R. D. (2000) *J Cell Biol* **149**(6), 1179-1192

29. Shumaker, D. K., Solimando, L., Sengupta, K., Shimi, T., Adam, S. A., Grunwald, A., Strelkov, S. V., Aebi, U., Cardoso, M. C., and Goldman, R. D. (2008) *J Cell Biol* **181**(2), 269-280

30. Luka, Z., Moss, F., Loukachevitch, L. V., Bornhop, D. J., and Wagner, C. (2011) *Biochemistry* **50**(21), 4750-4756

31. MacFarlane, A. J., Perry, C. A., McEntee, M. F., Lin, D. M., and Stover, P. J. (2011) *Carcinogenesis* **32**(3), 427-433

32. Herbig, K., Chiang, E. P., Lee, L. R., Hills, J., Shane, B., and Stover, P. J. (2002) *J Biol Chem* **277**(41), 38381-38389

33. Reed, M. C., Nijhout, H. F., Neuhouser, M. L., Gregory, J. F., 3rd, Shane, B., James, S. J., Boynton, A., and Ulrich, C. M. (2006) *J Nutr* **136**(10), 2653-2661

34. Szebenyi, D. M., Liu, X., Kriksunov, I. A., Stover, P. J., and Thiel, D. J. (2000) *Biochemistry* **39**(44), 13313-13323

35. Zanetti, K. A., and Stover, P. J. (2003) *J Biol Chem* **278**(12), 10142-10149

36. Anguera, M. C., Field, M. S., Perry, C., Ghandour, H., Chiang, E. P., Selhub, J., Shane, B., and Stover, P. J. (2006) *J Biol Chem* **281**(27), 18335-18342

37. Abdel-Aziz, W., Malkas, L. H., Wills, P. W., and Hickey, R. J. (2003) *Crit Rev Oncol Hematol* **48**(1), 19-33

38. Ahuja, D., Saenz-Robles, M. T., and Pipas, J. M. (2005) *Oncogene* **24**(52), 7729-7745

39. Bekesi, A., Pukancsik, M., Muha, V., Zagyva, I., Leveles, I., Hunyadi-Gulyas, E., Klement, E., Medzihradszky, K. F., Kele, Z., Erdei, A., Felfoldi, F., Konya, E., and Vertessy, B. G. (2007) *Biochem Biophys Res Commun* **355**(3), 643-648

40. Deutsch, W. A., and Spiering, A. L. (1982) *J Biol Chem* **257**(7), 3366-3368

41. Girgis, S., Suh, J. R., Jolivet, J., and Stover, P. J. (1997) *J Biol Chem* **272**(8), 4729-4734

42. Huang da, W., Sherman, B. T., and Lempicki, R. A. (2009) *Nat Protoc* **4**(1), 44-57

43. Huang da, W., Sherman, B. T., and Lempicki, R. A. (2009) *Nucleic Acids Res* **37**(1), 1-13

44. Dudley, M. A., Nichols, B. L., Rosenberger, J., Perkinson, J. S., and Reeds, P. J. (1992) *J Nutr* **122**(3), 528-534

45. Lichtenstein, A. H., Cohn, J. S., Hachey, D. L., Millar, J. S., Ordovas, J. M., and Schaefer, E. J. (1990) *J Lipid Res* **31**(9), 1693-1701

46. Reeds, P. J., Hachey, D. L., Patterson, B. W., Motil, K. J., and Klein, P. D. (1992) *J Nutr* **122**(3), 457-466

CHAPTER SIX

CONCLUSIONS AND FUTURE DIRECTIONS

Part I: Introduction

Folate-mediated one-carbon metabolism is a requirement for the synthesis of purines, thymidylate, and methionine. These pathways, however, compete for a limited pool of available folate cofactors. This competition is most pronounced for methyleneTHF which is required for *de novo* dTMP synthesis. The enzymes required for *de novo* dTMP synthetic cycle include SHMT1, TYMS, and DHFR. SHMT1 transfers one-carbon groups from C3 of serine to tetrahydrofolate to form glycine and MethyleneTHF (1). MethyleneTHF is then used by TYMS for the reductive methylation of dUMP to form dTMP and dihydrofolate. DHFR catalyzes the reduction of dihydrofolate in a NADPH dependent reaction which regenerates THF for continuing the cycle. SHMT1 is the rate limiting enzyme in *de novo* dTMP synthesis (2) and regulates the flux of one-carbon units towards dTMP at the expense of homocysteine remethylation (3). SHMT1 achieves this regulation through the import of the *de novo* dTMP pathway in a SUMO dependent fashion during S and G2/M phases (4,5). Although the mechanisms for nuclear import are known, direct evidence of dTMP synthesis within the nucleus was lacking. We also wanted to understand if *de novo* dTMP synthesis occurs in mitochondria to support DNA replication within that compartment. Regulation of nuclear dTMP synthesis and how SHMT1 exits the nucleus was also unknown. Furthermore, how SHMT1 acts as a rate-limiter in *de novo* dTMP synthesis was investigated. The results of these studies and other studies in the lab show that SHMT has a central uracil misincorporation limiting function within the cell.

Part II: Nuclear *de novo* dTMP synthesis

The data presented herein show directly the existence of nuclear one-carbon metabolism and in particular nuclear *de novo* dTMP synthesis. Previous work by Pardee and co-workers identified a nuclear multi-enzyme complex they termed the replitase which contained TYMS and DHFR activities (6,7). However, they never directly showed nuclear *de novo* dTMP synthesis. Using *Shmt1*$^{wt/wt}$ and *Shmt1*$^{-/-}$ whole mouse liver nuclei treated with L-[^{3}H]-serine, nuclear *de novo* dTMP synthesis was observed to occur. These activities were inhibited by sonication of nuclei which suggested a role for nuclear architecture and/or multi-enzyme complex formation in nuclei. Interestingly, we found that *Shmt1*$^{-/-}$ whole mouse liver nuclei retained 25% of the activity found in wild-type mice. We were able to identify that this activity was due to another nuclear isoform of SHMT made from the SHMT2 gene, we termed SHMT2α. SHMT2α was observed to be expressed through alternate promoter usage. The SHMT2 gene contains a mitochondrial leader sequence in exon 1 followed by a promoter region that controls SHMT2α. Exon 2 contains another start methionine codon which lacks the mitochondrial leader sequence and is translated to make the nuclear and cytosplasmic isoform of SHMT2, SHMT2α.

These studies also solidified the mechanism of SHMT1 import to the nucleus as mutation of the conserved SUMO motif (K38R/K39R) on SHMT1 completely abolished nuclear localization. Cells expressing a human SNP of SHMT1 present in the population, L474F, also show a decrease in nuclear localization. The presence of another nuclear isoform of SHMT provided evidence for how the L474F polymorphism persisted over evolutionary time and gave insight into the functional redundancy of SHMT and its importance in *de novo* dTMP synthesis.

Part III: Mitochondrial *de novo* dTMP synthesis

We had identified that nuclear *de novo* dTMP synthesis occurs and that in these mice that nuclei were isolated from also exhibited increased uracil misincorporation in nuclear DNA. We formed the hypothesis that perhaps mitochondrial *de novo* dTMP synthesis occurs in order to support mtDNA replication and limit uracil misincorporation in that compartment. It has been reported that in plant mitochondria, *de novo* dTMP synthesis occurs using SHMT2 and a bifunctional enzyme TS-DHFR which contains both activities (8). TYMS has also been reported in mitochondria of mammalian cells (9). SHMT2 has long been known to be a mitochondrial protein and is present on mtDNA (10). DHFR however, has not been identified in mammalian mitochondria. We set out to find a DHFR transcript with a mitochondrial localization signal (MLS) in the human hepatic cell line using 5'-RACE. We identified a transcript that was previously thought to be a pseudogene called DHFRL1. The sequence of DHFRL1 and DHFR are 92% identical and DHFRL1 localizes to mitochondria. We also show that TYMS localized to mitochondria. The submitochondrial localization of SHMT2, TYMS, and DHFRL1 were also determined with all of these enzymes present in the matrix and in association with the inner membrane. The matrix is the mitochondrial compartment that houses mtDNA. Treating HepG2 cells with siRNA directed towards DHFRL1 completely inhibited DHFR activity in mitochondrial extracts that were isolated. The mechanisms whereby DHFRL1 and TYMS localize to mitochondria are still unknown as no canonical MLS of either protein was identified.

We went on to show that mitochondrial *de novo* dTMP synthesis does occur and were able to isolate nascent ^{3}H-dTMP made from ^{3}H-serine in whole purified mitochondria. We found that mitochondrial *de novo* dTMP synthesis occurred in HepG2 cells and Chinese hamster ovary (CHO) cells and that this activity was markedly decreased in samples treated with the DHFR inhibitor methotrexate (MTX) and in the SHMT2 mutant CHO cell line, *glyA*. Furthermore, in order to see how deficiencies in mitochondrial *de novo* dTMP synthesis

affected uracil misincorporation in mtDNA, we used the *glyA* cell line that we knew was deficient in dTMP synthesis and assayed levels of uracil in mtDNA. We found 40% increased uracil in mtDNA in the *glyA* CHO cell line as compared to wild-type CHO cells. We were also able to complement a previously uncharacterized CHO glycine auxotroph called *glyC* with DHFRL1 cDNA, rescuing the glycine auxotrophy. This also solidifies a role for DHFRL1 in mitochondrial one-carbon metabolism.

Part IV: Regulation of SHMT1 through Ubiquitination

Previous work had shown the importance of SUMO-1 in the nuclear import of SHMT1. Prior observations also indicated that SHMT1 interacted with the ubiquitin E2 conjugase, Ubc13 (4). We wanted to know how SHMT1 was regulated through the ubiquitin pathway and if a competition existed for the same consensus motif that is SUMOylated for regulation of SHMT1, as has been shown for other proteins (11).

We found that SHMT1 levels are most prevalent during S-phase of the cell cycle when it is required for dTMP synthesis in the nucleus. This was not due to an increase in mRNA levels and it was determined that ubiquitination was lowest during S-phase. These data suggested an important role for ubiquitination in regulating SHMT1 levels in the cell. We found that inhibition of the translational machinery using cycloheximide (CHX) showed that SHMT1 has a half-life of approximately 2 hours. Concomitant inhibition of the proteasome rescued SHMT1 levels and lead to increases in ubiquitinated SHMT1. Mutation of the SHMT1 SUMO site resulted in increased stability of SHMT1 and drastic decreases in ubiquitination at K39. Furthermore, SHMT1 co-localizes with both the 19S cap and 20S core of the proteasome in both the nucleus and cytoplasm suggesting that degradation can occur in either compartment.

To determine whether degradation is compartment specific, cells were treated with the nuclear export inhibitor leptomycin B (LMB). Nuclei isolated from cells treated with LMB accumulated higher molecular weight bands which identified to be ubiquitin whereas nuclei isolated from cells treated with LMB and the proteosomal inhibitor Mg132 exhibited a prominent 75 kDa band which was determined to be a SUMO-2/3 conjugate of SHMT1. In conjunction with nuclear export and proteosomal inhibition, both ubiquitin and SUMO-2/3 chains became prominent. Mixed SUMO-2/3-Ubiquitin chains have been reported to be important mediators of protein degradation (12) suggesting that SHMT1 proteasomal dependent degradation does occur in the nucleus.

Because Ubc13 is generally involved in K63-linkage specific poly-ubiquitin chains, which are not involved in proteosomal degradation, we wanted to understand the role that Ubc13 played. We observed compartmental differences in K63 ubiquitination between the nucleus and cytosol. Extensive K63 polyubiquitin chains were observed in nuclei throughout S and G2/M phases, but were lacking in G1 phase. In the cytosol, only bands consistent with K63 linked di-ubiquitin were present with the same cell cycle profile. We found that normal cycling HeLa cells exhibited decreased nuclear SHMT1 in response to Ubc13 siRNA treatment and in cells over-expressing Ubc13 a reduction of nuclear SHMT1 was observed. The reduction of nuclear SHMT1 in response to Ubc13 over-expression was partially rescued by treatment with LMB. This suggests that SHMT1 is exported from the nucleus in a Ubc13 and K63 linkage specific manner as has been observed for p53(13). SHMT1 was less stable in both the cytosol and nuclei of cells treated with CHX and Ubc13 siRNA whereas over-expression of Ubc13 lead to an increase in stability of SHMT1 in the cytosol. In response to transfection of the mutant ubiquitin K48R which is involved in proteosomal degradation, and increase in stability of SHMT1 was observed in the cytosol, whereas the K63R mutant showed a decrease in SHMT1 stability in the nucleus. Lack of Ubc13 in siRNA treated samples lead to

decreased nuclear SHMT1 accumulation, suggesting that a competition between Ubc13 and Ubc9 does exist in the nucleus, where Ubc9 can add SUMO-2/3 to SHMT1 which is then selectively degraded. These data are also indicative of Ubc13 playing a role in stabilization of SHMT1 within nuclei and export out of nuclei. The tight regulation of SHMT1 through ubiquitination and SUMOylation at the same sites gives insight into the important regulatory events governing nuclear *de novo* dTMP synthesis. SHMT1 is the rate-limiter in *de novo* dTMP synthesis (2,14) so degradation of nuclear SHMT1 would serve to shut *de novo* dTMP synthesis off.

Part V: Lamin Binding of SHMT1 and its role in nuclear dTMP biosynthesis.

Because SHMT1, SHMT2α, TYMS, and DHFR are all required for *de novo* dTMP synthesis, we wanted to determine if a *de novo* dTMP multi-enzyme complex existed. Multi-enzyme complexes are required for *de novo* purine synthesis in the cytosol (15-18) and nuclear complexes containing TYMS and DHFR activity has also been reported (6,7). Using a tandem affinity approach coupled with peptide sequencing, we were able to determine that SHMT1 is a lamin binding protein and also interacts with multiple proteins involved in DNA replication and repair. Surprisingly, TYMS and DHFR were not present in the large-scale tandem affinity and peptide sequencing experiment. We found that this was due to the requirement of DNA for the interaction of the three enzymes. The interaction of SHMT1 with Lamin A/C and Lamin B1 was present even under high salt conditions (650 mM NaCl) but TYMS and DHFR did not interact with lamins in samples treated with nucleases. Furthermore, we went on to find the formation of LaminB1, SHMT1, SHMT2α, TYMS, and DHFR co-localizing filament like structures which are present during S and G2/M phases of the cell cycle.

Unlike the purinosome, the *de novo* dTMP multi-enzyme complex is not sensitive to nucleoside levels (16). It was also shown that SHMT1 and SHMT2α are requirements for the

recruitment of TYMS and DHFR to LaminB1 co-localizing structures, whereas TYMS and DHFR are not required for SHMT1 and SHMT2α localization.

Previous studies in SHMT1-deficient mice (14) and cell culture models (2,3) demonstrated positive correlations between the expression of SHMT1 and capacity for *de novo* thymidylate synthesis, although kinetic studies do not indicate SHMT1 is catalytically rate-limiting for *de novo* dTMP synthesis (19). To distinguish between the contributions of SHMT1 catalytic activity and scaffold function to nuclear *de novo* dTMP biosynthesis, a dominant negative (DN2) Y82A/Y83F/K257Q mutant fluorescent SHMT1 vector and SH-SY5Y neuroblastoma cells lines expressing a tet-inducible DN2-SHMT1 were produced (for a full description, see chapter 5). The SH-SY5Y cells and HeLa cells used in these experiments both contain endogenous levels of SHMT1. SHMT is a tetramer, best described as a dimer of obligate dimers, in which amino acid residues from each monomer in the obligate dimer contribute to both active sites in the dimer (20,21). Cells containing endogenous SHMT1 and expressing dominant negative mutants would result in a statistical mixture of active and inactive SHMT1 tetramers which would decrease SHMT1 specific activity in the cell. The effects of these mutants on scaffold function and *de novo* dTMP synthesis were determined. DN2-SHMT1 co-localized with LaminB1 and was similar to WT-SHMT1 localization. Surprisingly, DN2-SHMT1 increased *de novo* dTMP synthesis while suppressing methionine biosynthesis. These data confirm the importance of SHMT1 scaffold function for the biosynthesis of dTMP and indicates that the scaffold function is a major contributor to nuclear *de novo* dTMP synthesis.

Because of the requirement of DNA for multi-enzyme *de novo* dTMP synthesis complex formation, and due to the interaction of multiple DNA replication and repair proteins, we wanted to determine if SHMT1 was present on actively replicating DNA. We have reported the interaction of SHMT1 with the DNA processivity factor PCNA (4). This led to the hypothesis that the enzymes for *de novo* dTMP synthesis could be synthesizing dTMP right at

the replication fork for processive addition. We used a model of episomally replicating DNA in order to understand if *de novo* dTMP synthesis multi-enzyme complexes exist on DNA. Using tandem chromatin immunoprecipitations first against PCNA and then against SHMT1, TYMS, and DHFR we were able to show that all the enzymes necessary for *de novo* dTMP synthesis were present in association with PCNA and DNA and were highly enriched around origins of replication. These data support that the entire *de novo* dTMP synthesis pathway is present during DNA replication at replication forks for the processive addition of dT in order to limit uracil misincorporation.

Part VI: Future Directions

These studies have brought to light the importance of nuclear and mitochondrial *de novo* dTMP synthesis and have informed us in the capacity of SHMT to limit uracil misincorporation in both nuclear and mitochondrial DNA. Many new questions arise from the work presented here. The identification of SHMT2α as a functional replacement for SHMT1 in both scaffold function and activity suggests that SHMT function in the nucleus is crucial for maintaining cellular dTTP pools. The regulation of SHMT2α should be further investigated. The protooncogene, c-myc has been shown to be a regulator of both SHMT1 and SHMT2 transcription (22), but it is still unknown whether c-myc regulates both SHMT2 and SHMT2α or just one of them. The SHMT2α transcript also has a long 5'-UTR, similar to SHMT1 (23), which may indicate post-transcriptional regulatory events through internal ribosome entry sites (24). The similarity of SHMT2α to SHMT1 in structure also suggests that post-translational control of SHMT2α occurs. Understanding whether a similar interplay between SUMOylation and ubiquitination that exists for SHMT1 occurs for SHMT2α will further our understanding of the functional redundancy within this pathway.

The identification of mitochondrial *de novo* dTMP synthesis also has brought up many new questions. These data have shown the importance in dTMP synthesis in mitochondria for limiting uracil misincorporation in mtDNA. Future research must understand the regulation of the novel DHFRL1 gene described here. Although we and others have reported TYMS and DHFRL1 localization to the mitochondria, the lack of canonical MLS in either of these genes suggests a new mitochondrial import pathway exists that has yet to be determined. Identifying what residues are required in these enzymes for mitochondrial import and what other chaperones or import proteins are involved in mitochondrial import is required. Research into whether formation of multi-enzyme complexes for *de novo* dTMP synthesis in mitochondria should also be undertaken. SHMT2 has been shown to crosslink to mtDNA (10)and therefore may be playing a scaffold function within mitochondria similarly to what we report within nuclei. Furthermore, little research has gone into understanding how uracil in mtDNA affects mitochondrial biology. These studies may shed light on other mechanisms which lead to cellular dysfunction and risk of developmental defects and other pathologies in humans.

The data presented here have demonstrated how SHMT1 is rate-limiting in *de novo* dTMP synthesis. The lamin binding scaffold function of SHMT1 is critical for the formation of multi-enzyme complexes and for efficient *de novo* dTMP synthesis. Tight regulation of SHMT1 has also been reported here with ubiquitination and SUMOylation playing a role in maintaining appropriate levels of SHMT1 within the nucleus. Future work must go into understanding what other ubiquitin pathway enzymes are required for regulation of SHMT1. More direct evidence of SHMT1 degradation within the nucleus should also be undertaken.

The data presented here regarding DN2-SHMT1 in SH-SY5Y cells indicates that the scaffold function of SHMT1 contributes significantly to its ability to direct *de novo* dTMP synthesis. If cytoplasmic *de novo* dTMP synthesis were to occur, one would expect a decrease in *de novo* dTMP synthesis efficiency as was seen with methionine, but this was not the case.

Methionine represents cytoplasmic folate-mediated one carbon metabolism and was suppressed while dT synthesis was increased. This data along with the identification of *de novo* dTMP synthesis in both compartments that require DNA synthesis suggest that cytoplasmic *de novo* dTMP synthesis is not substantial, if it occurs at all. Future work will need to knock out nuclear *de novo* dTMP synthesis completely in order to understand the contribution of cytoplasmic *de novo* dTMP synthesis, if any. This could be achieved by making mice with a SUMO site mutant knock-in of SHMT1, along with mutation of the start methionine in the SHMT2 gene which leads to the production of SHMT2α.

We have also presented that SHMT1 interacts with a variety of proteins and enzymes required for DNA replication and repair, including PCNA, UNG2, and DNA polymerases δ and ε. These data are indicative of an important role for SHMT1 in delivering one-carbon units for *de novo* dTMP synthesis at the replication fork both during replication and repair and limiting uracil misincorporation within DNA.

REFERENCES

1. Fox, J. T., and Stover, P. J. (2008) *Vitam Horm* 79, 1-44
2. Oppenheim, E. W., Adelman, C., Liu, X., and Stover, P. J. (2001) *J Biol Chem* 276, 19855-19861
3. Herbig, K., Chiang, E. P., Lee, L. R., Hills, J., Shane, B., and Stover, P. J. (2002) *J Biol Chem* 277, 38381-38389
4. Woeller, C. F., Anderson, D. D., Szebenyi, D. M., and Stover, P. J. (2007) *J Biol Chem* 282, 17623-17631
5. Anderson, D. D., and Stover, P. J. (2009) *PLoS One* 4, e5839
6. Noguchi, H., Prem veer Reddy, G., and Pardee, A. B. (1983) *Cell* 32, 443-451
7. Prem veer Reddy, G., and Pardee, A. B. (1980) *Proc Natl Acad Sci U S A* 77, 3312-3316
8. Neuburger, M., Rebeille, F., Jourdain, A., Nakamura, S., and Douce, R. (1996) *J Biol Chem* 271, 9466-9472
9. Samsonoff, W. A., Reston, J., McKee, M., O'Connor, B., Galivan, J., Maley, G., and Maley, F. (1997) *J Biol Chem* 272, 13281-13285
10. Bogenhagen, D. F., Rousseau, D., and Burke, S. (2008) *J Biol Chem* 283, 3665-3675
11. Ulrich, H. D. (2009) *DNA Repair (Amst)* 8, 461-469
12. Schimmel, J., Larsen, K. M., Matic, I., van Hagen, M., Cox, J., Mann, M., Andersen, J. S., and Vertegaal, A. C. (2008) *Mol Cell Proteomics* 7, 2107-2122
13. Laine, A., Topisirovic, I., Zhai, D., Reed, J. C., Borden, K. L., and Ronai, Z. (2006) *Mol Cell Biol* 26, 8901-8913
14. MacFarlane, A. J., Liu, X., Perry, C. A., Flodby, P., Allen, R. H., Stabler, S. P., and Stover, P. J. (2008) *J Biol Chem* 283, 25846-25853
15. An, S., Deng, Y., Tomsho, J. W., Kyoung, M., and Benkovic, S. J. (2010) *Proc Natl Acad Sci U S A* 107, 12872-12876

16. An, S., Kumar, R., Sheets, E. D., and Benkovic, S. J. (2008) *Science* 320, 103-106

17. An, S., Kyoung, M., Allen, J. J., Shokat, K. M., and Benkovic, S. J. (2010) *J Biol Chem* 285, 11093-11099

18. Field, M. S., Anderson, D. D., and Stover, P. J. (2011) *Frontiers in Genetics* 2, 1-13

19. Reed, M. C., Nijhout, H. F., Neuhouser, M. L., Gregory, J. F., 3rd, Shane, B., James, S. J., Boynton, A., and Ulrich, C. M. (2006) *J Nutr* 136, 2653-2661

20. Szebenyi, D. M., Liu, X., Kriksunov, I. A., Stover, P. J., and Thiel, D. J. (2000) *Biochemistry* 39, 13313-13323

21. Zanetti, K. A., and Stover, P. J. (2003) *J Biol Chem* 278, 10142-10149

22. Nikiforov, M. A., Chandriani, S., O'Connell, B., Petrenko, O., Kotenko, I., Beavis, A., Sedivy, J. M., and Cole, M. D. (2002) *Mol Cell Biol* 22, 5793-5800

23. Woeller, C. F., Fox, J. T., Perry, C., and Stover, P. J. (2007) *J Biol Chem* 282, 29927-29935

24. Fox, J. T., Shin, W. K., Caudill, M. A., and Stover, P. J. (2009) *J Biol Chem* 284, 31097-31108